Wood and paint layers aging and risk analysis of ancient panel painting

Julien Froidevaux

Thèse N° Année 2012

THÈSE

De l'Université Montpellier 2

Pour l'obtention du grade de

Docteur de l'Université Montpellier 2

Ecole doctorale

Information, Structure, Systèmes (I2S)

Laboratoire - Spécialité

Laboratoire de Mécanique et Génie Civil (LMGC)

Wood and paint layers aging and risk analysis of ancient panel painting

Par

JULIEN FROIDEVAUX

Soutenue le 1 octobre 2012 devant le jury composé de :

Frédéric Dubois	Prof. Université de Limoges, France	Rapporteur
Marco Fioravanti	Prof. Université de Florence, Italie	Rapporteur
Joseph GRIL	Dir. Recherche CNRS, Montpellier, France	Directeur de thèse
Parviz Navi	Prof. HESB-AHB, Bienne/Biel, Suisse	Directeur de thèse
Julien Colmars	Dr, Université Paris 6, France	Examinateur
Emmanuel Le Clézio	Prof. Université Montpellier 2, France	Examinateur
Patrick Perré	Prof., Ecole Centrale, Paris, France	Examinateur
Ernst Zürcher	Prof. HESB-AHB, Bienne/Biel, Suisse	Examinateur

au

Laboratoire de Mécanique et Génie Civil
860 rue de St Priest – 34090 Montpellier

Je dédie ce travail

A mes parents, Nicolas & Pia

A ma femme, Stéphanie

Remerciements

Tous les travaux effectués dans ce projet n'auraient pas pu être réalisés sans l'implication de nombreuses personnes que je tiens à remercier pour les excellentes collaborations. Tout d'abord je remercie les membres de mon jury d'avoir accepté de rapporter et d'évaluer mes travaux. Plus particulièrement je tiens à remercier mes deux directeurs de thèses :

Parviz Navi qui a initié la thématique des panneaux peints à la Haute Ecole Spécialisée Bernoise et qui m'a donné la chance de travailler sur ce sujet très varié. Je lui suis reconnaissant pour sa grande disponibilité ainsi que l'autonomie et la confiance qu'il m'a accordée tout au long de mes travaux.

Joseph Gril qui a su concentrer son attention lors de mes visites (toujours trop courtes hélas) à Montpellier qui n'étaient pas aussi nombreuses qu'escompté. Ses conseils et remarques ont été d'une aide très précieuse. Un grand merci également pour le temps passé à corriger mes fautes d'anglais lors de la rédaction de ce mémoire….

Finance & Infrastructure

Ce projet n'aurait évidemment pas eu lieu sans soutien financier. Je remercie particulièrement le *Fonds National Suisse de la recherche scientifique (FNS)* (projet N° K21K-122336/1) pour le financement principal du projet. Remerciement également à la *Haute Ecole Spécialisée Bernoise* pour son soutien financier, logistique et administratif.

Merci aussi au programme *Germaine de Staël* de *l'Académie Suisse des Sciences Techniques* (SATW) pour le soutien financier de la collaboration franco-suisse entre Bienne et Montpellier.

Merci à *l'Université Montpellier 2* de m'avoir accepté comme étudiant doctorant et pour la mise à dispositon de leurs infrastructures.

Personnes

Bienne - HESB-AHB

Premièrement, je tiens à remercier **Christelle Ganne-Chédeville** pour son excellent travail sur la caractérisation des changements chimiques de mes échantillons. Un grand merci également à **Marion Noël**, pour son soutien administratif lors du développement des enceintes de sorption et à **Thomas Volkmer** pour son aide et ses précieux conseils lors de l'analyse anatomique des vieux bois. Merci aussi à ma collègue et voisine de bureau **Marìa-Inès Plancencia Peña**, elle-même doctorante à l'HESB-AHB, avec qui nos discussions sur nos thèses respectives ont été l'occasion d'un foisonnement d'idée ! Un grand merci à toutes l'équipe du labo de chimie, notamment **Estelle Graf**, **Maillard Aline** et **Moser Regula** pour leur aide et patience à m'expliquer les manips de chimie. Merci à **Martin Lehmann** pour ses conseils et aide sur la modélisation numérique avec ANSYS ainsi que pour les nombreuses heures passées pour l'administration des Workstations et des licences ANSYS….

Je tiens également à remercier, **Frédéric Pichelin** le chef de l'équipe *matériaux et technologie du bois*, ainsi que **René Graf** le directeur Recherche et Développement HESB-AHB, pour l'organisation générale ainsi que la mise de place et spécificité du statut de doctorant à la HESB.

Merci à tous les collaborateurs de l'HESB-AHB pour la bonne ambiance de travail.

Montpellier - UM2

Un grand merci à toutes l'équipe de mécanique de l'arbre et du bois MAB de l'Université Montpellier 2, pour leurs remarques et conseils scientifiques sur mes travaux. Je citerai notamment, **Delphine Jullien**, **Tancrède Alméras**, **Olivier Arnould**, **Bruno Clair** et **Arthur Gronvold**. Ce fut un plaisir et une chance pour moi de travailler en collaboration avec cette équipe de grande perspicacité scientifique. Merci à **Julien Colmars**, précédent doctorant de J. Gril, pour tous ses conseils en simulation numérique.

HESB-HKB

Un grand merci aux personnes du département des arts (HKB) pour la bonne et fructueuse collaboration que nous avons eue et qui continuera durant le prochain projet. Merci tout d'abord, à **Stefan Zumbhül**, **Renate Kühnen**, **Martina Müller**, **Giovanna Di Pietro** et **Sandra Hons** qui ont initié le projet à la HKB et pour leurs travaux sur le vieillissement de la peinture. Merci en tout particulier à **Martina** pour ses commentaires et conseils dans le domaine de la conservation et restauration ainsi que pour ses nombreux travaux sur la perméabilité de la peinture, mesure de

déformation des panneaux par le « Deformometric Kit » et bien sur la préparation des panneaux de peinture.

RINO Sàrl, alias Fred Girardet

Un constructeur et expérimentateur hors pair, associé à une grande maîtrise théorique, voici comment je peux qualifier **Fred Girardet**. Ean effet, grâce à lui, le design et la construction des réacteurs TH, éléments piliers de ce projet, ont été un grand succès. Mais ce n'est pas tout, ses conseils pratiques et théoriques ont été d'une très grande aide. MERCI !

Autres institutions

Merci à l'**EMPA** et au **Dr. Erwin Hack** pour les mesures par projection de franges. Merci aussi au **Prof. Marco Fioravanti** et **Luca Uzielli** pour notre formation sur le « Deformometric Kit ».

Remerciement personnel

Finalement un IMMENSE merci à mes parents Nicolas et Pia pour leur soutien inconditionnel tout du long de mes études.

Merci également pour son amour et sa patience (notamment lors de mes nombreuses excursions à travers l'Europe), à ma pomme d'amour : Stéphanie. Je t'aime à la folie….

Table of content

Version française abrégée

Introduction

Les anciennes peintures sur bois représentent une part importante du patrimoine culturel européen. Depuis longtemps, il est connu que les conditions de stockage peuvent entraîner des dégradations et des endommagements aux tableaux. En effet, les variations thermiques et hygroscopiques génèrent des déformations et des contraintes dans le support en bois, qui sont ensuite transférés aux couches picturales. La solution optimale connue pour la conservation d'objet artistique en bois est de les conditionner sous un climat contrôlé avec des variations thermo-hydrique (TH) minimales. Malheureusement, de tels systèmes de conditionnement sont relativement onéreux et ne sont pas applicables à toutes les situations (dans les églises par exemple). De plus, les systèmes de contrôles climatiques sont techniquement très sensibles et ne conviennent pas pour des temps de maintien très longs. En outre, une panne d'un système climatique peut induire des variations TH plus drastiques que les variations naturelles.

L'un des sujets importants de la conservation préventive et de la restauration est la définition des conditions ambiantes admissibles pour le tableau et l'évaluation des risques pour une variation climatique donnée. Une bonne compréhension du comportement de ces peintures sur bois dans diverses conditions climatiques est donc essentielle. Des techniques d'analyses telles que l'imagerie multispectrale par UV ou IR, la microscopie optique et acoustique et radiographie aux rayons X ont été mises en œuvre pour le diagnostic des peintures sur bois. Bien que ces techniques soient extrêmement importantes pour identifier des endommagements, elles ne peuvent pas fournir des informations sur leurs causes ou les prédictions de leurs évolutions.

De telles analyses, capables de prédire et de comprendre l'état actuel d'une ancienne peinture peuvent être faites par le biais de la modélisation numérique afin de virtuellement soumettre une peinture sur bois à différents scénarios climatiques. De telles analyses ont été effectuées par exemple sur la célèbre peinture de Léonard de Vinci : *La Joconde*. L'exécution des différentes parties de ces travaux ont mobilisé plusieurs groupes en 2004 - 2005 et ont combiné des mesures expérimentales et des modélisations numériques. Ces travaux sont résumés dans un livre "Au Cœur de la Joconde" (J. P. Mohen *et al.*, 2006).

Cette approche interdisciplinaire favorise des changements majeurs dans l'analyse des risques des peintures sur bois. Toutefois, la modélisation numérique de ces œuvres d'arts est complexe et requière un modèle multi-physique couplant la mécanique à l'hygroscopicité et à la thermique du bois. Ces méthodes ont été appliquées avec succès par différents auteurs (J. Colmars, 2011, D. Dureisseix and B. Marcon, 2011). Cependant, la modélisation numérique ne peut réaliser de bonnes prédictions que si les paramètres du matériau sont mesurés ou déterminés de façon adéquate. Les derniers travaux cités ci-dessus, intègrent dans leurs modèles les paramètres de bois et de peinture non-vieillis.

Le premier objectif de ce travail de doctorat a été de déterminer comment les propriétés mécaniques et physiques du bois et de la peinture sont modifiées par un vieillissement (de plusieurs siècles) et si ce vieillissement peut être estimé en utilisant des méthodes de vieillissement accéléré par traitement thermo-hydrique (TH). Le deuxième objectif a été de simuler numériquement et d'analyser le comportement de peintures sur bois non âgés. Finalement, une étude de cas a été effectuée sur une ancienne peinture.

Vieillissement du bois

Le bois fait partie du cycle du carbone dans la nature et sa dégradation en constitue l'un des éléments essentiels. Plusieurs processus de dégradation sont imposés au bois tel que les attaques biologiques (insectes ou fongiques), les conditions extrêmes de chaleur, de gel ou de hautes charges mécaniques, l'exposition à la lumière UV, la dégradation chimique due à la pluie ou la pollution de l'air, etc… Tous ces processus de dégradation dépendent étroitement des conditions d'utilisation ou de stockage du bois. Si le bois est maintenu dans un environnement raisonnable, elles peuvent être évitées. Cependant, un phénomène de vieillissement à long terme a lieu dans le bois. Ce vieillissement du bois sans autre dégradation, est typiquement généré dans des conditions intérieures ou abritées à l'extérieures. L'origine de ce vieillissement est thermodynamique : Des réactions chimiques entre les composants du bois ont lieu sur de longues périodes de temps et vont tendre vers un équilibre.

Investigation sur le vieux bois

Plusieurs études ont été réalisées sur le vieillissement du bois (K. Borgin *et al.*, 1975a, K. Borgin *et al.*, 1975b, D. Erhardt *et al.*, 1996, J. Kohara, 1952, J. Kohara, 1953, J. Kohara, 1954a, J. Kohara, 1954b, J. Kohara, 1955a, J. Kohara, 1955b, M. Matsuo *et al.*, 2011, E. Obataya, 2007, M. Yokoyama *et al.*, 2009). La première partie de ce travail de doctorat a été de développer des méthodes expérimentales afin de caractériser les modifications mécaniques et physiques du vieux bois.

Dans un premier temps, une sélection de vieux bois provenant de bâtiments anciens en Suisse a été effectuée. Une seule essence de bois a été étudiée dans ce

travail : le bois d'épicéa (*Picea abies Karst. (L.)*). L'âge des échantillons de vieux bois a été déterminé par dendrochronologie. De plus, afin de pouvoir isoler les modifications dues au vieillissement, seul les échantillons ne présentant aucun autre type de dégradation (notamment d'insecte et champignon) ont été retenus. Au final, seulement trois catégories de vieillissement ont été retenues : 200, 400 et 500 ans.

Dans un second temps, des tests mécanique et hygroscopique ont été effectués sur ces échantillons. Un appareil de micromécanique (figure 2.8) a été utilisé afin de déterminer en traction dans la direction radiale le module élastique, la contrainte de rupture, le comportement viscoélastique et mécanosorptif des vieux bois et de références modernes comprenant trois différents régimes de croissance de l'arbre. Les résultats de cette étude sont présentés dans les figures 3.4à 3.7. Concernant les mesures hygroscopiques, un système de chambres isothermes a été développé et construit comme on peut le voir sur le croquis de la figure 2.13 et en photographie de la figure 2.14. La perte de masse d'échantillons de bois est mesurée après un saut d'humidité relative (HR). Par une méthode inverse, le coefficient de diffusion de l'eau dans le bois peut en être déduit. Les résultats de ces mesures sont présentés dans les tableaux 3.3 et 3.4 .

En conclusion, et en accord avec la littérature, peu de modification ont été décelée dans les échantillons de vieux bois par rapport aux bois récents. En effet, aucun changement significatif n'a été observé pour le comportement radial élastique, viscoélastique et mécanosorptif des vieux bois. Egalement, pas de changement de la sorption des vieux bois par rapport aux bois récents. Cependant, la résistance radiale en tension est fortement dégradée (figure 3.5) ainsi que la couleur (figure 3.10) (J. Froidevaux *et al.*, 2012).

Vieillissement accéléré du bois

Afin de pouvoir prédire les propriétés d'un vieux bois, une méthode basée sur l'accélération du vieillissement a été développée. En effet, étant donné que l'origine du vieillissement naturel du bois est d'ordre chimique, une élévation de la température pourrait accélérer les réactions chimiques de vieillissement. Une étude chimique a été effectuée par C. Ganne-Chédeville, afin de déterminer quels sont les modifications chimiques apportées au bois par différentes variantes de traitements TH (C. Ganne-Chédeville *et al.*, 2011). Ces résultats ont montré que des traitements TH à des températures supérieures ou égales à 160°C induisent des réactions chimiques différentes des bois vieillis naturellement. Dès lors, les traitements TH imposés aux échantillons de bois pour cette étude du vieillissement accéléré ont été limités à 150°C et aux HR faibles (< 25 %).

Des systèmes de traitements TH ont été conçus et construits (RINO Sàrl, Blonay, Suisse) afin de précisément contrôler la température et l'HR de traitement. Un de ces réacteurs TH est présenté ci-dessous en figure a.

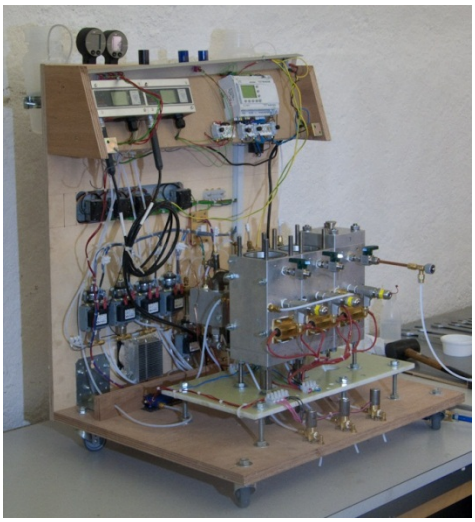

Figure a: Photographie d'un des deux réacteurs thermo-hydrique (TH) sans son isolation.

Les effets des traitements TH sur les propriétés du bois sont présentés dans les figures 3.15 à 3.23. Ces effets sont en accord avec la littérature et des tendances similaires au vieillissement naturel ont été observées sur les propriétés mécaniques. En effet, les modules élastiques radiaux ne sont pas affectés par les traitements thermiques alors que, comme pour le vieillissement naturel, la couleur et la résistance radiale sont fortement réduites.

Loi de vieillissement du bois d'épicéa

Afin de prédire, dans un premier temps les propriétés de bois traités TH, un ajustement de l'évolution de la résistance radiale et de la luminosité de la couleur a été effectué sur la loi de cinétique chimique. Une loi de vieillissement en a été déduite :

$$\begin{cases} \sigma_f(t) &= \sigma_0 e^{-k(T,m)\cdot t^n} \\ L^*(t) &= L_0^* e^{-k(T,m)\cdot t^n} + L_\infty^* \end{cases}$$

avec :

$$k(T,m) = k_0 \cdot e^{Bm} \cdot e^{-\frac{E_a}{RT}}$$

où σ_0 et L_0 sont la résistance radiale et la luminosité du bois non-vieillis, L_∞ est la luminosité du bois après un vieillissement de temps infini, $k(T,m)$ est la constante de vitesse et T, t et m sont respectivement la température, le temps et la teneur en eau durant le traitement TH. Les paramètres n, k_0, B et E_a sont les constantes ajustées. Le tableau 3.7 récapitule leurs valeurs.

Etonnement, une relation linéaire entre la luminosité et la résistance mécanique a été trouvée comme on peut le voir sur la figure b.

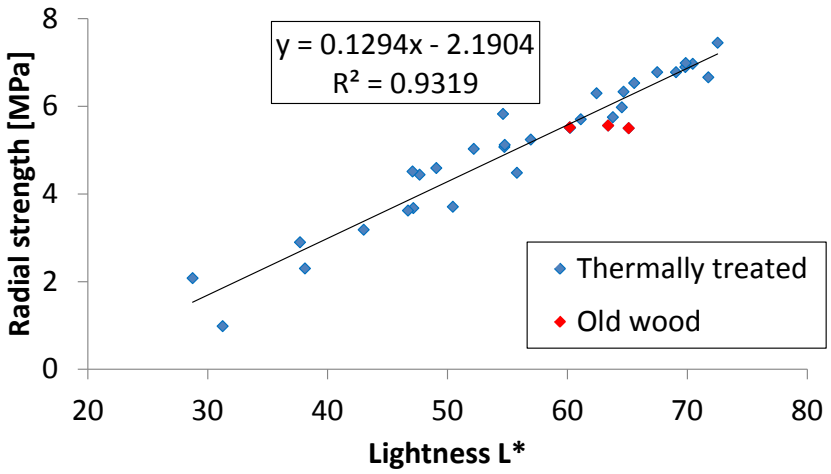

Figure b: Représentation de la relation linéaire entre la résistance radiale et la luminosité de bois vieillis par traitements TH et naturellement.

En extrapolant la loi de vieillissement à des conditions de vieillissement naturel, le vieillissement peut-être prédit. Cette extrapolation est présentée dans la figure c. Par exemple, on peut voir qu'une condition de stockage moyenne de 20°C et de 25% HR suffit réduire la résistance à la traction de 20% après 200 ans.

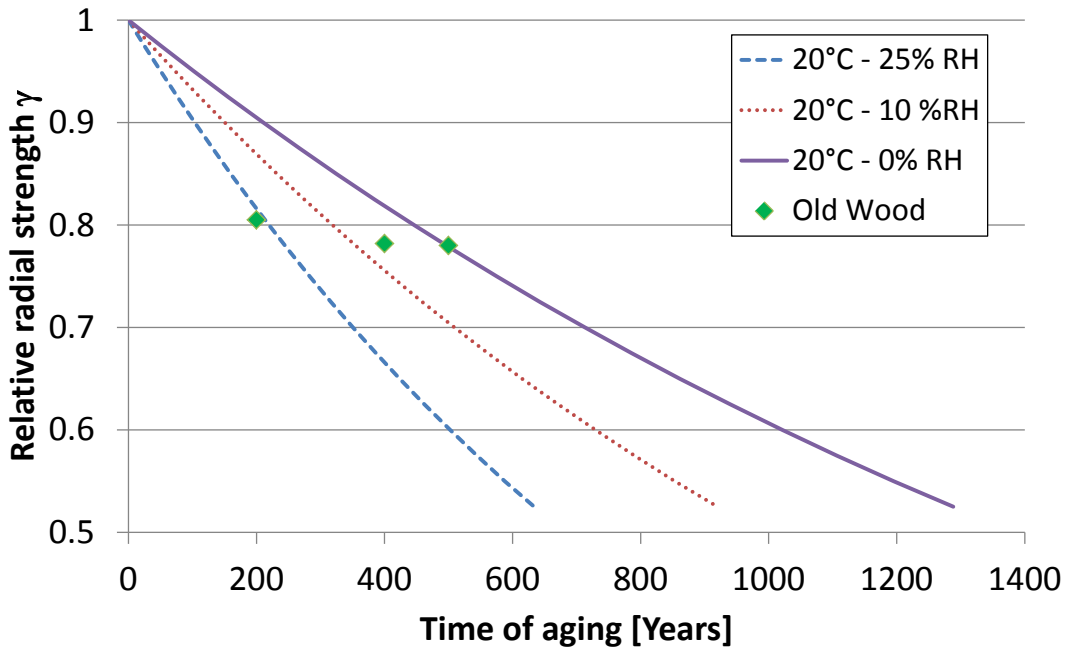

Figure c: Extrapolation de la loi de vieillissement. La perte de résistance radiale est présentée pour trois conditions de stockage en température et HR. Les trois points verts correspondent au trois variantes de vieux bois étudiés.

Cet outil pourrait servir d'aide à l'estimation de la résistance radiale d'un ancien panneau de peinture sur bois. En effet, en mesurant la couleur d'une ancienne œuvre d'art, sa résistance pourra en être déduite ainsi que ses conditions de stockages moyennes, ce qui servira à prédire son évolution dans le futur. Cela suppose toutefois

d’avoir accès à une partie non peinte de l’œuvre qui soit demeurée protégée de la lumière ou autre source de vieillissement de surface, et qui puisse être rafraîchie.

Vieillissement des couches de peintures

Grâce à la collaboration avec l'université des arts de Berne (HESB-HKB), une étude sur le vieillissement des couches de peinture a été effectuée. Les matériaux utilisés pour les couches de peinture peuvent varier considérablement de tableaux en tableaux. Une peinture multicouche médiévale typique a été sélectionnée. Elle est composée d’une couche de peinture (huile de lin avec des pigments de blancs de plomb) et d’une couche de base (mélange de craie et de colle) comme représentée à la figure d.

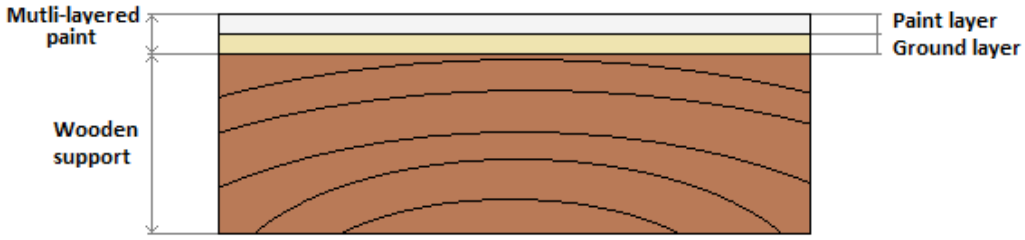

Figure d: Croquis de la peinture multicouche sélectionnée dans ce projet, composée de deux couches: une couche de peinture et une couche de base.

Comme pour l’étude du vieillissement du bois, un traitement thermique (incluant des irradiations UV) de vieillissement accéléré a été étudié. Une couche de peinture non-vieillis, vieillis naturellement et des peintures vieillis par ces traitements accélérés ont été chimiquement comparées. Des réactions chimiques différentes ont été mises en évidence (S. Zumbühl *et al.*, 2011). Par conséquent, les traitements accélérés ne peuvent pas être considérés comme similaires au vieillissement naturel. La multitude de réactions qui se produisent lors du vieillissement naturel ne peut pas être accélérée également, même à 40 °C.

Modélisation numérique de panneaux peints

Les premières étapes de la modélisation numérique ont été faites dans mon mémoire de Master: "*Simulation of the mechanical behavior of wood under relative humidity changes*" (J. Froidevaux, 2009). Dans ce travail, le comportement hygro-mécanique de panneaux de bois a été calculé par éléments finis en 2D dans le plan TR (déformation plane).

Dans le présent travail, le modèle a été étendu en 3 dimensions et le bois est considéré comme un matériau viscoélastique anisotrope.

Modèle numérique

Le modèle est donc multi-physique, calculant dans un premier temps la diffusion de l'eau dans le bois en fonction de conditions aux limites imposées dans le temps. Ensuite le modèle est couplé à un modèle mécanique. L'expansion hygroscopique est déduite du champ d'humidité et les contraintes sont calculées. Le modèle mécanique considère l'anisotropie du bois (notamment l'orientation des cernes annuels) et le comportement viscoélastique du bois. Pour ce faire, une loi de comportement viscoélastique a été implémentée dans le programme d'élément finis ANSYS. Cette loi est basée sur des modèles trouvés dans la littérature (Z. A. Taylor *et al.*, 2009, H. Poon and M. F. Ahmad, 1998, A. Guidoum, 1994), et considère un modèle rhéologique : le modèle de Maxwell généralisé tel que présenté à la figure 5.1. Ce modèle a été étendu au cas tridimensionnel (équations (5-7), (5-10) et (5-11)).

Ensuite, la couche de peinture a été ajoutée sous forme d'éléments plaques: sa rigidité a été prise en compte et le comportement hygroscopique de la peinture a été introduit comme une condition aux limites (équation (5-12)).

Les propriétés mécaniques et hygroscopiques du bois ont été pour la plupart mesurées expérimentalement dans le cadre de ce travail. Certains paramètres tels que les modules de cisaillement et les coefficients de Poisson, ont été estimés sur les bases de la littérature. Les propriétés mécaniques sont présentées dans le tableau 5.3.

Validation du modèle

Afin de confirmer le modèle, deux techniques expérimentales et une formulation analytique ont été utilisées pour déterminer la déformation de panneaux de bois peints soumis à un changement d'HR. La première approche expérimentale, appelée "*Deformometric Kit*", mesure en continue la flèche d'un panneau. Un schéma de cette méthode est donné à la figure 5.9 et une photographie de l'installation est présentée ci-dessous en figure e(a).

La seconde technique expérimentale est une technique optique par projection de franges permettant de mesurer la forme tridimensionnelle d'un panneau à un instant donné. Une photographie de l'installation est présentée à la figure e(b).

Finalement, une formulation analytique correspondant à la différence entre deux conditions d'équilibre est présentée.

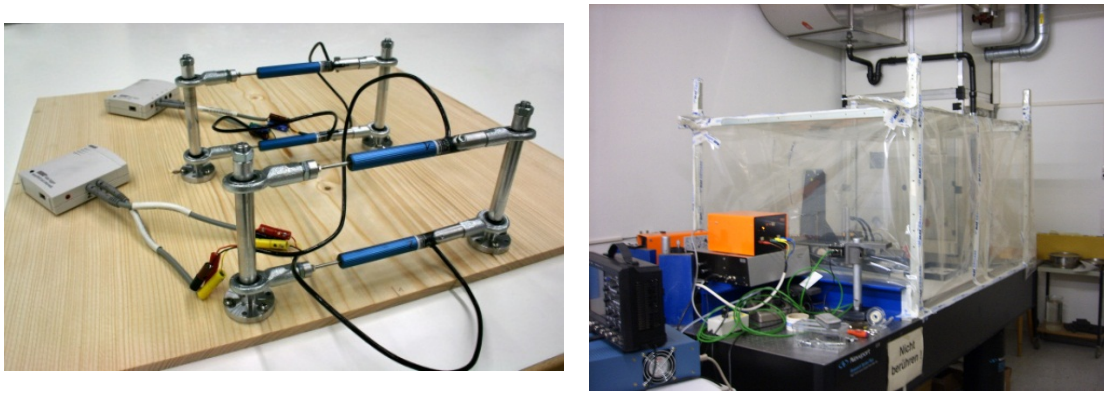

(a) (b)

Figure e: (a) Installation du « Deformometric Kit » sur un panneau de bois. (b) Système de mesure par projection de franges. Une tente climatique a été construite autour de l'installation afin de garantir un climat stable.

Les comparaisons entre les mesures expérimentales et numériques sont en bon accord comme on peut le voir aux figures 5.13 à 5.22.

Etude de cas d'un ancien panneau peint

Une étude de cas a été effectuée sur une ancienne peinture sur bois, présentée dans la figure f. Cette peinture nous a été confiée par le *Musée National Suisse - Centre de Collection* (Sammlungszentrum). Il s'agit d'une reproduction (contrefaçon) d'un artiste inconnu et se compose d'une peinture multicouche et d'un support en bois d'épicéa, daté par dendrochronologie d'environ 270 ans.

Figure f: L'ancienne peinture sur bois utilisé pour l'étude de cas. Une ligne de colle est bien visible (flèche verte). Le cadre rouge indique la zone de mesure de la technique de projection de franges.

La technique de projection de franges a été utilisée pour mesurer la déformation de cet ancien panneau peint soumis à une variation d'HR. Le système de mesure

couvre une superficie de 35x25cm^2 présenté par le rectangle rouge dans la figure f. L'évolution du climat (température et HR) que cette ancienne peinture a subit durant nos tests est présentée dans la figure 6.3. La déformation mesurée après une heure est présentée ci-dessous dans la figure g.

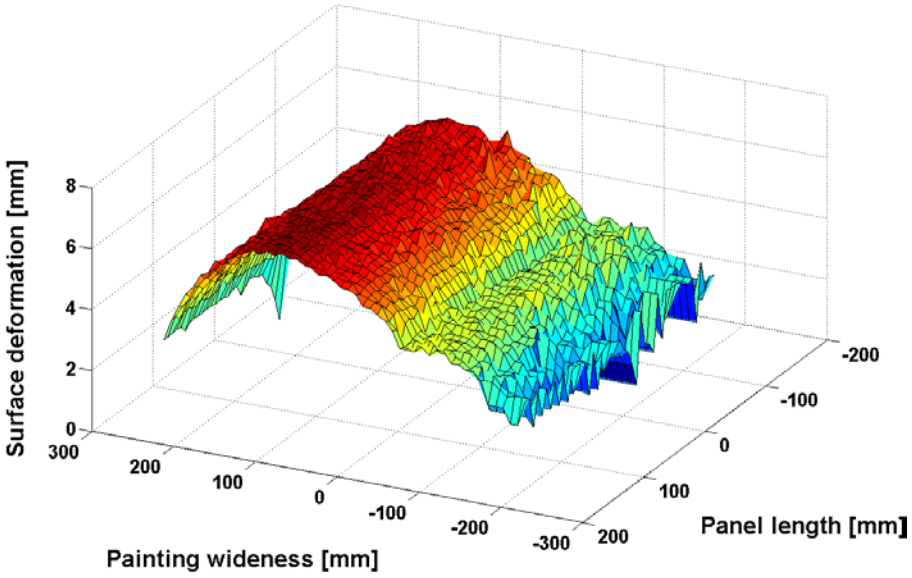

Figure g: Forme de la surface de l'ancien panneau peint après une heure du changement d'HR. La ligne de colle sur le panneau de bois apparait aux alentours de la position -50 mm sur la largeur.

Identification du tableau

La caractérisation de cette ancienne peinture sur bois est plus difficile que celle des panneaux de bois modernes produits pour les expériences de confirmation du modèle. En effet, aucun essai destructif ne peut être effectué sur des panneaux réels. Cependant, comme ce tableau est une contrefaçon, nous avons été autorisés à poncer la face TR comme le montre la figure g.

Figure h: Face TR poncée de l'ancienne peinture sur bois. La flèche verte indique l'endroit d'un joint de colle.

Cette coupe nous a permis de déterminer l'essence du bois, l'orientation des cernes annuels, la couleur du bois, l'épaisseur du bois et des couches de peinture et l'âge du bois (analyse dendrochronologique). Les propriétés mécaniques globales telles que les propriétés viscoélastiques et élastiques ont été considérées égales à ceux du bois non-vieillis de référence étant donné qu'aucun effet de vieillissement n'a été détecté sur ces valeurs. La contrainte de rupture radiale peut être estimée par

la couleur avec la relation linéaire tel que présentée à la figure b. Cette résistance vaut **5.0 MPa**.

Malheureusement, nous n'avons pas réussi à prédire les propriétés d'une peinture vieillie. De plus, la perméabilité et la rigidité de la peinture multicouche de l'ancien panneau peint ne peuvent être mesurées qu'avec des essais destructifs. Par conséquent, le vieillissement de la rigidité et de la perméabilité a été négligé. Etant donné que cette ancienne peinture correspond à la peinture non-vieillie utilisée précédemment, les propriétés de cette dernière ont été utilisées dans le modèle numérique.

Comparaison avec le modèle et analyse de risque

La figure i montre la comparaison entre la flèche mesurée expérimentalement par la technique de projection de franges et la flèche calculée par le modèle numérique. L'évolution de la masse de la peinture au cours du temps est également représentée.

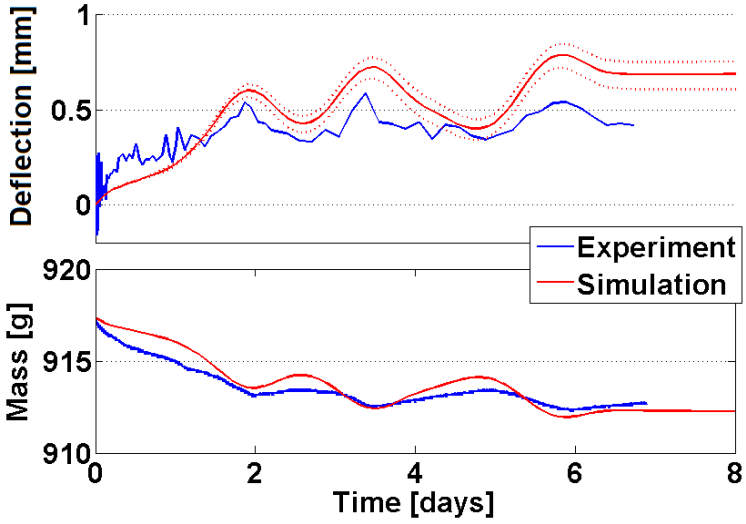

Figure i: Evolution temporelle de la flèche et de la masse de l'ancienne peinture sur bois durant un changement d'HR de 50 à 40% (condition climatique à la figure 6.3). Les lignes en pointillées correspondent à l'incertitude de la caractérisation.

La simulation de la flèche est légèrement supérieure à celle mesurée expérimentalement, même en tenant compte de l'incertitude (représentée par la ligne en pointillée) sur les paramètres des couches de peinture et du bois (rigidité, épaisseur et la perméabilité des couches de peintures et l'orientation des cernes annuels du bois). Cette déviation peut être due à la rigidité et la perméabilité inconnues de la peinture qui peuvent modifier de façon significative la déformation du panneau. Les changements climatiques, illustrés par la fluctuation de masse, ont été correctement simulés.

Les contraintes radiales maximales dans l'ancienne peinture sur bois pendant le changement hydrique précédent sont présentées à la figure 6.12. Il peut être observé que les fluctuations climatiques induisent d'importantes variations de contraintes. Cependant, la contrainte radiale maximale subite par le panneau est de 0.48 MPa. Cette contrainte est loin de la résistance à la rupture calculée du vieux bois.

En prenant en compte un changement d'HR plus important, typiquement atteint lors d'un déménagement du tableau, imposant dans un temps très court une HR de 65 à 44%, la contrainte maximale radiale devient: 2,7 MPa. Cette contrainte est également inférieure à la contrainte de rupture radiale. Cependant, à l'aide de la loi de vieillissement, nous pouvons estimer que la contrainte de rupture atteindra ces 2.7 MPa dans environ 1500 ans.

Analyse des contraintes dans la couche de peinture

Les contraintes dans la peinture multicouche sont localisées dans la couche de base. En effet, la couche de peinture n'est pas rigide et sa déformation à la rupture est importante. Les contraintes maximales calculées par le modèle numérique étaient de 1,6 MPa dans la couche de base pendant le changement d'HR expérimentale. C'est moins que la contrainte de rupture de la couche de base qui est 4,4 ± 1,0 MPa.

En reconsidérant un déménagement du tableau avec un rapide changement d'HR, la contrainte dans la couche de base monte à 6,4 MPa. Cette valeur est supérieure à la contrainte de rupture ce qui amènerait la couche de base à se fissurer.

Conclusion

Nous remarquons donc que si l'ancienne peinture sur bois est maintenue sous des conditions ambiantes respectables avec des changements limités d'HR, il n'y a pas de risque particulier d'endommagement du support en bois ou de la couche picturale. Cependant, une modification brutale de l'HR pouvant intervenir par exemple lors d'une panne d'un système de climatisation, d'un déménagement du tableau ou d'un accident, peut endommager la couche de base et dans une moindre mesure le support en bois en cas de fortes variations hygroscopiques ou d'un âge avancé de la peinture.

Cette analyse montre comment la science des matériaux peut aider dans la conservation des œuvres d'art en bois. Il faudra cependant encore améliorer le niveau de précision du modèle en incluant les phénomènes mécanosorptifs du bois par exemple.

Références

BORGIN, K., FAIX, O. & SCHWEERS, W. 1975a. The effect of Aging on Lignins of wood. *Wood Science and Technology*, 9**,** 207-211.

BORGIN, K., PARAMESWARAN, N. & LIESE, W. 1975b. The effect of aging on the ultrastructure of wood. *Wood Science and Technology,* 9**,** 87-98.

COLMARS, J. 2011. *Hygromécanique du matériau bois appliquée à la conservation du patrimoine culturel : Etude sur la courbure des panneaux peints.* PhD, Université de Montpellier 2 (UM2).

DUREISSEIX, D. & MARCON, B. 2011. A partitioning strategy for the coupled hygromechanical analysis with application to wood structures of cultural heritage. *International Journal for Numerical Methods in Engineering,* 88**,** 228-256.

ERHARDT, D., MECKLENBURG, M. F., TUMOSA, C. S. & OLSTAD, T. M. 1996. New versus old wood: differences and similarities in physical, mechanical, and chemical properties. *ICOM Preprints, 11th Triennial Meeting,* 2**,** 903-910.

FROIDEVAUX, J. 2009. *Simulation of the mechanical behavior of wood under relative humidity changes.* EPFL (Ecole Polytechnique Fédérale de Lausanne).

FROIDEVAUX, J., VOLKMER, T., GANNE-CHÉDEVILLE, C., GRIL, J. & NAVI, P. 2012. Viscoelastic behaviour of aged and non-aged spruce wood in the radial direction. *Wood Material Science and Engineering,* 7**,** 1-12.

GANNE-CHÉDEVILLE, C., JÄÄSKELÄINEN, A. S., FROIDEVAUX, J., HUGHES, M. & NAVI, P. 2011. Natural and artificial ageing of spruce wood as observed by FTIR-ATR and UVRR spectroscopy. *Holzforschung,* 66**,** 163-170.

GUIDOUM, A. 1994. *Simulation numérique 3D des comportements des bétons en tant que composites granulaires.* EPFL (Ecole Polytechnique Fédérale de Lausanne).

KOHARA, J. 1952. Studies on the durability of wood I, mechanical properties of old timbers. *Bulletin of Kyoto Prefectural University,* 2**,** 116-131.

KOHARA, J. 1953. Studies on the permanence of wood V, shrinkage and swelling of old timbers about 300-1300 years ago. *Bulletin of Kyoto Prefectural University,* 5**,** 81-88.

KOHARA, J. 1954a. Studies on the permanence of wood VI, the changes of mechanical properties of old timbers. *Bulletin of Kyoto Prefectural University,* 6**,** 164-174.

KOHARA, J. 1954b. Studies on the permanence of wood VII, the influence of age on the components of wood (Chamaecyparis obtusa Endlicher). *Bulletin of Kyoto Prefectural University,* 6**,** 175-182.

KOHARA, J. 1955a. On permanence of wood II, differences between the ageing processes of cypress wood and zelkova wood. *Wood industry,* 10**,** 395-399.

KOHARA, J. 1955b. Studies on the permanence of wood XV, the influence of age on the components of wood (Zelkowa serrata Makino). *Mokuzai Gakkaishi,* 1**,** 21-24.

MATSUO, M., YOKOYAMA, M., UMEMURA, K., SUGIYAMA, J., KAWAI, S., GRIL, J., KUBODERA, S., MITSUTANI, T., OZAKI, H., SAKAMOTO, M. & IMAMURA, M. 2011. Aging of wood: Analysis of color changes during natural aging and heat treatment. *Holzforschung,* 65**,** 361-368.

MOHEN, J. P., MENU, M. & MOTTIN, B. 2006. *Au coeur de La Joconde: Léonard de Vinci décodé - Centre de recherche et de restauration des musées de France*, Gallimard.

OBATAYA, E. 2007. Caractéristiques du bois ancien et technique traditionnelle japonaise de revêtement pour la protection du bois. *Actes de la journée d'étude Conserver aujourd'hui : les vieillissements du bois.* Cité de la Musique, Paris, France.

POON, H. & AHMAD, M. F. 1998. A material point time integration procedure for anisotropic, thermo rheologically simple, viscoelastic solids. *Computational Mechanics*, 21**,** 236-242.

TAYLOR, Z. A., COMAS, O., CHENG, M., PASSENGER, J., HAWKES, D. J., D., A. & S., O. 2009. On modelling of anisotropic viscoelasticity for soft tissue simulation: Numerical solution and GPU execution. *Medical Image Analysis*, 13**,** 234-244.

YOKOYAMA, M., GRIL, J., MATSUO, M., YANO, H., SUGIYAMA, J., CLAIR, B., KUBODERA, S., MISTUTANI, T., SAKAMOTO, M., OZAKI, H., IMAMURA, M. & KAWAI, S. 2009. Mechanical characteristics of aged Hinoki wood from Japanese historical buildings. *Comptes Rendus Physique*, 10**,** 601-611.

ZUMBÜHL, S., SCHERRER, N., FERREIRA, E., HONS, S., MÜLLER, M., KÜHNEN, R. & NAVI, P. 2011. Accelerated ageing of drying oil paint - an FTIR study on the chemical alteration. *Journal of Art Technology and Conservation / Zeitschrift für Kunsttechnologie und Konservierung*, 2**,** 137-149.

Chapter 1
Introduction

Ancient wood panel paintings represent an important part of the European cultural heritage and are omnipresent in museums, churches, states buildings and private collections. Since long time it is known that the storing conditions can degrade and damage wood panel paintings. Indeed, temperature and relative humidity (RH) fluctuation induce strains and stresses in the wooden support, which are transferred to the paint layers.

1.1 Context

1.1.1 History of conservation and restoration of panel paintings

Since long time, conservation and restoration of panel paintings exist. Until about the middle of 18th century, the persons involved in restorations were divided into the paint-restorers and the artisans (A. Acidini *et al.*, 2006). Paint-restorers were responsible of the aesthetical phases of panel paintings such as cleaning and retouching. The artisans were responsible to structural operation such as the wood support repairing. Therefore, during long period the structural elements in panel paintings and the paint layers were considered independent from each other. Such thinking of conservators had often important and regrettable consequences on the wooden objects. (A. Acidini et al., 2006) in the book introduction (p. 7) refers to this problem by noting that:

> *"The research and work carried on at the Opificio – not only in years but since the time of Ugo Proccacci and Umberto Baldini – have proven without doubt the fundamental importance of the structural aspects of panel paintings.*
>
> …
>
> *We find ourselves too often regretting the scarce or even total lack of respect for the wood support, in the face of the consequences of past operations on one or another painting. We are forced to realize that certain drastic decision, such as*

removal of crossbars, for example, or the thinning down or cradling of panels, have actually resulted in compromising the stability of the ground and paint layers, causing damage it might have been possible to avoid"

An example of such problems can be highlighted with the winged altars (known as *triptych*). Triptych are paintings or carving in three panels: two exterior shutters with double sided paint that can be closed on the middle one. These artworks have been developed mainly in the 12th and 13th centuries, as part of religious painting in Europe. Figure 1.1 shows two typical triptychs. Generally, when the altar is closed, religious motives to be seen during the week are shown. On the other side of the wings are motives to be shown on Sundays, when the altar is open during religious ceremonies in church.

The presentation in museum of such artworks cause a problem: The paintings in the open and closed condition cannot be seen at the same time. The repeated closing and opening movement can also induce unacceptable wear. In 19th century a solution that have been tried by restorers where to cut the shutters along the thickness, when they had to be shown in museums and so both sides could be seen all the time. Important cupping of the panel paintings was generated. Next the restorers tried to block these deformations by putting the panels in frames for examples. Mechanically, it is clear that this solution induces important stresses to the wooden supports which can develop cracks.

Actually, it is clear that for conservation and restoration of panel paintings one should consider them as a multi-layered structure with interdependent layers, composed of a wood support and a multi-layered paint (generally composed of a paint layer and a ground layer).

(a) (b)

Figure 1.1: (a) Gothic winged altar in Hungarian National Gallery-medieval altars & stones in Budapest. (b) The Eggenberg altarpiece in Eggenberg castle in Austria.

1.1.2 Recent techniques for panel paintings investigation

The known solution for conservation of wood panel paintings is to keep them under controlled climate with minimal variations. Unfortunately such conditions are expensive and cannot be satisfied everywhere (in churches for example). Moreover, climatic control systems are technically quite sensitive and not appropriate for long processing time. Furthermore, a breakdown of the system can induce more drastic climate change than natural variations.

Understanding of the actual state of old panel paintings and the prediction of their behaviour under various climatic conditions is essential to better conserve and restore them. It is known that transportation of panel paintings, for example, can induce stresses due to rapid RH changes. Such understanding should verify that these changes were supportable by the wooden support and the paint layers without producing irreversible damages.

One of the important topics of preventive conservation and restoration is the definition of optimal ambient conditions and risk assessment. Analytical techniques like multispectral imaging, UV, IR, optical and acoustical microscopy and X-ray radiography were implemented for diagnosing panel paintings. Although these techniques have been extremely important for depicting of object damaging, they cannot provide information either on the causes or on the prediction of the evolution of existing damages.

A known solution for predicting and analysing an old panel painting could be done by virtual testing via numerical simulation. Such techniques can provide information for risk analysis, to predict if an old panel painting would remain stable, undamaged under various scenarios.

In the 1990's, (M. F. Mecklenburg *et al.*, 1998, M. F. Mecklenburg and C. S. Tumosa, 1991) investigated the mechanical behaviour of historic wood and paint materials in equilibrium conditions at different relative humidity levels. They show a primary stage of stress analysis for a panel painting under ambient variation for assessing the potential for damage. In their work the panel is considered as a layered composite and the stresses at each layer are calculated by a finite element method. More recently the deformation of the famous Leonardo's Mona Lisa panel painting was measured and calculated by numerical modelling using finite element method. From the calculated results risk analysis has been carried out. Execution of different parts of this work have mobilized several groups and have combined experimental measure and numerical modelling (J. Gril *et al.*, 2007, J. Gril *et al.*, 2006, P. Perré *et al.*, 2006, L. Uzielli *et al.*, 2006). These works are summaries in a book "*Au Coeur de la Joconde*" (J. P. Mohen et al., 2006).

This interdisciplinary approach promotes major changes in risk analysis of panel paintings. However, the precise numerical modelling of such problems required

complex multi-physic coupling between mechanics, thermal conductivity and water sorption and diffusion. Such methods have been successfully applied by different authors (J. Colmars, 2011, D. Dureisseix and B. Marcon, 2011, B. Marcon, 2009), including the time dependent behaviour of wood and the hydro-mechanical coupling (known as *mechanosorptive* behaviour). However, numerical modelling can achieve good predictions only if the material parameters are measured or determined adequately. The late cited works incorporate in their models the parameters of non-aged wood and non-aged paint.

1.2 About the thesis

1.2.1 Objectives & strategy

The first purpose of this PhD thesis is to determine which and how the mechanical and physical properties of wood and paint are modified by long aging time (several centuries) and if the aging could be obtained by accelerated methods using mild thermo-hydrous treatment. The second purpose is to simulate numerically and to analyse the behaviour of non-aged and old painted panels under ambient variations, and verify the modelling by experiments.

This research project includes the following objectives:

Objective N°1:

Investigation of the mechanical, physical and chemical deterioration of wood during aging.

To achieve this first objective, parameters of old wood samples such as Young's modulus, strength, diffusion coefficient, etc… have been quantified and compared with non-aged wood samples.

Objective N°2:

Investigation of the possibilities to accelerated the aging of wood and a typical medieval multi-layered paint by thermo-hydro treatments.

Two thermo-hydrous reactors have been designed and built to treat wood samples under controlled temperature, time, humidity and pressure. Next, the treated wood characteristic have been measured and compared with non-aged and naturally aged wood. Chemical analysis by FTIR (Fourier transform infrared spectroscopy), UVRR (Ultraviolet Resonance Raman spectroscopy) and XPS (X-ray photoelectron spectroscopy) has been carried out as well.

Accelerating aging treatments chambers have been built to thermally treat paint layers under controlled temperature, humidity and UV light exposure (done by the team from HKB). Permeability, stiffness and strength of the treated paint have been measured and compared with untreated ones. Moreover, chemical analysis by FTIR and GCMS (Gas chromatography mass spectrometry) has been carried out.

Objective N°3:

Definition and fitting of a law of wood aging.

The radial strength and the colour lightness of thermally aged wood have been fitted on a chemical kinetics law. This law is dependent upon the treatment time, temperature, pressure and relative humidity. Then, the law has been extrapolated to ambient condition to predict the radial strength and the colour lightness of old wood samples.

Objective N°4:

Investigation of the long term ambient variation effects on the mechanical behaviour of ancient panel paintings through the application of wood science and computational analysis (virtual experimentations).

A numerical model using finite element method has been developed to calculate the mechanical and hygroscopic behaviour of panel painting under RH variation. This model has been verified by experiments.

Objective N°5:

Case study on an old panel painting using the numerical model and the prediction of the wood aging law.

An old panel painting has been subjected to an RH step and its deformation has been measured by optical techniques. The result has been compared with the prediction of the numerical model and finally a stress analysis has been carried out.

1.2.2 Collaborations

The subjects of this project were multidisciplinary and have required the collaboration of research teams with different expertise. This project was conjointly investigated by 2 teams. A first one in *Bern University of Applied Science – Architecture, wood and Civil Engineering* (BUAS - AWCE) and in *University of Montpellier II - Laboratoire de mécanique et génie civil* (UM2 - LMGC). The second team was in *Bern University of Applied Science - Bern University of the Arts* (BUAS-BUA).

1.2.3 Structure of the report

To present and detail the works done during this PhD thesis, this report is divided in the following 7 chapters:

Chapter 1 gives the introduction.

Chapter 2 summaries the wood behaviour and describes the development of the experimental procedures and methods used in the following chapters. The hygroscopic and mechanical behaviour of wood is presented, including some numerical tools that have been used in the experimental and numerical investigation. Then, the experimental development, machines and procedures are described. Mechanical testing using a micro-tensile device is detailed. The microscopes with their respective sampling are shown. Finally, the development of the isothermal sorption chambers used to determine the hygroscopic parameters of wood and paint layers are detailed.

Chapter 3 investigates the wood aging. A first part recapitulates the aging of wood in terms of physical, chemical and mechanical behaviour. Then, the potential of mild thermo-hydrous treatments to accelerate the aging of wood is investigated and finally the results from the thermo-hydrous treatments have been extrapolated in a law of wood aging.

Chapter 4 investigates the behaviour of multi-layered paint aging. The first part defines the selected typical medieval multi-layered paint and then the accelerated aging treatment that have been developed. Finally, the chemical, physical and mechanical behaviour of the different components of the multi-layered paint have been measured.

Chapter 5 explains the numerical model that has been developed for the simulation of wooden panel paintings under varying relative humidity conditions. The first section presents the model and then the experimental procedures which have been used for confirming the model. Finally, the comparison between experiments and numerical simulation are shown and analysed.

Chapter 6 investigates an old panel painting with the numerical model. The first part describes the characterisation of the old panel painting and next a stresses analysis has been carried out by taking into account the modification of the wood properties due to aging.

Chapter 7 gives the general conclusion and the future developments of these works.

1.3 References

ACIDINI, A., CIATTI, M., BONSANTI, G., FROSININI, C., UZIELLI, L., CASTELLI, C. & SANTACESARIA, A. 2006. *Panel Painting - Technique and conservation of wood supports*, EDIFIR - Edizioni Firenze.

COLMARS, J. 2011. *Hygromécanique du matériau bois appliquée à la conservation du patrimoine culturel : Etude sur la courbure des panneaux peints.* PhD, Université de Montpellier 2 (UM2).

DUREISSEIX, D. & MARCON, B. 2011. A partitioning strategy for the coupled hygromechanical analysis with application to wood structures of cultural heritage. *International Journal for Numerical Methods in Engineering,* 88**,** 228-256.

GRIL, J., RAVAUD, E., UZIELLI, L., DUPRÉ, J. C., PERRÉ, P., DUREISSEIX, D., ARNOULD, O., VICI, D. P., JAUNARD, D. & MANDRON, P. 2007. Le cas de la Joconde : modélisation mécanique de l'action du châssis-cadre. *Actes de la journée d'étude Conserver aujourd'hui : les vieillissements du bois.* Cité de la Musique, Paris, France.

GRIL, J., RAVAUD, E., UZIELLI, L., DUPRÉ, J. C., PERRÉ, P., DUREISSEIX, D., ARNOULD, O., VICI, P. D., JAUNARD, D. & MANDRON, P. Mona Lisa saved by the Griffith theory: Assessing the crack propagation risk in the wooden support of a panel painting. International Conference on Integrated Approach to Wood Structure, Behavior and Applications, ESWM and COST Action E35, May 2006 Florence (Italy).

MARCON, B. 2009. *Hygromécanique des panneaux en bois et conservation du patrimoine culturel : des pathologies...aux outils pour la conservation.* PhD, Université Montpellier 2 - Università degli studi di Firenze.

MECKLENBURG, M. F., TUMOSA, C. & ERHARDT, D. Structural Response of Painted Wood Surfaces to Changes in Ambient Relative Humidity. Painted Wood: History and Conservation, 1998. Los Angeles: Getty Conservation Institute, 464-484.

MECKLENBURG, M. F. & TUMOSA, C. S. Mechanical behavior of paintings subjected to changes in temperature and relative humidity. *In:* MECKLENBURG, M. F., ed. Art in transit: studies in the transport of paintings, 1991. NATL GALLERY ART, 173-216.

MOHEN, J. P., MENU, M. & MOTTIN, B. 2006. *Au coeur de La Joconde: Léonard de Vinci décodé - Centre de recherche et de restauration des musées de France,* Gallimard.

PERRÉ, P., RÉMOND, R. & GRIL, J. La simulation des effets de variation de l'ambiance. *In:* MOHEN, J. P., MENU, M. & MOTTIN, B., eds. Au coeur de la Joconde: Léonard de Vinci décodé, 2006. Paris: Gallimard / Musée du Louvre, 53-55.

UZIELLI, L., DIONISI VICI, P. & GRIL, J. Caractérisation physico-mécanique du support. *In:* MOHEN, J. P., MENU, M. & MOTTIN, B., eds. Au coeur de la Joconde: Léonard de Vinci décodé, 2006. Paris: Gallimard / Musée du Louvre, 52-53.

Chapter 2
Development of experimental procedures

Studying of wood and paint aging has required experimental and numerical tools. In this chapter, the wood behaviour is briefly summarised and some common numerical tools are presented. Finally, the developments of the experimental procedures are described.

2.1 Summary of wood hygroscopic behaviour

Wood is a *hygroscopic* material (it absorbs or desorbs water). It reaches an *equilibrium moisture content* (EMC) with the relative humidity (RH) of the surrounding atmosphere. The wood *moisture content* (MC) affects almost every properties of wood and induces swelling or shrinkage, known as *hygroexpansion*. The MC can vary highly during the use of wood. Indeed, the RH can vary within a quite big range of 10 to 80% for indoor conditions in the absence of climate control. The worst case can appear in winter, when the air becomes particularly dry due to the heating.

The understanding of the absorption/desorption and also the motion of water inside wood are important for this study on panel paintings. Indeed, the fluctuation of the MC induces mechanical stress in the wood as well as in the paint layer. This section will summarise the basis of wood-water relations and the common models that has been used during this investigation.

2.1.1 Water in wood

The definition of the wood moisture content m is the relative mass variation from the anhydrous state:

$$m = \frac{w_m - w_0}{w_0} \tag{2-1}$$

where w_0 and w_m are the mass of wood in the anhydrous state (oven dry-mass) and in the wet state respectively. The quantity of water in wood ($w_m - w_0$) is strongly dependent on the thermodynamic variables such as pressure, temperature (T) and, especially, relative humidity (RH).

Water can be found in four different forms in wood: as free water in the ice, liquid or vapour state and as bound water (hydrogen bonding). The enthalpy of liquid free water in wood is a little less than the enthalpy of normal water (J. F. Siau, 1984). This comes from capillarity forces which reduce the energy of the liquid free water. Therefore, water tends to be absorbed in wood in order to minimize its free energy. The enthalpy of bound water is less than the free water enthalpy but it depends on the MC level. At a certain moisture concentration in wood, the enthalpy of bound water is equal to the enthalpy of liquid free water. This point is called: *Fibre Saturation Point* (FSP). At FSP, no additional water can be bounded inside wood components. All the sorption sites are saturated. Therefore, in theory, only above the FSP does free water appear. FSP is reached at 100% RH.

The level of moisture content of the FSP depends on temperature and wood species. However, as an example, the works of Burmester can be cited (A. Burmester, 1978). He found that the exposure (Nord, East, South, West) within a same tree induces dissimilar wood FSP. E. Zürcher *et al.* show sensitivity on sorption parameters against the date of cutting are more specifically the Moon phases (E. Zürcher *et al.*, 2012).

It can be seen with these examples, how the wood-water relations are sensitive. The following models represent only a simplified version of these relations.

2.1.2 Absorption and desorption of water

The absorption or desorption of water occurs in wood to attain an equilibrium (EMC) with the external conditions, characterized by RH and temperature. The relationship between MC and RH for a given temperature is called *sorption isotherm*. The sorption isotherms exist in 8 different shapes, but only three of them are applicable to wood-water relation (C. Skaar, 1988). Type I corresponds to a simple sorption isotherm when only one layer of molecules is absorbed on the substrate (figure 2.1). Type III corresponds to multi-molecular absorbed layers. The wood sorption isotherm is the type II with a sigmoid shape, which is a mix between type I and III. Sorption isotherms are temperature dependent and a hysteresis is observed between absorption and desorption.

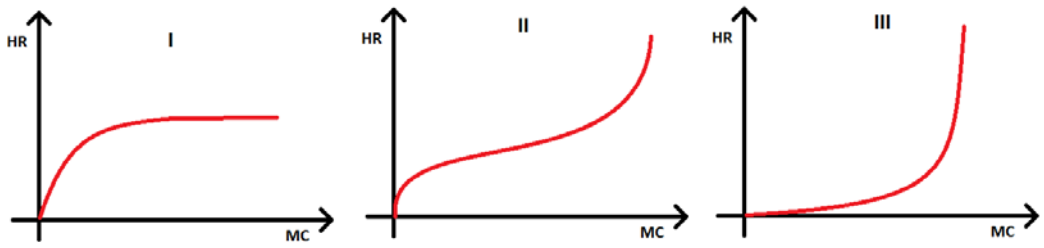

Figure 2.1: Schematic representation of the three types of sorption isotherm. Type II corresponds to wood-water relation.

Models of the sorption isotherm

More than 77 equations exist in the literature for describing the isotherm of sorption of hygroscopic materials (C. Skaar, 1988). These equations have been classified into four categories: Monolayer sorption models, multilayer models, empirical and semi-empirical models. All these equations can be mathematically written in a parabolic form. The BET model (Brunauer - Emmett - Teller) is the most used one and it has been selected during my master works (J. Froidevaux, 2009). BET model is written, in the parabolic form, as:

$$\frac{h}{m} = A + Bh + Ch^2 \tag{2-2}$$

with h the RH and m the wood EMC. A, B and C are parameters depending on the wood species and on the temperature.

F. Heger in his thesis proposes an extension of the BET model that takes into account the temperature exceeding 100°C (F. Heger, 2004). He fit the parameters of the BET model using an Arrhenius relation. The extended model becomes:

$$m(h,T) = \frac{c_1 c_2 h e^{(c_2+c_4)/RT}}{[1 + h(c_3 e^{c_4/RT} - c_5 e^{c_6/RT})](1 - h c_5 e^{c_6/RT})} \tag{2-3}$$

The six parameters c_i of this model are tabulated in table 2.1.

Table 2.1: Parameters of the extended BET model for spruce wood by (F. Heger, 2004).

c_1	$4.023 \cdot 10^{-3}$
c_2	$6.703 \cdot 10^{3}$
c_3	$4.075 \cdot 10^{-1}$
c_4	$7.819 \cdot 10^{3}$
c_5	$9.756 \cdot 10^{3}$
c_6	$-4.816 \cdot 10^{2}$

2.1.3 Water movement inside wood

Water can move through wood by fluid flows in case of liquid free water or by diffusion for bound water and free vapour. As free water appears only above FSP, only the diffusion process will be taken into account in this study. Moreover, it is commonly assumed that a single diffusivity coefficient can be used for both bound water and vapour (J. F. Siau, 1984).

Steady-state diffusion can be described by Fick's first law:

$$J = -D \cdot \nabla c(\vec{r}) \tag{2-4}$$

where J is the steady flux of moisture, D the diffusion coefficient and c the moisture concentration depending on space $\vec{r} = (x; y; z)$. Concerning transient diffusion, the second Fick's law has to be used:

$$\frac{\partial c(\vec{r},t)}{\partial t} = -\frac{\partial}{\partial \vec{r}}\left(D(c,T) \cdot \frac{\partial c(\vec{r},t)}{\partial \vec{r}} \right) \tag{2-5}$$

The diffusion coefficient D depends on the MC and on the temperature. The moisture concentration $c(r,t)$ is not a common variable to describe the water in wood. The moisture content $m(r,t)$ as defined by (2-1) is a more appropriate variable. Therefore, a variable change is made: $c(\vec{r},t) = m(\vec{r},t) \cdot G\rho_w / 100$, where G is the specific gravity of wood and ρ_w is the density of water. In order to keep only one constant value, the diffusivity coefficient D_m is defined as:

$$D_m(m,T) = \frac{G\rho_w D(c,T)}{100} \tag{2-6}$$

Finally the second Fick's law for wood moisture content takes the form:

$$\frac{\partial m(\vec{r},t)}{\partial t} = -\frac{\partial}{\partial \vec{r}}\left(D_m(c,T) \cdot \frac{\partial m(\vec{r},t)}{\partial \vec{r}} \right) \tag{2-7}$$

2.2 Wood mechanical behaviour

Wood can be seen as a continuous, cellular or fibrous material depending on the scale of observation. In this study, wood will be assumed to be a continuum medium. Therefore, the continuum mechanics will be applied to model the mechanical behaviour of wood.

By neglecting the volume forces (mainly gravity) and the material inertia, the local conservation equation of momentum becomes:

$$\mathbf{div}\,\boldsymbol{\sigma} = 0 \tag{2-8}$$

where $\boldsymbol{\sigma}$ is the stress tensor, containing 6 independent variables for three equations. In order to resolve this equation, constitutive equations that link the stress with the deformation have to be incorporated.

2.2.1 Constitutive equations for linear elasticity

The linear elastic strain is defined by the Hook's law:

$$\varepsilon_{ij} = C_{ijkl}\sigma_{kl} \tag{2-9}$$

with σ_{ij} the stress tensor, ε_{kl} the strain tensor and C_{ijkl} the compliance tensor. Wood is an orthotropic material. Therefore the compliance is described by 9 independent variables, which makes in the matrix notation (P. Navi and F. Heger, 2005, P. Navi and D. Sandberg, 2012):

$$C = \begin{pmatrix} \frac{1}{E_r} & \frac{-\upsilon_{tr}}{E_t} & \frac{-\upsilon_{lr}}{E_l} & 0 & 0 & 0 \\ \frac{-\upsilon_{rt}}{E_r} & \frac{1}{E_t} & \frac{-\upsilon_{lt}}{E_l} & 0 & 0 & 0 \\ \frac{-\upsilon_{rl}}{E_r} & \frac{-\upsilon_{tl}}{E_t} & \frac{1}{E_l} & 0 & 0 & 0 \\ 0 & 0 & 0 & \frac{1}{G_{tl}} & 0 & 0 \\ 0 & 0 & 0 & 0 & \frac{1}{G_{rl}} & 0 \\ 0 & 0 & 0 & 0 & 0 & \frac{1}{G_{tr}} \end{pmatrix} \tag{2-10}$$

E_i, G_{ij} and υ_{ij} are respectively the Young's modulus, the Poisson's ratio and shear's modulus. The compliance matrix has to be symmetric, hence:

$$\begin{cases} \upsilon_{rt} &= \dfrac{\upsilon_{tr}E_r}{E_t} \\ \upsilon_{rl} &= \dfrac{\upsilon_{lr}E_r}{E_l} \\ \upsilon_{tl} &= \dfrac{\upsilon_{lt}E_t}{E_l} \end{cases} \tag{2-11}$$

Finally, 9 parameters have to be identified to completely represent the elastic behaviour of wood. The stresses can be calculated by inversing the compliance matrix

$$\sigma_{ij} = D_{ijkl}\varepsilon_{kl} \tag{2-12}$$

with $D = C^{-1}$. Each Young's and shear modulus is temperature and MC dependent. This dependency can be linearly fit on experimental data (S. Ormarsson, 1999, S. Ormarsson *et al.*, 1998):

$$Z_i(m,T) = Z_{i,0}\left(1 + Z_{i,T}\left(T - T_0\right) + Z_{i,m}\left(m_f - m\right)\right) \tag{2-13}$$

where Z_i represent Young's modulus and shear modulus, $Z_{i,0}$ are the reference values at the reference temperature T_0 and at the fibres saturation moisture content m_f. The variation of Z_i with respect to the temperature is given by $Z_{i,T}$ and to the moisture content by $Z_{i,m}$.

2.2.2 Hygroexpansion

In the simplest formulation, the total strain of wood is composed of the elastic strain and the free shrinkage or swelling, known as hygroexpansion ε_m:

$$\varepsilon = \varepsilon_{el} + \varepsilon_m \tag{2-14}$$

so that the generalized Hook's law in equation (2-9) becomes:

$$\sigma_{ij} = D_{ijkl}\left(\varepsilon_{kl} - \varepsilon_{kl,m}\right) \tag{2-15}$$

The hygroexpansion is defined as:

$$\varepsilon_{ij,m} = \alpha_{ij}\left(m - m_0\right) \tag{2-16}$$

with:

$$\alpha = \begin{bmatrix}\alpha_r & \alpha_t & \alpha_l & 0 & 0 & 0\end{bmatrix}^T \tag{2-17}$$

α_{ij} are the material coefficients of hygroexpansion. These parameters describe the relative strain induced by an MC variation from 0 to FSP.

2.2.3 Time-dependent behaviour

Wood exhibits a time-dependent behaviour: it is a viscoelastic material. Hooke's law can be extended to take into account the time dependency under constant climate (P. Navi and D. Sandberg, 2012). For example, creep and relaxation constitutive equations are the following:

$$\begin{cases}\sigma_{ij}(t) = R_{ijkl}(t)\varepsilon_0 \\ \varepsilon_{ij}(t) = J_{ijkl}(t)\sigma_0\end{cases} \tag{2-18}$$

with ε_0 and σ_0 the constant strain and stress during the relaxation and creep tests, respectively. J and R are tensors of forth order and are respectively the viscoelastic compliance and the relaxation functions. In order to generalize to all loading condition, the Boltzmann principle is applied: the response of some solicitations is equal to the sums of the responses of each individual solicitation. This leads to the heredity equation:

$$\varepsilon_{ij}(t) = \int_0^t J_{ijkl}(t-\tau) \cdot \frac{d\sigma_{kl}}{d\tau} d\tau \tag{2-19}$$

The heredity equation requires to know and to sum all the stresses history of the system.

Rheological models

Viscoelastic materials can be modelled using rheological models. In these models, viscoelastic behaviour is seen as linear combinations of elastic and viscous components represented by springs and dashpots, respectively (figure 2.2). Each model differs in the arrangement of these elements. The two simplest combinations can be seen in figure 2.3: the *Maxwell* model where one spring is connected in series with a dashpot, and the *Kelvin-Voigt* model where a spring is connected in parallel with a dashpot.

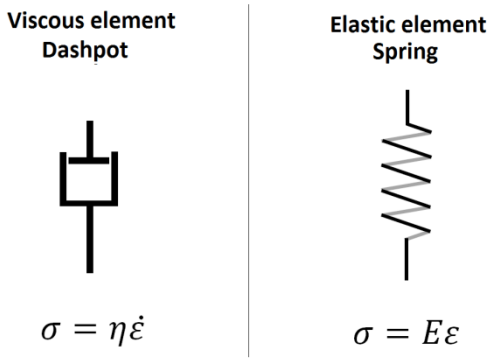

Figure 2.2: Rheological elements used to represent the viscoelastic behaviour. The spring and the dashpot correspond to an elastic and viscous behaviour, respectively, with E the Young's modulus and η the viscosity.

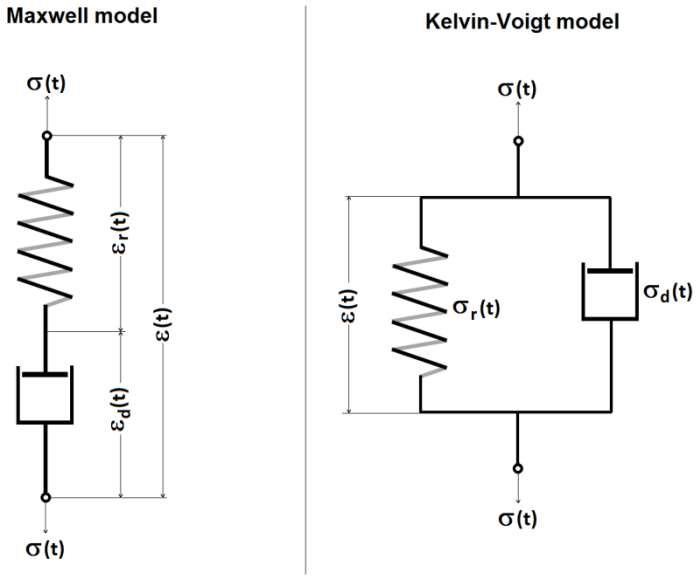

Figure 2.3: Maxwell and Kelvin-Voigt rheological models.

Maxwell element is suitable for stress relaxation simulation but not for creep. On the other hand, Kelvin-Voigt model is suitable for creep simulation but not for relaxation. The *Generalized Maxwell Model (GMM)*, an assembling of multiple Maxwell elements in parallel with one spring in parallel as presented in figure 2.4, is able to model both creep and relaxation. It takes into account the relaxation occurring not around a single time, but along a large distribution of times.

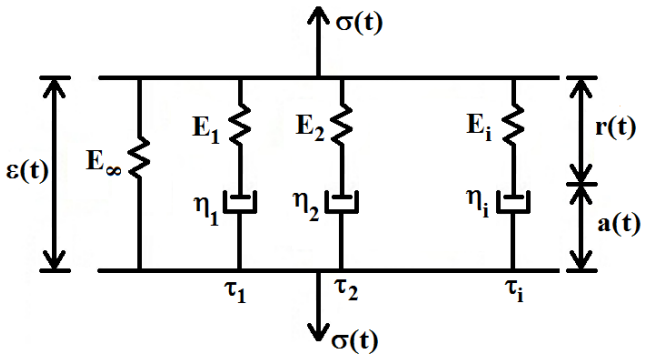

Figure 2.4: Rheological Generalized Maxwell model.

Solving - Generalised Maxwell model

The stresses in the GMM are the sum of all parallel branches stresses:

$$\sigma(t) = E_{\infty}\varepsilon(t) + \sum_{i=1}^{N}\sigma_i \qquad (2\text{-}20)$$

where N is the number of Maxwell elements put in parallel in the GMM. In a Maxwell element, due to the serial assembling, the stresses in the spring $\sigma_{r,i}(t)$ and in

the dashpot $\sigma_{d,i}(t)$ are equal. Therefore the total strain rate $\dot{\varepsilon}(t)$ in a Maxwell element is the sum of the spring $\dot{r}_i(t)$ and the dashpot $\dot{a}_i(t)$ strain rates:

$$\dot{\varepsilon}(t) = \frac{\dot{\sigma}_i(t)}{E_i} + \frac{\sigma_i(t)}{\eta_i} \tag{2-21}$$

where E_i and η_i are the Young modulus of the spring and the viscosity of the dashpot, respectively. For example, in case of a relaxation test, the strain rate is zero, therefore the stresses in one branch *i* becomes:

$$\sigma_i(t) = \varepsilon_0 e^{-\frac{t}{\tau_i}} \tag{2-22}$$

with $\tau_i = E_i / \eta_i$ the relaxation time of the branch *i*. The resolution of equation (2-21) for the general case and creep case required numerical time integration. This numerical solving is presented in chapter 5.

2.2.4 Hygro-mechanical couplings: mechanosorption

The previous chapter takes into consideration the creep behaviour of wood under constant MC. Coupling between the moisture changes and mechanical loading appears in wood and is known as *mechanosorption.* Figure 2.5 highlights this behaviour. Many works has been carried out on observation of this behaviour (J. Gril, 1988, P. Grossman, 1976, D. Hunt, 1982, V. Pittet, 1996, P. Navi *et al.*, 2002, A. Ranta-Maunus, 1975, T. Toratti and S. Svensson, 2000). However, the phenomenon is still not well understood and its modelling is still challenging.

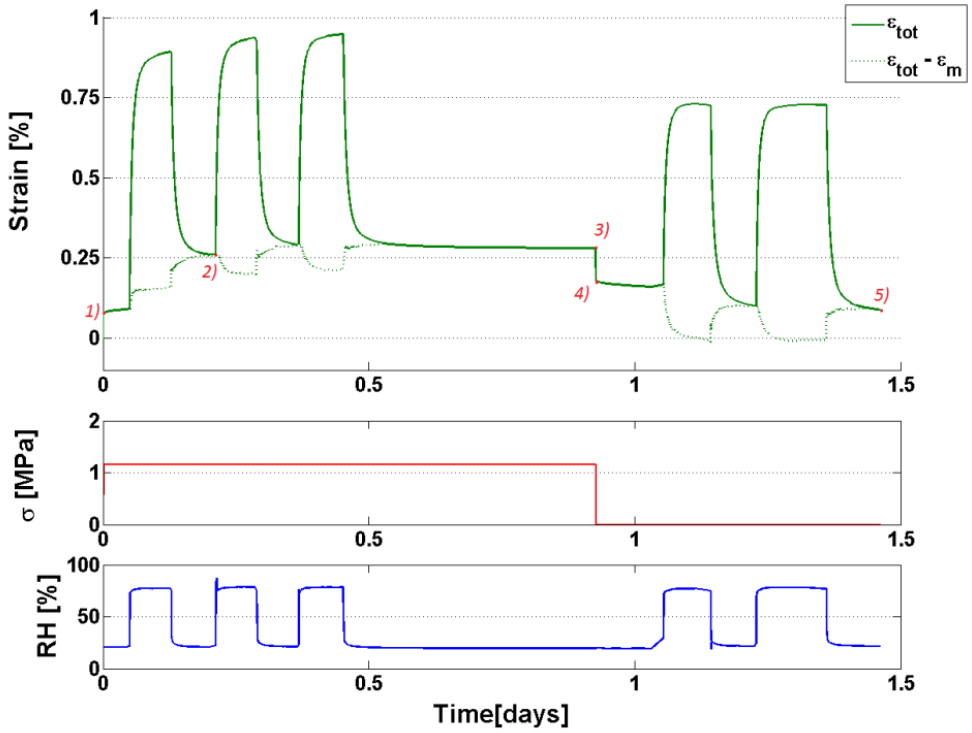

Figure 2.5: Highlighting of the mechanosorptive behaviour of wood. A stress of 1.2 MPa is applied during about 1 day (red) and RH cycles (blue) are imposed during the loading and unloading phases. The total strain is shown by the full line (green) and the dashed line shows the same strain where the free hygroexpansion has been removed. At position N°4, the stress level is the same as the initial condition; the remaining strain is the mechanosorptive and viscoelastic strain.

On the other hand, the mechanical loading can influence the sorption behaviour of wood (A. Negi, 1999). A compressive load reduces the sorption of water and a tensile load increase the sorption. Finally, thermal coupling occurs as well and at each level:

- Thermo-hydrous coupling - Influence of the temperature on the water sorption and diffusion. Influence of MC on temperature: MC dependency of the heat capacity and thermal conductivity. Heating and cooling due to absorption desorption of water.
- Thermo-mechanical coupling - Thermal dilatation and thermal activation of creep. Heating due to mechanical work.
- Thermo-hygro-mechanical coupling - Influence of the temperature on the mechanosorptive behaviour).

2.2.5 Local coordinate system

The constitutive equations described in the previous sections are defined in the local coordinate system of wood. This local coordinate system is represented in figure 2.6. It is composed of the three main direction of wood *RTL*: radial, tangential and longitudinal. The transformation from the global *XYZ* coordinate system is done by the following rotation of the local coordinate system:

- Rotation around the *z* axis to turn the *X* and *Y* axis in the direction of *R* and *T*.
- Rotation around the tangential axis *T* for taking into account of the conical angle of the trunk of the tree.
- Rotation around the radial axis *R* for taking into account the spiral grain angle of the tree rings.
- Rotation around the *R* and *T* axis for a plank which has been cut not parallel to the fibres direction.

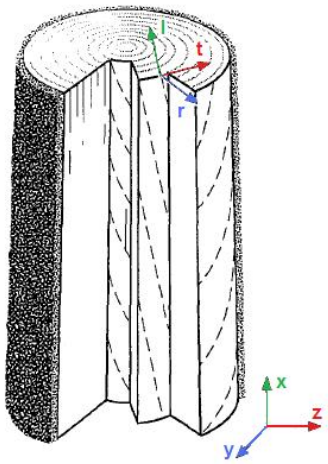

Figure 2.6: Representation of the local RTL and global XYZ coordinate system.

2.3 Mechanical testing

This section describes all the mechanical testing procedures used during this study. The sub-sections 1 to 3 show the micro-mechanical testing. In sub-section 1, the equipment is described; in sub-section 2 the sample preparation is explained and sub-section 3 describes the different testing procedures that have been carried out. Finally, sub-section 4 describes the longitudinal tensile tests.

2.3.1 Micro-mechanical tensile device

The equipment used in this study for the micro-mechanical characterisation was developed at EPFL (*Swiss Institute of Technology, Lausanne)* and was used by V. Pittet in her investigation of transient moisture effects in wood (V. Pittet, 1996, P.

Navi et al., 2002). This device consists of two units: the mechanical testing part and the climatic control unit such as can be seen in figure 2.8. Both T and RH can be precisely controlled during the test. The mechanical testing device is a horizontal testing machine with 500 N load capacity. The machine can operate under force or deformation control. The deformation is measured with an inductive extensometer of 20.2 mm length mechanically fixed to the samples with two springs as shown in figure 2.7.

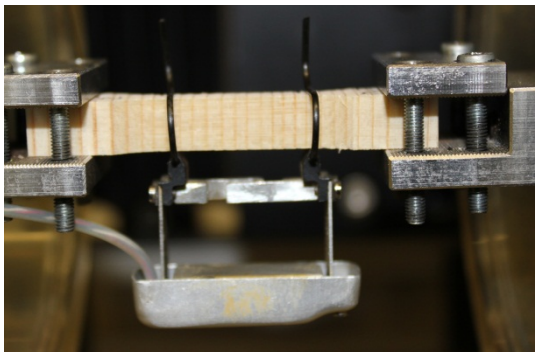

Figure 2.7: Inductive extensometer used to measure the deformation of the samples.

The second unit comprises all devices of the climatic control system. A cylindrical hygro-thermal cell of *20 cm* long and *8 cm* of diameter surrounds the sample fixed in the testing machine. The walls of this cell are made of double-layered Plexiglas. The temperature inside the cell is kept constant by running water through the cell walls. The water temperature is regulated with a thermostatic bath and the relative humidity is controlled by mixing dried and wet air. Dry air comes from the air pressure system of the building and has about 6–7% RH. The wet air is produced with a cylinder filled with water. The back of this cylinder is made of a ceramic foam which is permeable to the air and impermeable to water. By injecting dried air at the back through the ceramic and next through the water, the air output on the top is saturated with water at 97–98% RH. The humidified air is pre-heated, in order to avoid local condensation, and conveyed into the Plexiglas testing chamber.

2.3.2 Samples preparation

Two kinds of samples have been prepared during this study. Firstly, due to the limited amount of naturally aged wood available, micro-samples were made. Next, more representative samples were made for the testing of the thermally aged.

2.3.2.1 Micro-samples

The advantage to work along the radial direction is that the representative cross section (L x T) is about *2 x 0.1* mm. Therefore, relatively small samples can be

tested. These samples are particularly welcome for naturally aged wood where the amount of wood was limited.

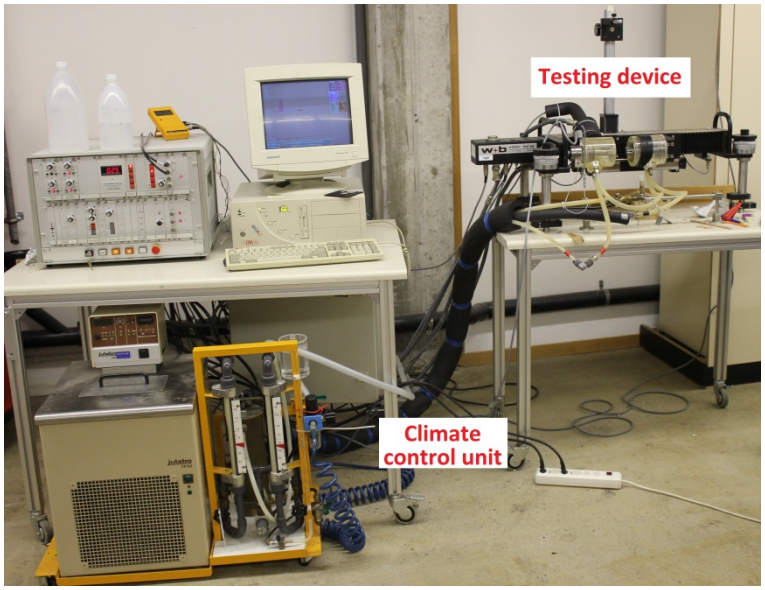

Figure 2.8: Picture of the micro-tensile testing device.

Samples of *3x3* mm of cross section were prepared. The preparation consisted of the following steps as presented in figure 2.9(a): the wood samples were cut into small square rods with dimensions *50x3x3* mm (R x T x L). Next, the rods were put into a silicone mould and the two ends of the rods were reinforced with an epoxy resin to avoid any damage due to fixing in the clamps of the testing device. The silicone moulds were made with a metal mould as shown in figure 2.9(b).

(a) (b) (c)

Figure 2.9: (a) Micro-samples preparation: reinforcement of the tops in silicone mould using epoxy resin. (b) Metallic mould used to prepare the silicone mould. (c) Standard samples.

2.3.2.2 Standard samples

A second type of sampling was done for the accelerated aging tests. Standard shape samples were produced with a section of about *50x6x8* mm (R x T x L) as shown in figure 2.9(c).

The production of these samples was done according to the following steps: First wood planks of *50x8* mm (R x T) were cut and planed. Next, the planks were moulded in order to reduce the section in the centre of the planks. Finally, the planks were cut across the fibres in pieces 8 mm long.

2.3.3 Mechanical tests

2.3.3.1 Samples conditioning

All mechanical tests carried out with the micro-tensile device, where done under controlled climate condition. Due to the relative small size of our samples, any variation of the RH induces strains and stresses. Therefore, all samples have been preconditioned before testing for at least 2 hours. This conditioning included the following steps: The samples were placed in the climate chambers of the testing device and stored for one night. Next, the sample were fixed in the clamps of the testing device. The climatic chamber was then closed and the loading program was run. The system maintained zero force on the samples so that the shrinkage or swelling could be followed. After 2 hours the sample was ready for testing.

2.3.3.2 Elastic and failure tests

First tests were done to determine the Young's modulus and the failure stress. These tests were done under force control with the following program (figure 2.10): The speed of the force increase was set at 0.5 N/s for the micro-samples (section *3x3 mm*) and at 2.5 N/s for standard shape samples (section *6x8 mm*). At these speeds, about two minutes are required to reach the failure stress. Two force cycles were done at respectively 12.5% and 25% of the failure stress. Therefore a mean of 4 Young's moduli can be calculated.

Finally, the extensometer was removed and the force increased up to rupture.

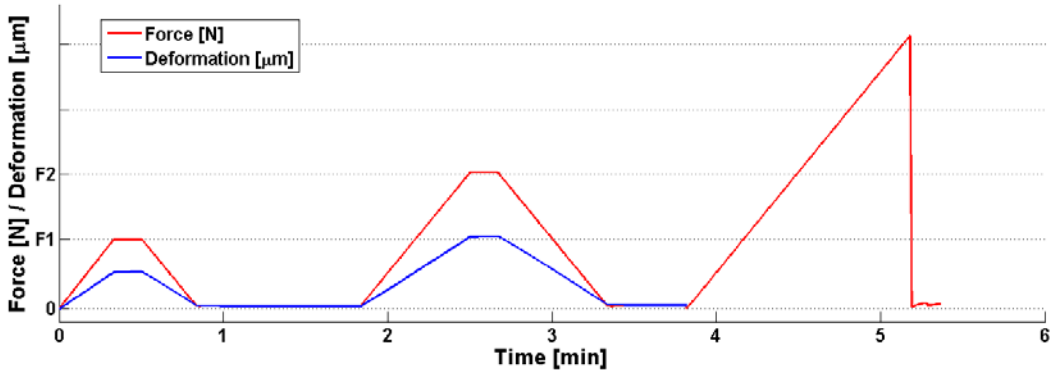

Figure 2.10: Elastic tests under load control in order to determine the Young's modulus and rupture stress.

2.3.3.3 Viscoelastic tests

The time-dependent behaviour of the wooden samples was determined with two different tests: creep test and relaxation tests. First, the EMC was controlled by maintaining the sample under zero force for at least 6 hours. Indeed, for such long test the hydrous stabilisation of the samples is capital. The creep-recovery tests were carried out at a constant stress of 1.6 MPa (~25% of the failure stress) as shown in figure 2.11. The load was maintained during two days. Next the loading was realised and the deformation recovery recorded during a half day.

The stress relaxation-erasing tests were performed at a constant deformation of 0.25% as shown in figure 2.11. The deformation was maintained during two days. Afterwards the deformation was run to zero and the load erasing was recorded during a half day.

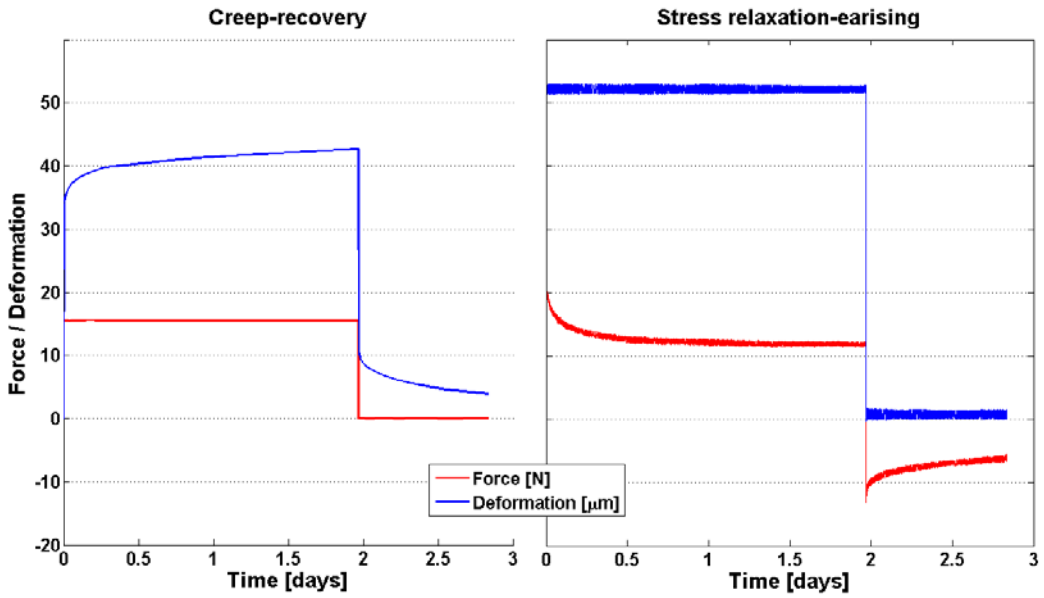

Figure 2.11: Creep-recovery and stress relaxation-erasing tests program.

Data processing

The creep and even more the relaxation curves show small fluctuation as shown in figure 2.11. Therefore some data processing was done to better represent these curves. First, a smoothing was applied using a local second-order polynomial interpolation. Then, in order to compare different samples, relative values were calculated:

$$\varepsilon_{VS} = \frac{\varepsilon - \varepsilon_{El}}{\varepsilon_{El}}$$
$$\sigma_{VS} = \frac{\sigma - \sigma_{El}}{\sigma_{El}} \qquad (2\text{-}23)$$

where σ_{VS} and ε_{VS} are the relative stress relaxation and relative creep, respectively, and σ_{El} and ε_{El} are the instantaneous elastic stress and strain, respectively. Finally, the results were plotted against log time.

2.3.3.4 Mechanosorption tests

Tests under varying climate conditions were carried out to compare the mechanosorptive behaviour between different samples. These tests were performed as follows: First, the samples were equilibrated at the starting EMC m_1 during one night. Then, in order to quantify the free shrinkage and swelling of the samples, zero force was maintained and 3 humidity cycles from m_1 to m_2 were applied. Next, as shown in figure 2.12, a stress of 1.2 MPa (~20% of the failure stress) was applied to the samples and the same three humidity cycles were repeated. After these humidity cycles, the force was unloaded totally and two further humidity cycles were imposed in order to quantify the strain recovery.

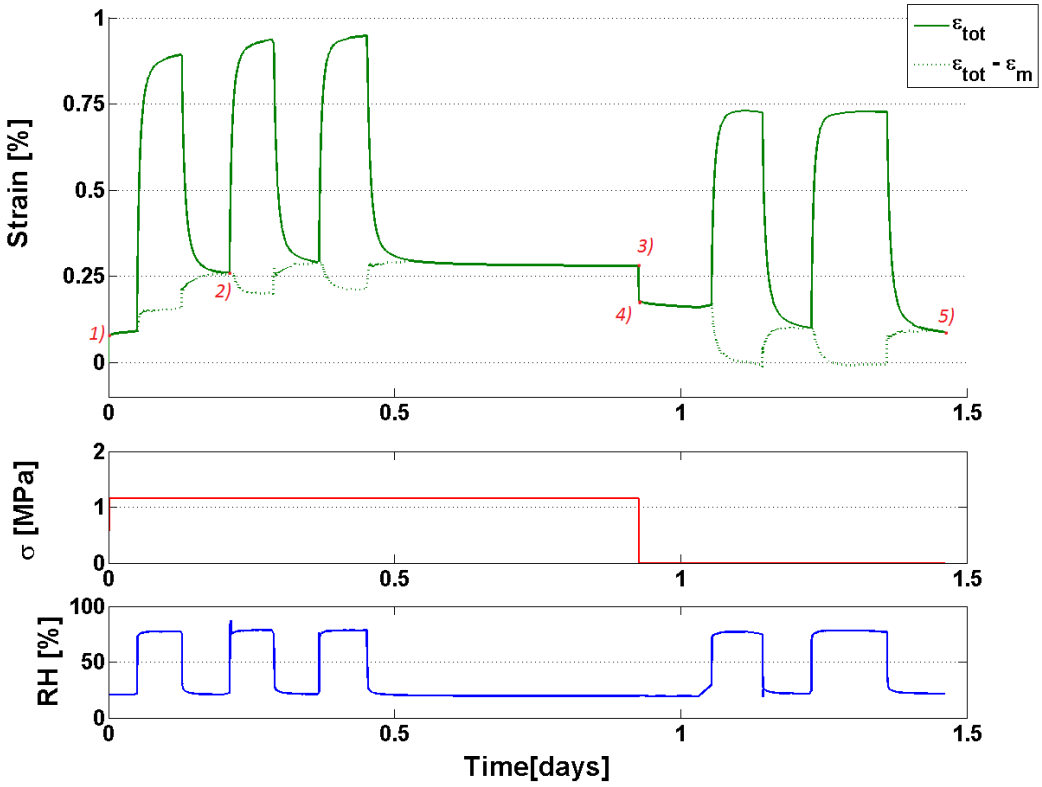

Figure 2.12: Mechanosorption tests program. A stress of 1.2 MPa is applied during about 1 day (red) and RH cycles are imposed during the loading and unloaded phases. The first graph shows with the full line the total recorded strain and the dashed line show the same strain where the free hygral swelling/shrinkage has been removed.

Data processing

As the objective of the study was to compare the mechanosorptive behaviour between different ages of wood, no specific fitting on mechanosorption models has been carried out.

The free swelling or shrinkage has been removed from the total strain as shown in figure 2.12. The following values have been extracted and compared:

1) ε_0 : Elastic strain.
2) $\varepsilon_{ms,c1}$: Strain after one humidity cycle.
3) $\varepsilon_{ms,c3}$: Strain after three humidity cycles.
4) ε_{ms}: Mechanosorption strain after total unloading (stress and RH).
5) $\varepsilon_{ms,irr}$: Remaining irreversible mechanosorption strain.

2.3.4 Longitudinal tensile testing

Some longitudinal tensile testing has been carried out on thermally aged wood samples. Standard-shape sample were produced following the same procedure as the micro-samples described in section 2.3.2.2. The section of the samples was *10x8 mm* and their length was *80 mm*.

The test was carried out on a universal tensile testing device Zwick/Roell Z050 of 50kN of load capacity. The room climate was regulated at 23°C and 50% RH. In order to determine the longitudinal Young's modulus, the deformation was measured optically with a video extensometer: Zwick/Roell videoXtens 5.26.0.0. The device was set under load control at a speed of 50 N/s. Two load cycles were imposed to the sample up to 2'000 N.

To determine the failure stress of the samples, the central zone of the samples were reduced to a section of *5x4 mm*. Next, the tensile device was set under displacement control and a speed of 4 mm/min was used up to failure.

2.4 Isothermal sorption chambers

Isothermal sorption chambers (ISC) have been developed and constructed to identify the sorption and diffusion parameters of wood samples. The following sub-sections show the structure and principles of the system. Next the measurement procedure is shown and finally the data processing is described.

2.4.1 System description

The entire ISC is composed of five chambers: 3 conditioning chambers (CC) and 2 analysis chambers (AC). A sketch can be seen in figure 2.13 and pictures in figure 2.14.

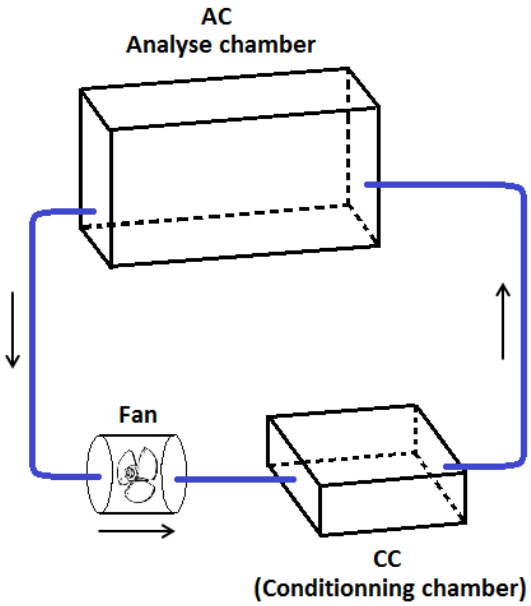

Figure 2.13: Sketch of the principle of the isothermal sorption chambers.

The principle of the system is the following: The air is conditioned at a targeted relative humidity (RH) in one of the CC using salt saturated solution. These chambers are made with an important surface in order to evaporate or condensate water quickly. In table 2.2, a list of salt saturated solution is shown with their respective RH at 20°C. Next, an air flux is created through the CC up to AC with a fan as shown in the sketch in figure 2.13. The fan is installed between AC and CC. A picture of the fan is shown in figure 2.16. The fan speed can be controlled with an electrical potentiometer. The air RH in AC will then tend to the RH of the CC. The AC are made with a minimal volume in order to be able to quickly change the RH.

Note: The RH is not the same in AC and in CC due to losses or the height difference between them. However, the RH is stable as shown in figure 2.17: The RH after the RH step is kept between 26.5% and 25.5% (during 14 days). The RH stabilisation takes about one day. However, after 15 min. the RH drops by 80% of the RH step. The stabilisation is perturbed by the water released by the wood samples.

Table 2.2: Salt saturated solutions and their corresponding relative humidity (J. Froidevaux, 2009).

HR en % à 20°C	Nom de la solution	Formule chimique	Concentration [g/100ml H_2O]		Toxicité
			20°	30°	
9	Hydroxyde de potassium	KOH	107(15°)	136 (40°)	2
12	Chlorure de lithium	LiCl H2O	111.86	120.42	3
22	Acétate de potassium	CH3 COOK	253	368.3 (50°)	5
33	Chlorure de magnésium	MgCl2 6H2O	116.4	-	5
44	Carbonate de potassium	K2CO3 2H2O	139.3	143.3	4
55	Nitrate de magnésium	Mg(NO3)2 6H2O	121.2	129.3	-
55	Dichromate de sodium	Na2Cr2O7 2H2O	204.8	223.75	3
66	Nitrite de sodium	NaNO2	84.5	91.6	2
76	Chlorure de sodium	NaCl	36	36.5	libre
81	Sulfate d'ammonium	(NH4)2 SO4	75.4	78	5
86	Chlorure de potassium	KCl	34	37	4
93	Nitrate de potassium	KNO3	31.6	45.8	4
97	Sulfate de potassium	K2SO4	11.11	12.97	-

This stabilisation can be achieved only if the temperature is stable as well. No control of the temperature has been designed. The stabilisation is done by installing the system in a location with slight variation of temperature. To avoid a slight and brief change in temperature, which can happen if a door or a window is opened for example, the system has been installed in an old freezer out of order. Indeed, a freezer is a well isolated box which minimizes the temperature variations.

The switching of the RH in the AC is done by connecting another CC in the air flux cycles. To record the RH and the temperature in the AC or also in CC, a logger can be placed in the chambers.

The samples are placed in the AC and they weights can be measured with a scale placed on the top of the AC as shown in figure 2.15. Hooks, made with iron wire, are attached to the samples. Next, the conveyor belt is rotated to bring the samples below the scales and next it is put down to hang the sample at the scales hook.

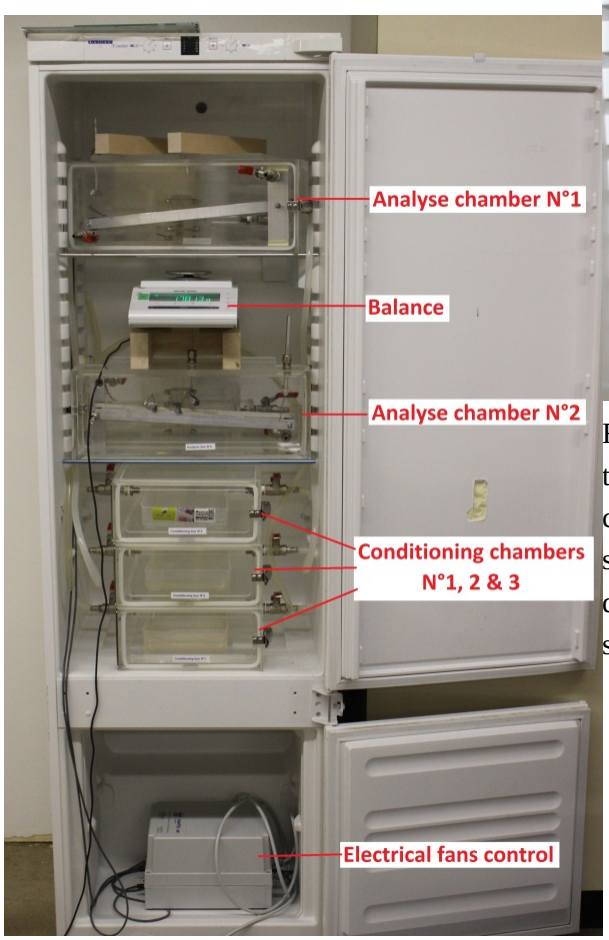

Figure 2.14: Picture of the sorption chambers. The overall system is placed in an old freezer in order to keep the temperature constant.

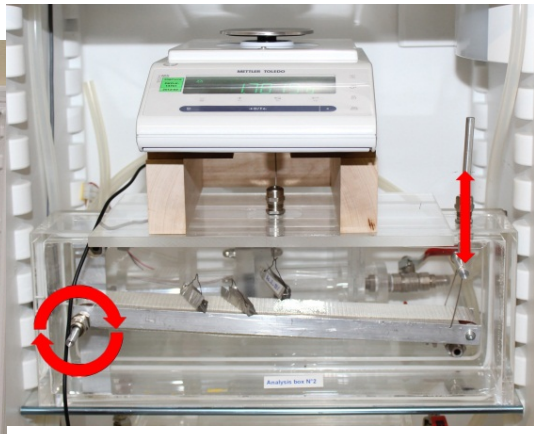

Figure 2.15: Conveyor belt used to place the samples below the scales. First the conveyor belt is rotated to bring the samples below the scales and next it is put down in order to hang the sample at the scales hook.

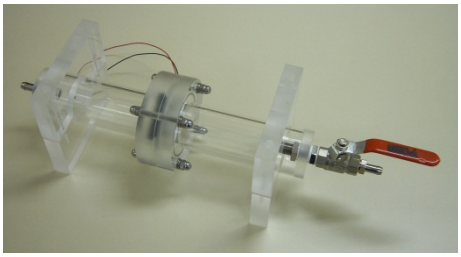

Figure 2.16: Picture of the fan placed between AC and CC.

2.4.2 Experimental procedure

2.4.2.1 Samples preparation

Samples have been designed to determine the diffusivity coefficient of massive wood along one of the principal wood direction as shown in figure 2.18. The thickness of the sample was set at 10 mm to avoid size effect (A. Pfriem *et al.*, 2010). A hook of iron wire is attached to the samples in order to be able to hang them with the balance hook. Moreover, the other faces are sealed from water sorption to ensure a unidirectional diffusion. The surface of the samples as well as the mass of the metal wire and sealing aluminium tape were determined prior to the experiments.

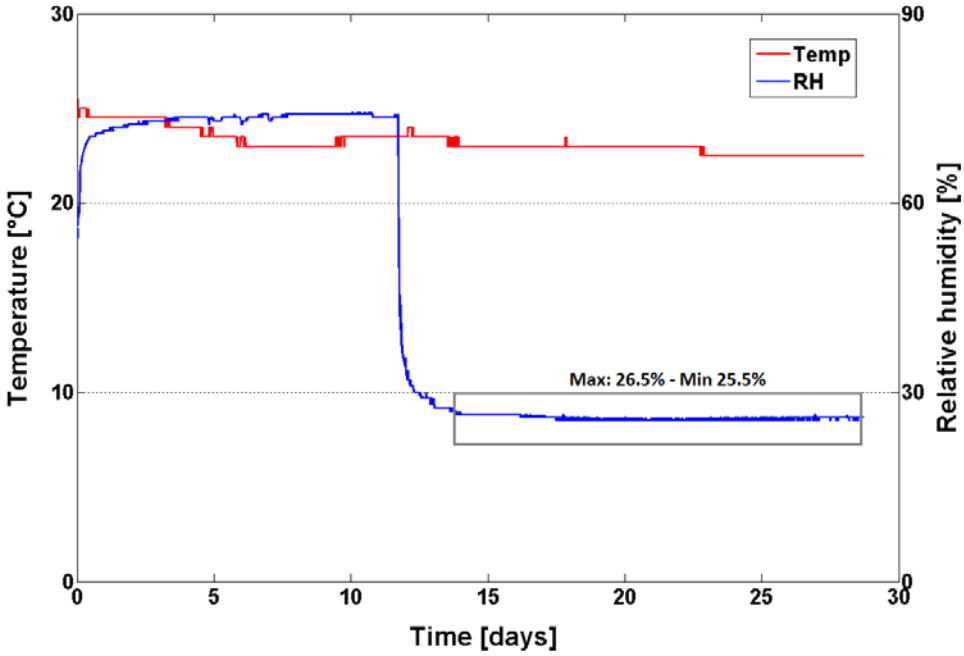

Figure 2.17: RH and temperature inside an analyse chamber (AC). After 11 days, the RH was changed from 70 to 30%.

Figure 2.18: Sample used for the measurement of the diffusivity coefficient along one of the principal wood anisotropic direction. The faces perpendicular to the measured direction are sealed with aluminium foil and a hook of iron wire is fixed on the sample.

2.4.2.2 Measurements

To control the climate, and in view of measuring the sorption isotherm, the RH of the AC has to be recorded. Therefore, an RH logger was placed in the AC.

The samples were then placed on the conveyor belt. The AC was closed and the tubes connected to the CC. Next, the samples were conveyed below the scale using the conveyor belt as shown in figure 2.15. When the sample's hook was brought below the scale hook, the conveyor belt was put down in order to weight the sample. To determine the sorption isotherm, the weights of the samples have to be recorded at different RH when the EMC is reached.

To determine the diffusion coefficients of the samples, the mass evolution during an RH step has to be recorded. The RH step has to be done from an equilibrium state and up to another EMC state. The mass loss or gain should be then recorded about twice a day. At the end, the anhydrous mass of the samples is determined to calculate the MC.

2.4.3 Data processing

The sorption chambers give only the mass evolution over time of a sample. To determine the water diffusivity coefficient, one way is to use an inverse method.

2.4.3.1 Resolution of Fick's law

The second Fick's law (2-7) is a partial derivative equation (PDE) of the second order. An analytical solution for the one dimensional case with a constant diffusivity coefficient is:

$$m(x,t) = m_L + \frac{4(m_0 - m_L)}{\pi}\sum_{n=0}^{\infty}\left(\frac{1}{2n+1}\sin\left(\frac{2n+1}{L}\pi x\right)\exp\left(-\frac{(2n+1)^2}{L^2}\pi^2 Dt\right)\right) \qquad (2\text{-}24)$$

where m_L and m_0 are the boundary and initial moisture content respectively and L is the length of the one dimensional rod.

Solving

The second Fick's law in one dimension and with a constant diffusivity coefficient becomes:

$$\frac{\partial m(x,t)}{\partial t} = -D\cdot\frac{\partial^2 m(x,t)}{\partial x^2} \qquad (2\text{-}25)$$

where D is a constant diffusivity coefficient, independent on $m(x,t)$ the moisture content. The MC function depends on time t and on the position x in the sample. A sketch of this 1D case is shown in figure 2.19. The initial and boundaries condition are the following:

$$\begin{cases} m(0,t) = m_L & \text{B.C. (a)} \\ m(x,0) = m_0 & \text{I.C. (b)} \\ \partial m(L/2,t)/\partial x = 0 & \text{B.C. (c)} \end{cases} \qquad (2\text{-}26)$$

The boundary condition (c) states that the problem is symmetric. The resolution of equation (2-25) is done by making a variable change. The function $m(x,t)$ is split into two functions: $m(x,t) = G(x)\cdot F(t)$. Therefore, equation (2-25) becomes:

$$\frac{-1}{DF(t)}\frac{\partial F(t)}{\partial t} = \frac{1}{G(x)}\frac{\partial^2 G(x)}{\partial x^2} = K \qquad (2\text{-}27)$$

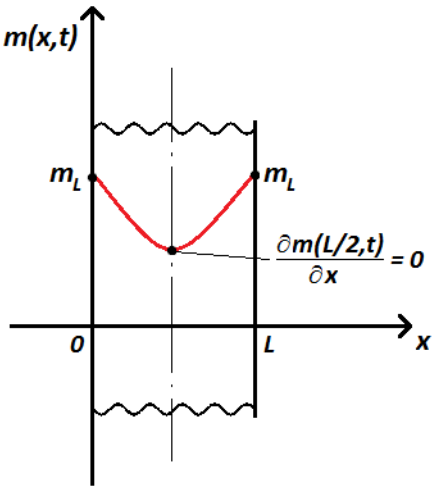

Figure 2.19: Sketch of one-dimensional moisture diffusion though a sample of length *L*. The problem is symmetric, therefore at the middle the partial derivate of *m(x,t)* with respect to *x* is null.

As the time and position variables *x* and *t* are independent from each other, the solution of the two members of this last equations should be equal to a constant *K*. Therefore the equation (2-27) can be split into two equations:

$$\begin{cases} \dfrac{\partial F(t)}{\partial t} + KDF(t) &= 0 \\ \dfrac{\partial^2 G(x)}{\partial x^2} - KG(x) &= 0 \end{cases} \qquad (2\text{-}28)$$

The solution of the function *G(x)* depends on the sign of *K*:

$$\begin{cases} G(x) &= ax + b & \text{if } k = 0 \\ G(x) &= C_1 e^{-\sqrt{K}x} + C_2 e^{\sqrt{K}x} & \text{if } k > 0 \\ G(x) &= C_1 \sin\left(\sqrt{K}x\right) + C_2 \cos\left(\sqrt{K}x\right) & \text{if } k < 0 \end{cases} \qquad (2\text{-}29)$$

By applying the boundary condition (2-26)(a) on these equations, only when $k < 0$ the solution is non-trivial. To enforce this we set $K = -\lambda^2$. The solution of the function *F(t)* is then:

$$F(t) = C_3 e^{-\lambda^2 Dt} \qquad (2\text{-}30)$$

Therefore, the moisture content becomes:

$$m(x,t) = e^{-\lambda^2 Dt}\left(C_1 \cos(\lambda x) + C_2 \sin(\lambda x)\right) \qquad (2\text{-}31)$$

It remains three constants, C_1, C_2 and λ that can be determined using the initial and boundaries conditions (2-26). Before applying the B.C., a variable change is set: $\theta(x,t) = m(x,t) - m_L$. Therefore the B.C. (2-26)(a) becomes $\theta(0,t) = 0$. This B.C. implies that $C_1 = 0$. Next, the B.C. (2-26)(c) is applied:

$$\frac{\partial\theta(x,t)}{\partial x} = 0 = e^{-\lambda^2 Dt} C_2 \lambda \cos\left(\lambda \frac{L}{2}\right) \tag{2-32}$$

The only non-trivial solution is when the cosine function is null. This is achieved when $\lambda L/2$ is an even multiple of $\pi/2$:

$$\lambda_n = \frac{2n+1}{L}\pi \tag{2-33}$$

The function $\theta(x,t)$ is then the sums for $n = 0$ to $n = \infty$:

$$\theta(x,t) = \sum_{n=0}^{\infty} C_n e^{-\left(\frac{2n+1}{L}\pi\right)^2 Dt} \sin\left(\frac{2n+1}{L}\pi x\right) \tag{2-34}$$

Finally, we apply the initial condition (2-26)(b):

$$\theta(x,0) = \sum_{n=0}^{\infty} C_n \sin\left(\frac{2n+1}{L}\pi x\right) = m_0 - m_L \tag{2-35}$$

This is known as the half-range sine series expansion. The C_n are calculated with:

$$C_n = \frac{2}{L}\int_0^L \theta(x,0) \sin\left(\frac{2n+1}{L}\pi x\right) \mathrm{d}\, x \tag{2-36}$$

which gives:

$$C_n = \frac{4\left(m_0 - m_L\right)}{\left(2n+1\right)\pi} \tag{2-37}$$

Finally, $m(x,t) = \theta(x,t) + m_L$ which yields the equation (2-24).

2.4.3.2 Inverse algorithm

The inverse method consists to calculate the diffusion problem and to compare it with experimental values (M. Rappaz *et al.*, 1998). The determination of the diffusivity coefficient *D* can be made with such methods (W. Olek *et al.*, 2005, W. Olek and J. Weres, 2007). It is done by minimizing the mean square difference between the experimental measurement of $m_e(x,t)$ and the calculated one $m_c(x,t)$. Experimentally, it is difficult to measure the local moisture content. However, the mass evolution can be easily measured. Therefore the mean square difference is calculated on the experimental weight $w_e(x,t)$ and the calculated weight $w_c(x,t)$ which is:

$$w_c(t) = \frac{1}{N}\sum_{i=1}^{N}\left(m_c(i,t)+1\right)\cdot w_{dry} \qquad (2\text{-}38)$$

where N is the number of nodes along the thickness of the sample and w_{dry} is the anhydrous mass of the sample. The function $m_c(x,t)$ is calculated with equation (2-24) or by a finite element model using ANSYS. The mean square difference is then:

$$S = \sum_{i=0}^{N}\left(w_e(t_i) - w_c(t_i, D)\right)^2 \qquad (2\text{-}39)$$

S is minimized when $\partial S / \partial D = 0$:

$$f(D) = \frac{dS}{dD} = -2\sum_{i=0}^{N}\left(w_e(t_i) - w_c(t_i, D)\right)\frac{dw_c(t_i, D)}{dD} = 0 \qquad (2\text{-}40)$$

The diffusivity coefficient D can be found using an iterative procedure with Newton-Raphson methods:

$$D_{k+1} = D_k - \frac{f_k}{\left(df / dD\right)_k} \qquad (2\text{-}41)$$

Where k is the iteration step and:

$$\frac{df(D)}{dD} = \frac{d^2S}{dD^2} = -2\sum_{i=0}^{N}\left(w_e(t_i) - w_c(t_i, D)\right)\frac{d^2w_c(t_i, D)}{dD^2} + 2\left(\frac{dw_c(t_i, D)}{dD}\right)^2 \qquad (2\text{-}42)$$

The first and second derivate of the calculated weights w_c can be calculated by finite difference approximations, specifically when ANSYS is used for the calculation:

$$\frac{dw_c(t, D)}{dD} = \frac{w_c(D+\varepsilon) - w_c(D-\varepsilon)}{2\varepsilon} \qquad (2\text{-}43)$$

Or by derivating the equation (2-24):

$$\begin{aligned}\frac{dm(x,t)}{dD} &= \frac{4m_0\pi t}{L^2}\sum_{n=0}^{\infty}(2n+1)\sin\left(\frac{2n+1}{L}\pi x\right)\exp\left(-\frac{(2n+1)^2}{L^2}\pi^2 Dt\right)\\ \frac{d^2m(x,t)}{dD^2} &= \frac{-4m_0\pi^3t^2}{L^4}\sum_{n=0}^{\infty}(2n+1)^3\sin\left(\frac{2n+1}{L}\pi x\right)\exp\left(-\frac{(2n+1)^2}{L^2}\pi^2 Dt\right)\end{aligned} \qquad (2\text{-}44)$$

Finally, the value of D^{k+1} is compared with D^k and if their absolute difference is above a targeted tolerance, another iteration step is performed; otherwise the diffusivity coefficient is set as D^{k+1}. In figure 2.20 the loop of the inverse method is presented.

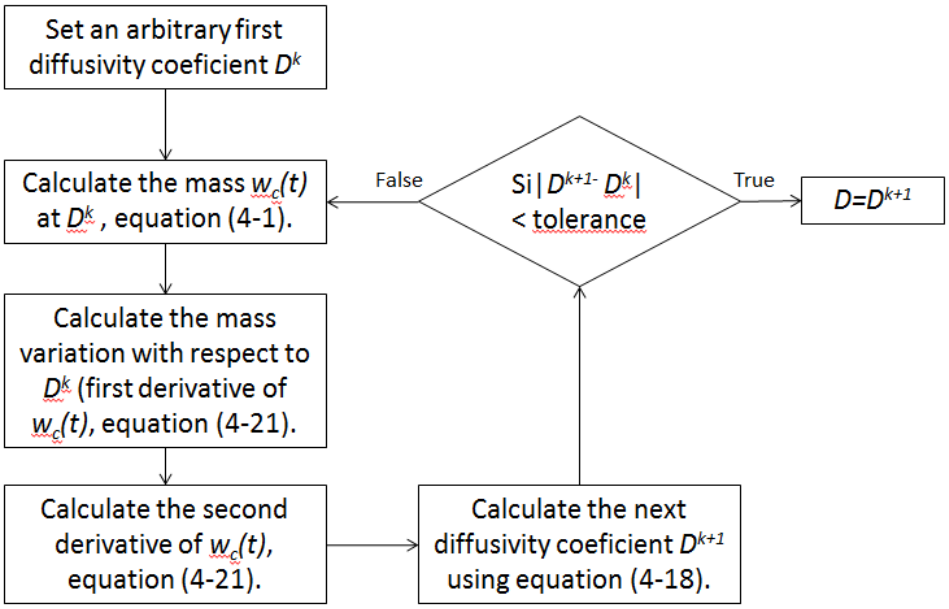

Figure 2.20: Procedure steps of the inverse algorithm implemented in Matlab.

2.5 Microscopy and colorimetry

2.5.1 Optical microscopy

Optical microscopy has been carried out on micro-cuts in the transverse plane. These micro-cuts were prepared with a thickness of 2 – 3 µm by the *Institut für Forstbotanik* at the *University of Freiburg* (Germany). The samples preparation included the following steps: cutting of the samples, dehydration of the samples for one week, soaking the samples in an acrylic resin, slicing the micro-cuts with a rotation microtome, colouring the samples with a mixture of three colours, and embedding the samples in resin. After the preparation, the micro-objects were analysed with a light microscope (Leica DMLM) at different magnifications of up to 400x. Different light sources were used: white and UV light. For a better differentiation of the wood components, polarization and different phase contrast filters were used.

2.5.2 SEM

Scanning electron microscopy has also been used (*Hitachi TM-1000*). The sample preparation procedure was as follows: the samples were first boiled in water at 110°C for six hours. Then they were placed in a solution of water and glycerine for one week. These steps are required to soften the samples. Afterwards, the T x R plane of the samples was cut with a sliding microtom, in order to achieve a clear cut. A final cut was made by hand with a fine razor blade. Finally, the samples were coated with a metal film.

2.5.3 Colorimetry

Colorimetry measurements have been carried out using *Microflash 200d* from datacolour international in CIRAD in Montpellier. The colour space used is CIELAB*: CIE 1976 (L*a*b*).* In CIELAB, colours are described by three components: The lightness *L** and two chromatic parameters *a** and *b**. The lightness goes from 0 for black up to 100 for white. The chromatic parameters *a** is from green (negative) up to red (positive) and *b** is from blue (negative) up to yellow (positive). A representation of the colour space is shown in figure 2.21.

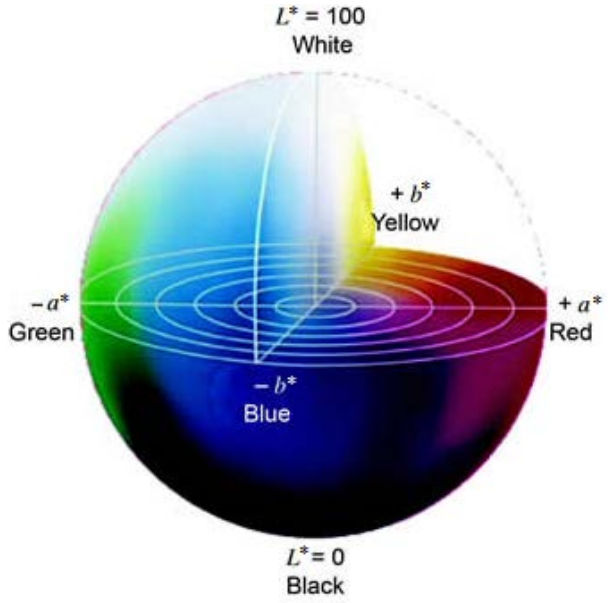

Figure 2.21: Representation of the CIELAB colour space with *L** the lightness and *a** and *b** the chromatic parameters.

The following values are calculated:

$$\begin{cases} \Delta L^* = L^* - L_0^* \\ \Delta a^* = a^* - a_0^* \\ \Delta b^* = b^* - b_0^* \end{cases} \quad (2\text{-}45)$$

where X_0^* are the colour values of a black reference.

Samples preparation

The samples used for the colour measurements were the same as for the radial testing. The samples were first sanded in the transverse plane to have a freshly cut section. Next, there were stored and stabilised in darkness in order to avoid any colour degradation due to UV light. The stabilisation and the measurements were done at 20°C and 65% RH. Before the measurements, the colorimeter has been calibrated using white and black gauges.

2.6 References

BURMESTER, A. 1978. Seasonal-Changes of Physical Wood Properties in Oak Wood (Quercus-Robur L). *Holz Als Roh-Und Werkstoff,* 36**,** 315-321.

FROIDEVAUX, J. 2009. *Simulation of the mechanical behavior of wood under relative humidity changes.* EPFL (Ecole Polytechnique Fédérale de Lausanne).

GRIL, J. 1988. *Une modelisation du comportement hygro-rhéologique du bois à partir de sa microstructure.* Université Paris 6, Sciences Physiques.

GROSSMAN, P. 1976. Requirements for a model that exhibits mechano-sorptive behavior. *Wood Science and Technology,* 10**,** 163-168.

HEGER, F. 2004. *Etude du phénomène de l'élimination de la mémoire de forme du bois densifié par post-traitement themo-hydro-mécanique.* EPFL (Ecole Polytechnique Fédérale de Lausanne).

HUNT, D. 1982. Limited mechano-sorptive creep of beech wood. *Journal of the Institute of Wood Science,* 9**,** 136-138.

NAVI, P. & HEGER, F. 2005. *Comportement thermo-hydromécanique du bois: applications technologiques et dans les structures*, PPUR.

NAVI, P., PITTET, V. & PLUMMER, C. J. G. 2002. Transient moisture effects on wood creep. *Wood Science and Technology,* 36**,** 447-462.

NAVI, P. & SANDBERG, D. 2012. *Thermo-Hydro-Mechanical Wood Processing,* EPFL Press - Distibuted by CRC Press.

NEGI, A. 1999. Turbulence in the wood system with small and short stresses. *Wood Science and Technology,* 33**,** 209-214.

OLEK, W., PERRÉ, P. & WERES, J. 2005. Inverse analysis of the transient bound water diffusion in wood. *Holzforschung,* 59**,** 38-45.

OLEK, W. & WERES, J. 2007. Effects of the method of identification of the diffusion coefficient on accuracy of modeling bound water transfer in wood. *Transport in Porous Media,* 66**,** 135-144.

ORMARSSON, S. 1999. *Numerical analysis of moisture-related distortions in sawn timber.* Chalmers university of technology - Department of structural mechanics, Göteborg, Sweden.

ORMARSSON, S., DAHLBLOM, O. & PETERSSON, H. 1998. A numerical study of the shape stability of sawn timber subjected to moisture variation - Part 1: Theory. *Wood Science and Technology,* 32**,** 325-334.

PFRIEM, A., ZAUER, M. & WAGENFUEHR, A. 2010. Alteration of the unsteady sorption behaviour of maple (Acer pseudoplatanus L.) and spruce (Picea abies (L.) Karst.) due to thermal modification. *Holzforschung,* 64**,** 235-241.

PITTET, V. 1996. *Etude expérimentale des couplages mécanosorptifs dans le bois soumis à variations hygrométriques contrôlées sous chargement de longue durée.* EPFL (Ecole Polytechnique Fédérale de Lausanne).

RANTA-MAUNUS, A. 1975. Viscoelasticity of wood at varying moisture content. *Wood Science and Technology,* 9**,** 189-205.

RAPPAZ, M., BELLET, M. & DEVILLE, M. 1998. *Modélisation numérique en science et génie des matériaux*, Presses polytechniques et universitaires romandes.

SIAU, J. F. 1984. *Transport processes in wood*, Springer-Verlag.

SKAAR, C. 1988. *Wood-water relations*, Springer-Verlag.

TORATTI, T. & SVENSSON, S. 2000. Mechano-sorptive experiments perpendicular to grain under tensile and compressive loads. *Wood Science and Technology,* 34**,** 317-326.

ZÜRCHER, E., ROGENMOSER, C., KARTALAEI, A. S. & RAMBERT, D. 2012. Reversible Variations in Some Wood Properties of Norway Spruce (Picea abies Karst.), Depending on the Tree Felling Date *In:* NOWAK, K. I. & STRYBEL, H. F. (eds.) *Spruce: Ecology, Management and Conservation.*

Chapter 3
Wood aging

Wood shows very good durability. Many examples of wood patrimonial architecture are still resisting against time, without specific treatment, as shown in figure 3.1. However, as an organic material, wood is part of the carbon cycle in nature and its formation and degradation are essential elements of this cycle. Wood degradation processes are numerous: firstly, wood can be degraded by extreme condition such as heat, frost or high mechanical loading; secondly, it can be modified by weathering such as UV-light degradation (surface degradation), chemical degradation due to rain, air pollution, etc.; and thirdly, it can be biologically degraded by insect or fungi. These last degradations processes depend closely on the conditions where wood is used and stored. If the wood is kept under reasonable environment they can be avoided. However, a long-term aging phenomenon takes place in wood even in such conditions.

Definition - Aged wood:

Wood that has been chemically modified by time and slight moisture (under FSP) and thermal variation only.

(a) (b)

Figure 3.1: Old wooden construction in Switzerland. (a) "Grand Chalet de Rossinière", built in 1750 in Rossinière. It is the biggest wooden house in Switzerland. (b) Farm "Auf der Kreuzgasse " built in 1556 in Schwarzenmatt (source: www.patrimoinesuisse.ch).

This aging is typically achieved under indoor condition or sheltered. Such chemical modifications can be explained by thermodynamics. Indeed, wood is a complex chemical structure which tries to minimise its free energy. The analysis of the changes during aging of wood is a new field in wood science where questions remain unresolved.

This chapter presents our investigation on the wood aging prediction. The first part investigates the natural aging effect on wood properties, including our results and a literature review. The second part considers the possibilities to accelerate the aging phenomenon by thermo-hydrous treatment. Finally, the third part proposes a theory about the law of wood aging.

3.1 Natural aging of wood

3.1.1 Literature review

The effects of aging in wood in terms of physical, mechanical and chemical degradation has been studied by Kohara (J. Kohara, 1955b, J. Kohara, 1955a, J. Kohara, 1954b, J. Kohara, 1954a, J. Kohara, 1953, J. Kohara, 1952), by Borgin (K. Borgin et al., 1975a, K. Borgin et al., 1975b), and more recently by Erhardt (D. Erhardt and M. Mecklenburg, 1996, D. Erhardt et al., 1996), Obataya (E. Obataya, 2007, E. Obataya, 2009) and Yokoyama (M. Yokoyama et al., 2009).

The main difficulty of such investigation is the sampling. Indeed, aging phenomenon is a slow process inducing a slight change in the wood structure. Therefore, it is impossible to extract the aging degradation if wood is degraded by another process, typically the biological degradation. The quantity of available old wood for carrying out destructive testing is therefore very limited. Indeed, generally the well-conserved aged wood of several centuries is present in art-works and cannot be tested.

Erhardt *et al*. found no clear differences of mechanical properties between aged and non-aged wood. However, on their figures, it can be clearly seen that the fracture energy along the radial and tangential direction is reduced. They detected some chemical changes such as xylan hydrolysis.

The experiments performed by Kohara on old hinoki wood [*Chamaecyparis obtusa Endl.*], summarised by (E. Obataya, 2007, E. Obataya, 2009) give more precise indication on aging phenomenon. His samples came from old constructions in Japan and were aged between 300 and 1300 years. He shows that the longitudinal Young's modulus of aged wood increases by around 20% during the first 300 years. After that time, the modulus decreases slowly. He explains this phenomenon by two chemical modifications occurring at the same times: Firstly by an increase of the crystallization of cellulose and secondly by the depolymerisation of the

hemicelluloses. Kohara shows also that the strength of old wood decreases with aging time. He explained this loss of strength by the degradation of the interface between the matrix and fibres. Yokoyama et al. show that the higher rigidity of old wood observed by Kohara was an indirect effect of density (M. Yokoyama et al., 2009). They found that the degradation of the mechanical properties of old wood is quite small along the longitudinal direction, but quite important along the radial direction where the strength is drastically decreased (by about 40%).

Borgin *et al.* work on old Egyptian wood varying in age from 900 to 4400 years (K. Borgin et al., 1975b). In their electron microscopy investigation, they found some degradation such as cracks across the cell wall and loss of adhesion of interfaces zone such as between middle lamella and S1 layer.

Objective N°1:

*Our first objective was to collect old wood samples of spruce (*Picea abies Karst. (L.)*) and look at the modification of the mechanical properties along the radial direction and next compare the results with the value from literature on other species. Moreover, more complex mechanical behaviour such as viscoelasticity and mechanosorption has been investigated and as well as the sorption and diffusion behaviour. The focus is set on the radial direction, because of our purpose, cultural heritage and specifically the paintings. The probability of damaging will appears along radial or tangential direction, the weakest one. Moreover, as it reported in literature, the major change of old wood is the radial strength.*

3.1.2 Properties of naturally aged spruce wood

The mechanical and sorption properties along the radial direction have been determined for non-aged and naturally aged spruce wood. Elastic, failure, creep, relaxation and mechanosorption tests have been carried out with a micro-tensile testing device. The sampling, the machines used and the testing procedures are described in the previous chapter in section 2.3. Results of this investigation on mechanical properties of old spruce wood have been published (J. Froidevaux et al., 2012).

The sorption and diffusion of water have also been determined. The sampling, machines and procedures have been described in the section 2.4.

3.1.2.1 Wood selection

Due to its simple structure and abundance in cultural heritage artworks in Switzerland, Spruce wood (*Picea abies Karst. (L.)*) has been selected for this study of wood aging.

The naturally aged wood samples were originated from different historical buildings in Switzerland. The ages of the samples were determined by dendrochronology as shown in figure 3.2. They varied between 100 and 700 years (considered from tree felling).

Figure 3.2: Examples of natural aged wood samples dated via dendrochronology.

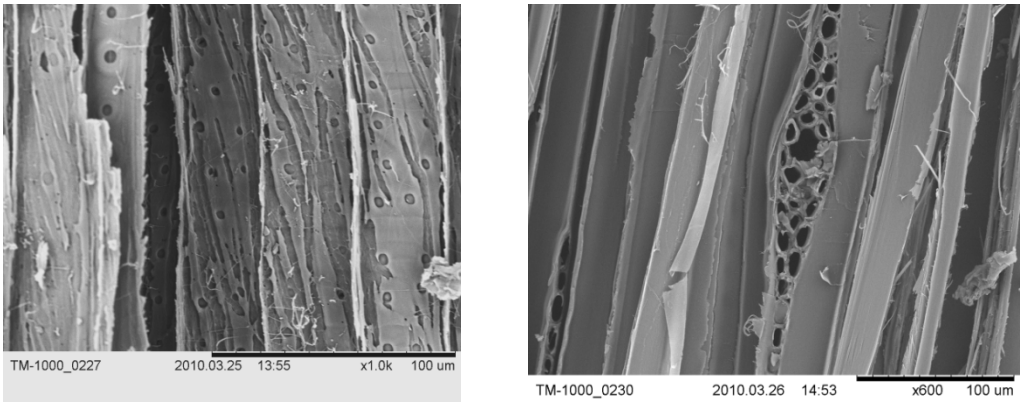

(a) (b)

Figure 3.3: (a) Old wood of 500 years old. Strong fungal degradation of the secondary wall in the tracheids of the early wood can be seen. This wood sample has been rejected. (b) 400 years old tested wood sample. No visible degradation has been detected.

Wood is a part of the biological cycle and so is always prone to attack by insects and micro-organisms, especially in the case of aged wood. To generate reproducible results it is necessary to perform the tests on wood that has not been degraded by fungi or insect attack. For this reason a comprehensive study was performed to select aged wood without such degradations. All aged wood samples were selected by optical and electronic microscopy. Thus the quality of the aged wood samples were examined and evaluated as presented in figure 3.3. Finally, three age categories were selected: 500 years old (1521), 400 years old (1610) and 200 years old (1760). The 200 and 500 years-old samples came from framework beams, and the 400 year-old sample from a parquet floor. Their air-dry density was 414, 392 and 394 $kg \cdot m^{-3}$ for the 200, 400 and 500 years-old samples respectively. All these wood samples can be

considered as aged under indoor conditions (slow temperature and RH variation, no contact with water, and low UV radiation).

The reference non-aged wood (modern wood) has been selected with similar air-dry density than the aged wood samples. They were grown in central Switzerland near Schattdorf (Department Uri) and were cut in 2007 (3 years old during the investigation). Three different annual ring width samples were included in the investigation, in order to quantify their effects: narrow (width < 2 mm), middle (width ~2 mm), wide (width > 2 mm). The air-dry density was 411, 404 and 388 $kg \cdot m^{-3}$, respectively.

3.1.2.2 Radial mechanical behaviour

The main objective of our investigation is to compare the long-term and the short-term micro-mechanical properties of non-aged and naturally aged wood along the radial direction. This direction is of great importance for the preservation of ancient wooden artworks such as old painting panels, where damage can frequently occur.

All mechanical tests presented in the following sections have been carried out with the micro-tensile testing device, following the experimental procedures described in section 2.3.2 and 2.3.3.

3.1.2.2.1 Linear elasticity behaviour

The Young's modulus for all samples is within the same range, as can be seen from figure 3.4. This shows that there is no clear tendency of a modification of the stiffness in the radial direction during the aging of the samples. The components which determine the stiffness of the wood depend on the principal directions. In the longitudinal direction the cellulose mainly governs the stiffness. Due to the probable increase of crystallinity during aging, an increase of stiffness is most likely ((J. Kohara, 1954b) in (E. Obataya, 2007)). But in the radial direction, the percentage of cellulose radially oriented is small. Only in the cell wall layers S1 and S3, micro-fibrils are radially oriented with angles of about 80°. Therefore, any modification of the crystallinity of cellulose would have a low influence. Lignin and hemicelluloses have a more dominant influence on the stiffness in the radial than in the longitudinal direction.

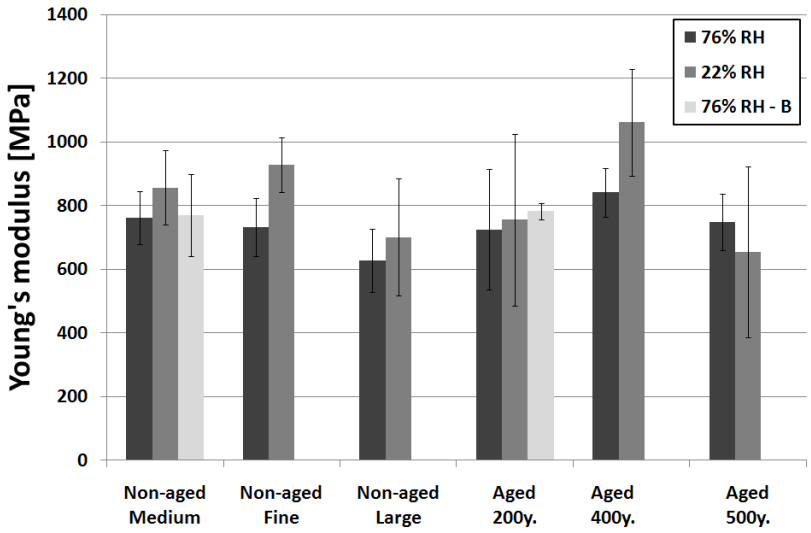

Figure 3.4: Average radial Young's modulus and the standard deviation at 76% and 22% relative humidity (RH) of non-aged and aged spruce wood samples. Each bar corresponds to a mean of 10 tests. The third series (light grey) corresponds to tests done at 76% RH with a bigger section sample (50 mm^2).

In figure 3.5 the radial tensile rupture stresses under the two different climatic conditions are shown. No significant difference can be seen between the three non-aged woods samples. This may indicate that the width of the annual rings in the samples does not influence the tensile strength in the radial direction. The mean value is about 5.5±15% MPa. This value is slightly greater than those in the literature: 2-5 MPa (F. Kollman, 1951). This is could be explained by size effect, with strength higher for small samples than for normalized samples, but variability related to differences in growth conditions cannot be ruled out.

Concerning the aged wood samples there is a clear difference between the 400-year-old sample and the two other samples of aged wood (namely of 200 and 500 years). The failure of all samples always takes place in the region of the first three cell rows of the early wood, i.e. in the vicinity of the annual ring border. According to the optical analysis outlined in section 3.1.2.3, the thickness of the radial cell walls in this zone is significantly greater for the 400-year-old wood than the others as tabulated in table 3.1. Comparing the density, the samples are similar. However, the density profile between late and early wood is different for the 400 years aged wood compared to the others. This is the most likely explanation for the high radial strength of the 400-year-old wood. The two other samples of aged wood show a distinct reduction of about 25% in rupture stress compared with the non-aged wood. Unfortunately, the precise history of usage of the aged sample is not known and no correlation with aging time can be observed.

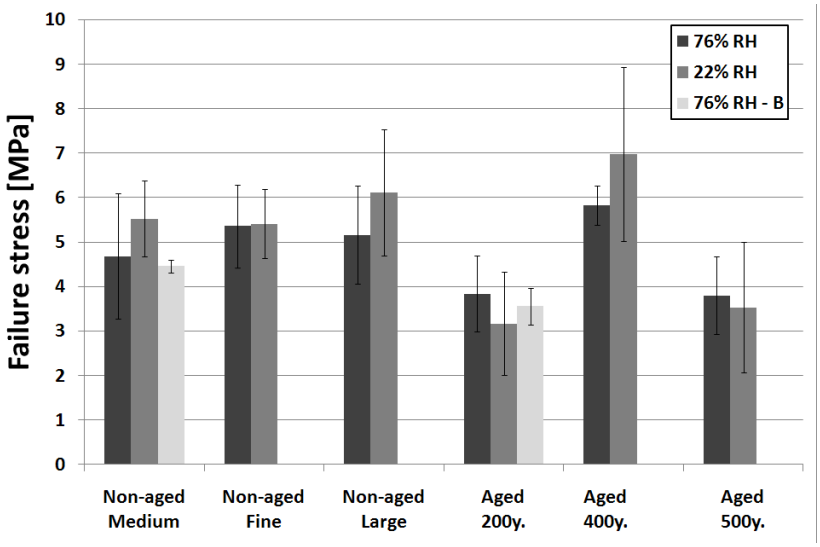

Figure 3.5: Average radial tensile failure stress and the standard deviation at 76% and 22% relative humidity (RH) of non-aged and aged spruce wood samples. Each bar corresponds to a mean of 10 tests. The third series (light grey) corresponds to tests done at 76% RH with a bigger section sample (50 mm^2).

Table 3.1: Dry density and radial cell wall thicknesses (mean of 60 measurements) in the second and third layer of cells in the earlywood region.

		Density [kg m^{-3}]	Earlywood cell-wall thickness [µm]
Non-Aged	Fine	411	-
	Medium	404	3.6
	Large	388	-
Aged	200 years	414	4.1
	400 years	392	5.1
	500 years	394	3.1

3.1.2.2.2 Time dependent behaviour

Creep and relaxation results are presented in figure 3.6 and 3.7 respectively. The results show significant creep for all specimens. At 22% RH during testing, the relative creep (define in section 2.3.3.3) after two days is between 35% and 65% of the elastic strain. As expected, the creep in a wetter state, at 76% RH, tends to be a little higher than in the dry state, and varies between 50% and 75% after two days.

There is little difference between the creep of aged and non-aged wood samples. At 22% RH, non-aged wood tends to creep a bit less than aged wood. At 76% RH (Figure 3.6 (b)), the difference between aged and non-aged wood samples is not perceptible.

Comparing the creep-recovery of the different samples, no significant change can be seen. Each sample shows an irreversible deformation after one day of recovery of about 20% of the instantaneous strain. It is important to note that for

most of the creep tests, only one sample could be tested. Although a tendency is visible, for a detailed interpretation more experiments would be necessary.

As in the creep tests, the stress relaxation tests confirm that the natural aging of several hundred years does not greatly change the time-dependent behaviour of wood. The relative relaxation for all samples in dry conditions is in the range 30–45% of the instantaneous stress. Similarly to the creep tests, it seems that aged wood relaxes a little more than non-aged wood.

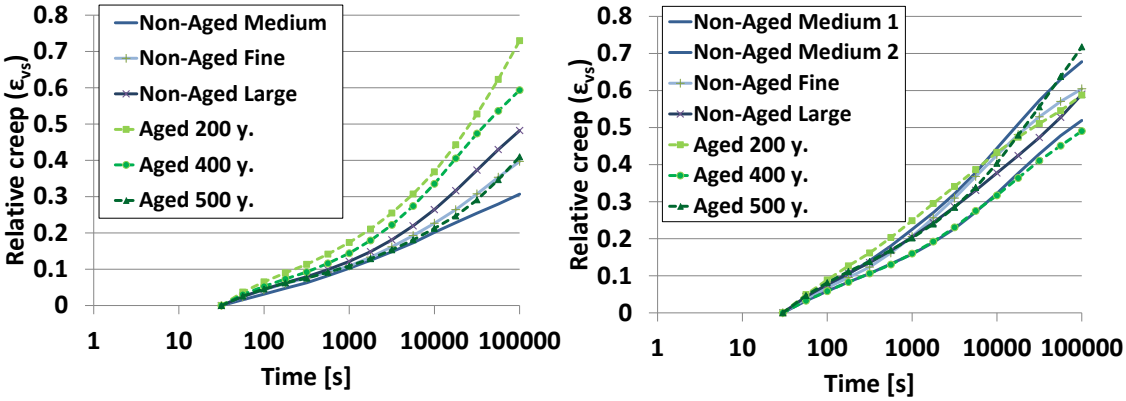

(a) (b)

Figure 3.6: Radial relative creep strain ε_{VS} versus the log of time under climatic conditions of 22% (a) and 76% (b) relative humidity.

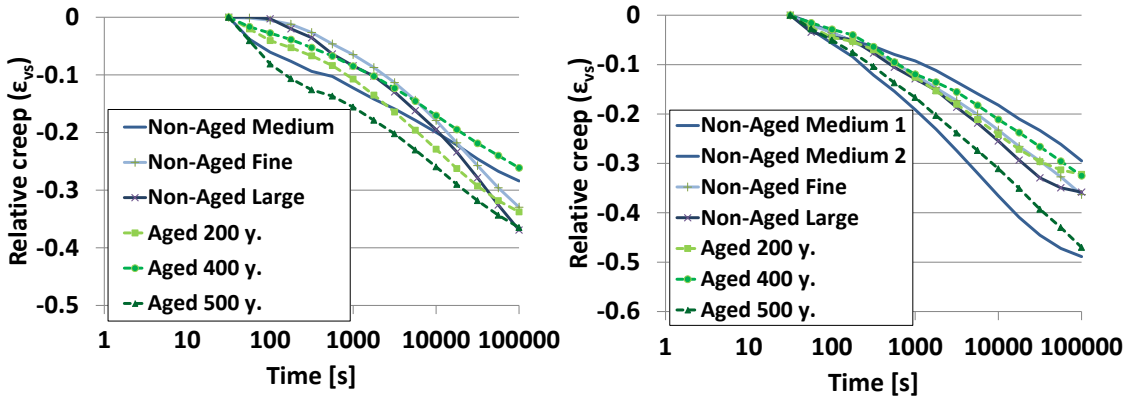

(a) (b)

Figure 3.7: Radial relative relaxation stress σ_{VS} versus the log of time under climatic conditions of 22% (a) and 76% (b) relative humidity.

In order to be able to compare the results obtained from the relaxation and creep tests, a generalized Maxwell rheological model was used (see section 2.2.3 for more information). First, the parameters of the model were determined for each creep test. Then, with these parameters, the stress relaxation test was simulated using:

$$\sigma(t) = E_\infty \varepsilon_0 + \sum_{i=1}^{N} E_i \varepsilon_0 \exp\left(\frac{-t}{\tau_i}\right) \qquad (3\text{-}1)$$

where ε_0 is the constant strain during the relaxation, N the number of spring-dashpot pairs of the model (here $N = 5$), E_i the moduli of elasticity of each spring, t the time and $\tau_i = E_i / \eta_i$ the relaxation times, with η_i the viscosities of the dashpots. The compatibility between creep and relaxation results was checked by comparing the relaxation data to calculated values using a model based on creep data (figure 3.8).

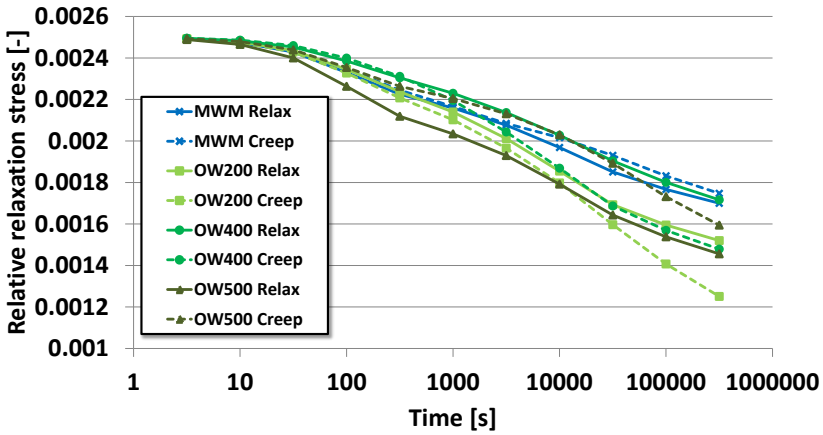

Figure 3.8: Comparison between measured (plain lines) and calculated (dotted lines) relaxation curves at 76% RH. Calculated values were obtained by simulation of the stress relaxation using a generalized Maxwell model fitted from creep data.

3.1.2.2.3 Mechanosorption

In the figure 2.12 in the section 2.3.3.4, the mechanosorption effect in the radial direction can be seen. In table 3.2, different strain and relative strain values are listed according to the definition given in section 2.3.3.4.

Table 3.2 : Mechanosorptive strain. ε_0 is the instantaneous strain; $\varepsilon_{ms,\,c1}$ and $\varepsilon_{ms,\,c3}$ are the strain after one and three cycles of relative humidity (RH) respectively; ε_{irr} is the final irreversible mechanosorptive strain after the final two RH cycles. Finally, each strain value is given relative to the instantaneous strain.

	Non-Aged Wood Medium	Aged Wood 200 y.	Aged Wood 400 y.
ε_0	0.096	0.134	0.077
$\varepsilon_{ms,\,c1}$	0.371	0.500	0.257
$\varepsilon_{ms,\,c3}$	0.398	0.600	0.283
ε_{irr}	0.099	0.189	0.089
$(\varepsilon_{ms,\,c1} - \varepsilon_0)/\varepsilon_0$	2.88	2.74	2.35
$(\varepsilon_{ms,\,c3} - \varepsilon_0)/\varepsilon_0$	3.16	3.48	2.68
$\varepsilon_{irr}/\varepsilon_0$	1.03	1.42	1.16

Comparing the relative mechanosorptive strain (relative to the instantaneous strain ε_0) of the different samples, it can be seen that no significant change occurs

during aging. It seems that the relative mechanosorptive strain is slightly higher for the non-aged compared to the aged woods. However, these slight modifications could come from a hygroscopic loss due to aging instead of a change in the mechanosorptive behaviour, although no significant change in the moisture behaviour of aged wood has been reported (T. Gereke, 2009).

On the other hand, the irreversible relative mechanosorption strain ε_{irr}, which has not been recovered at the end of the test, is greater for the two aged woods. This indicates that aged wood may undergo more non-recoverable deformation than non-aged wood.

3.1.2.3 Anatomical comparison

The basic idea behind the microscopy investigations was to investigate the correlation between the aging of the wood and the modifications of the micro-structure and the mechanical characteristics. Optical and scanning electron microscopy has been used. The description of the samples preparation and the systems used can be found in section 2.5. The micrographs are shown in figure 3.9 on page 75. They show cross-sectional cuts of wood. The following damage has been identified in the aged wood structure:

- Punctual degradation of the middle lamella (Figure 3.9 (a)),
- Delamination of the S3 wall (Figure 3.9 (b)),
- Cracking from the tertiary wall into the secondary wall,
- Delamination within the secondary wall,
- Delamination between middle lamella and secondary wall,
- Radial cracking in the secondary wall (Figure 3.9 (c)),
- Partial reduction of the cell wall thickness within the cell,
- Accumulation of defaults in the first rows of the early wood.

It is known that such damage is mainly caused by the sample preparation. Indeed, the cutting into fine slices and the drying of the samples can induce quite high local stresses. However, these damages were not observed in the non-aged wood structure. This shows that the structure of aged wood has become locally weaker than non-aged wood. Moreover, similar damage has been seen in optical and electron micrographs with different sample preparation.

The localized damage observed in aged wood microstructure partly explains why the strength in the radial direction is lower than that of non-aged wood. Indeed, this localized damage should decrease the failure stress, specifically when the damage is located in the early-wood region. Nevertheless, these types of damage should not have an important influence on the overall macro behaviour, such as Young's modulus or viscoelastic behaviour. It is important to note that it is not

possible to say which of these changes are correlated with aging. As already stated, the failure of wood in radial direction occurs mainly in the first rows of the early wood. Thus, any defect in this region directly impacts the radial strength of wood. Modifications or defects in the late-wood regions are probably not so important for the failure strength.

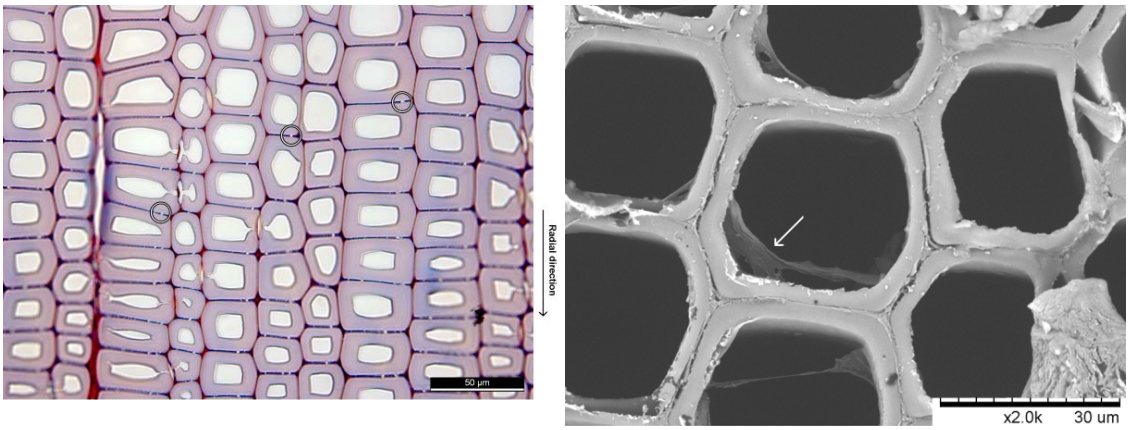

(a) (b)

(c)

Figure 3.9: Optical and scanning electron micrographs. a) Optical micrograph of 200-year-old aged wood. Punctual degradations are visible in the middle lamella (circled). b) Scanning electron micrograph of 500-year-old aged wood. Delamination of the S3 wall from the secondary wall is visible (arrow). c) Optical micrograph of 200-year-old aged wood. Delamination between the middle layer and the secondary wall (arrows) and radial cracking in the secondary wall (circled) are visible.

3.1.2.4 Colour change of old wood

Accordingly to the experimental procedures described in section 2.5.3, the colour of the old wood samples has been measured by colorimetry in the CIELAB colour space. The colour parameters of each sample correspond to a mean of nine values. The results with the coefficients of variation are presented in figure 3.10.

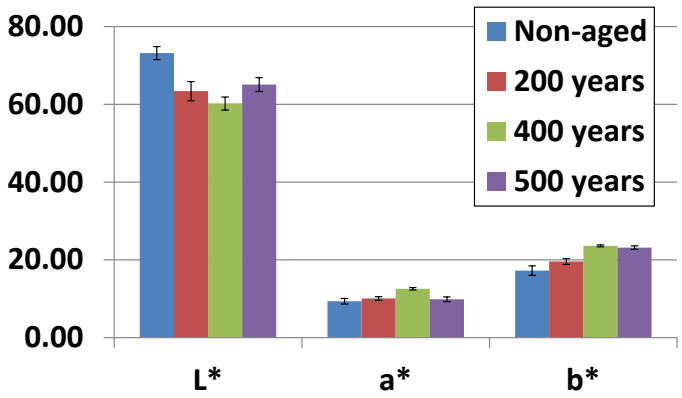

Figure 3.10: CIELAB colour values of non-aged and naturally aged spruce wood.

It can be seen that the lightness L^* decrease with age. The aged samples are more yellow: b^* increase with age. Concerning the chromatic parameters a^* (green to red), only a slight tendency of increasing is seen in the red.

3.1.2.5 Sorption and diffusion behaviour

3.1.2.5.1 Diffusivity

The diffusivity coefficients of non-aged and naturally aged samples have been determined using the isothermal sorption chambers. The description of the system, the samples preparation and the tests procedures are described in section 2.4.2. An RH step from 76 to 22% has been imposed to the samples and the mass evolution over time has been recorded. The data processing has been carried out with an inverse algorithm (section 2.4.3) using an analytical solution for the calculation of the diffusion.

The coefficients of diffusivity have been measured along the three main directions for non-aged wood. Due to the small size of the old wood samples available, certain directions could not be measured. The mean values are presented in table 3.3.

Table 3.3: Diffusivity coefficients of non-aged and naturally aged spruce wood samples. The coefficient of variation (CV) is shown as well as the number of measurements.

	Non-aged			200y		400y	500y	
	L	R	T	L	R	L	T	R
D [m^2 s^{-1}]	1.45E-10	4.70E-11	4.52E-11	1.05E-10	4.76E-11	1.07E-10	5.32E-11	6.19E-11
CV	12%	10%	11%	8%	-	-	3%	-
N measure	3	4	4	2	1	1	2	1

As known, wood shows a large anisotropy between transverse and axial directions. The diffusivity along L direction is three times greater than in R or T. On the other hand, no significant difference can be seen between R and T directions.

A clear reduction of the diffusion can be seen along the L direction between non-aged and aged wood. Indeed, a loss of 33% is seen after 200 and 400 years of natural aging. However, no time correlation between the aged samples can be seen. Concerning the transverse direction, no change is seen in R direction of the 200-years-old samples but increases of the diffusion of about 12% in R and 30% in T directions have been detected in the 500-years-old samples.

It is difficult to draw conclusion for the transverse directions due to lack of measurements and the absence of correlation between the measured values and the age of the samples. However, it seems that the natural aging tends to reduce the diffusion along the fibres direction. A tentative explanation could be the closing or obstructions of pits in old wood, although variations in the drying methods could also be invoked. Indeed, the diffusion of water in wood combines two processes: diffusion of bound water inside the cell wall (slow) and diffusion of vapour in the lumen (fast). To pass from cell to cell, water has to go through the cell walls, but this can be helped by the pits when they are open (J. F. Siau, 1984). In wood, the majority of the pits are closed as a result of drying although some remain open.

3.1.2.5.2 Sorption

During the measurements of the diffusion of water in the wood samples detailed above, the moisture content has been calculated at the two EMC states at the beginning and ending of the measurements. The mean results are shown in table 3.4. No significant change of the sorption behaviour can be seen between the samples.

Table 3.4: Moisture content of non-aged and naturally aged samples at two different relative humidity.

	Non-aged	200y.	400y.	500y.
76%	11.7%	12.0%	12.0%	11.8%
22%	7.2%	6.7%	7.2%	6.9%

3.2 Accelerated aging of wood by thermal treatment

As already mentioned, wood aging consists in chemical modifications (mainly oxidation and hydrolysis), occurring over time. It is well known that the rate of chemical reactions is temperature dependent following an Arrhenius law. Therefore, by increasing the temperature, it might be possible to accelerate the aging of wood.

In the following section, a brief description of the effect of the thermo-hydrous treatments will be described. Next, the thermo-hydrous reactors that we have designed and constructed with support of a Swiss company (RINO Sàrl, Blonay, Switzerland) will be presented and finally, a comparison between the accelerated aging and natural aging will be made.

3.2.1 Thermo-hydrous treatments – summary

The thermal modifications of wood are known and studied since 1915 (C. A. S. Hill, 2006). The main improvements than can be achieved with such treatments are the dimensional stability, hygroscopicity reduction and increased decay resistance. Moreover, there is a darkening of the wood that can be seen as an improvement or not. On the other hand, some properties are degraded, and specifically the mechanical properties. Generally, the rigidity along L direction is increased with the treatment time up to a certain point and next it is reduced (C. A. S. Hill, 2006). The strength of thermo wood is always decreased and specifically along the R direction. These modifications are strongly dependent on the treatment conditions. Indeed, many variables can be set during the treatment such as time and temperature but as well as the relative humidity, presence of liquid water, oxygen (air pressure), gases, closed or open system and use of catalyst.

The temperatures generally used are between 180 and 260°C. It has been seen that below 140°C under dried condition no major changes occurs and above 260°C, exothermal chemical reactions take place and strong degradation occurs. The objectives for actual commercial applications are to improve the wood properties with a minor degradation of the mechanical properties. The chemistry of treated wood is very complex, because the chemical reactions are temperature and atmosphere dependent. Indeed, the reaction pathway will be the one which minimise the free energy of the system. To reach more stable state, the overpassing of energetic barriers is required. Several of such processes, quantified by different activation energies, may coexist and compete. Therefore, some reactions can be activated under high temperature and take the place of reactions that normally occur at lower temperature.

3.2.2 Accelerated aging

As different reactions happen inside wood at relatively high temperature compared to natural aging, artificial aging at high temperature will not be compatible with natural aging. Temperature below 150°C is preferable, in order to keep chemical reactions closer to those occurring in standard condition.

Obataya has investigated the effect of dry and wet (saturated) thermal treatments compare to natural aging of wood (E. Obataya, 2007). It appears that the control of humidity level during the treatment is important to introduce some hydrolysis reactions. Indeed, water probably plays a role in the chemical modification during natural aging. Borgin *et al.* show evidence of lignin hydrolysis in their investigation (K. Borgin et al., 1975a). Therefore, the relative humidity during the accelerated aging treatments should be controlled and stabilised, in order to promote and control the hydrolysis.

On the other hand, Millet and Gerhards have investigated the change of mass, stiffness and strength of thermally treated wood along L direction (M. A. Millett and C. C. Gerhards, 1970). They compared the different treatments and fitted the results on an Arrhenius law. Finally, they extrapolated their Arrhenius equation to ambiance temperature. The prediction of the degradation of wood by the Arrhenius relation from Millet and Gerhards (1970) seems to work fine for thermal treatments. However, their results do not correspond to real natural aging when they extrapolate their data. This is probably due to the relatively high treatment temperature that they used (115 to 175°C): the extrapolation using an Arrhenius relation is possible only if the chemical reactions are the same for naturally aged and treated samples. Moreover, they have performed only dry thermal treatments. Therefore the possible hydrolysis reactions are not taken into account in their law.

Many works have been recently performed about the colour change of dry-thermally treated wood (M. M. Gonzalez-Pena and M. D. C. Hale, 2009a, M. Matsuo *et al.*, 2010). The prediction of colour change by applying kinetic analysis using the Arrhenius law has been successfully applied. Matsuo et al. compared the colour change of naturally aged wood coming from historical buildings with thermo-treated wood (M. Matsuo et al., 2011). They extrapolate their kinetic law at ambient temperature and found that the colour change after 921 years at ambient temperature was almost equivalent to a thermal treatment 6.7 h at 180°C. On the other hand Gonzàlez-Peña et al. used the colour change of thermally treated wood to predict other physical parameters such as density, weight losses or mechanical strength (M. M. Gonzalez-Pena and M. D. C. Hale, 2009b).

Objective N°2:

Our second objective will be to design and built thermo-hydrous reactors which can process wood under controlled temperature, time, humidity and pressure. Next, the spruce wood samples (Picea abies Karst. (L.)) will be treated at temperature from 110 to 150°C, under dry to 25% of relative humidity and under different pressure condition from vacuum to 6 bars. Finally, mechanical, sorption and diffusion parameters will be compared with literature and with our naturally aged wood.

3.2.3 TH-Treatments reactors

Two automatic thermo-hydrous reactors have been designed and constructed (by RINO Sàrl, Blonay, Switzerland) to control precisely the treatment temperature *T*, pressure *p* and relative humidity *h* for relatively long periods of time (several weeks). Pictures of these reactors can be seen in figure 3.11.

Figure 3.11: Pictures of the two automatic thermo-hydrous reactors designed.

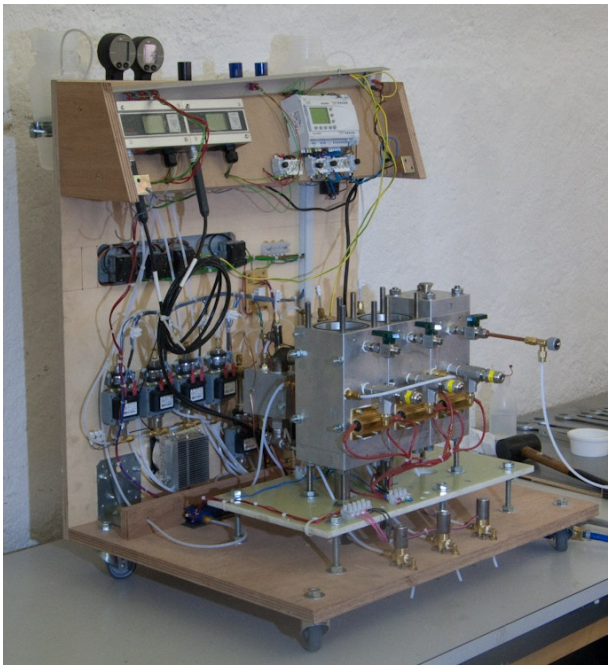

Figure 3.12: Tri-cellular pressure vessel TH-III in open condition.

The first reactor contains one closed treatment cell (TH-I). Its temperature, RH and pressure ranges are 100 to 150°C, 2 to 95% of RH and 0 to 8 bars respectively. The second one contains three treatment cells with controllable air flux (TH-III). TH-III can be seen in open condition in figure 3.12. Its temperature and pressure ranges are 30 to 200 °C and 0 to 8 bars respectively. The two first cells have an RH range from 1 to 95% and the third one does not have an RH control and is kept under a dry climate (less than 0.5%). Figure 3.13 shows a sketch of the system.

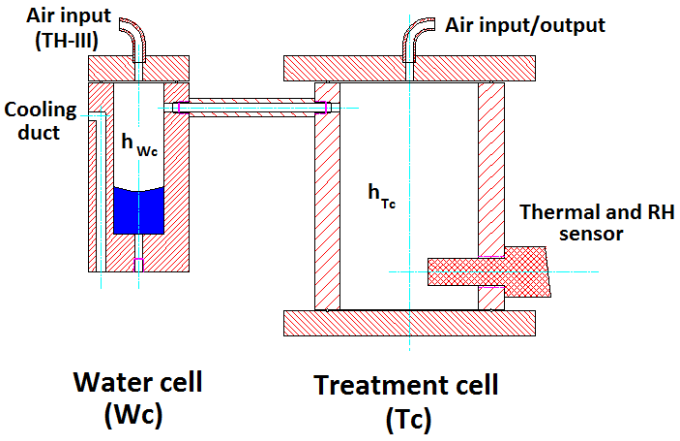

Figure 3.13: Sketch of the thermo-hydrous reactors principle. TH-III has an air input above Wc.

The pressure is controlled externally with the help of a vacuum pump or a compressor. The flux of the tri-cellular reactor is simply controlled with micro-valves placed at the air input and output. The pressure is important during the treatment because oxygen produces oxidation reactions of wood components. Of course the pressure will increase the quantity of oxygen. On the other hand, treatment under vacuum will suppress the oxidation reactions.

The treatment cells (Tc) can be heated with heating elements which are controlled by a PLC (*Programmable Logic Controller*). A thermal sensor measures continuously the temperature of the treatment cells and is linked to the PLC.

The relative humidity is conditioned in the "water cells" (Wc). These cells are directly connected to their respective Tc as can be seen on the sketch of figure 3.13. Wc are filled with water and therefore their relative humidity h_{Wc} is:

$$h_{Wc} = \frac{p_{vap}}{p_{sat}(T_{Wc})} = \frac{p_{sat}(T_{Wc})}{p_{sat}(T_{Wc})} = 100\% \qquad (3\text{-}2)$$

where p_{vap} is the vapour pressure in the Wc which is equal to $p_{sat}(T_{Wc})$, the pressure of saturation at the temperature of Wc T_{Wc}. In the treatment cell the RH h_{Tc} is then:

$$h_{Tc} = \frac{p_{vap}}{p_{sat}(T_{Tc})} = \frac{p_{sat}(T_{Wc})}{p_{sat}(T_{Tc})} \qquad (3\text{-}3)$$

Due to the connection between the two cells, the vapour pressure inside Tc is equal to the vapour pressure in Wc which is equal to the pressure of saturation at the temperature T_{Wc}. Therefore, by controlling the temperature of Wc, it is possible to control the RH of the treatment cell. This control is done with the PLC, which controls the heating and cooling system of Wc as a function of the RH sensors in Tc.

For both reactors, the temperature and relative humidity of the treatment cells can be recorded as can be seen in figure 3.14. The stabilisation of the temperature

(±0.5°C) and of the RH (±1%) is quite good. The thermal stabilisation of both reactors takes about 3 hours. The RH stabilisation is quite fast in TH-III, due to the air flux control (about 1hours). On the other hand, the RH stabilisation in the close mono-cellular reactor (TH-I) is slower. Indeed, the water vapour has to move in the treatment cell by diffusion instead of an air flux.

The PLC can be programmed to generate variable RH conditions (possible only with TH-III which can switch the RH relatively fast) as can be seen in figure 3.14(b), where the RH is cycled from 0 to 10 to 25% each days.

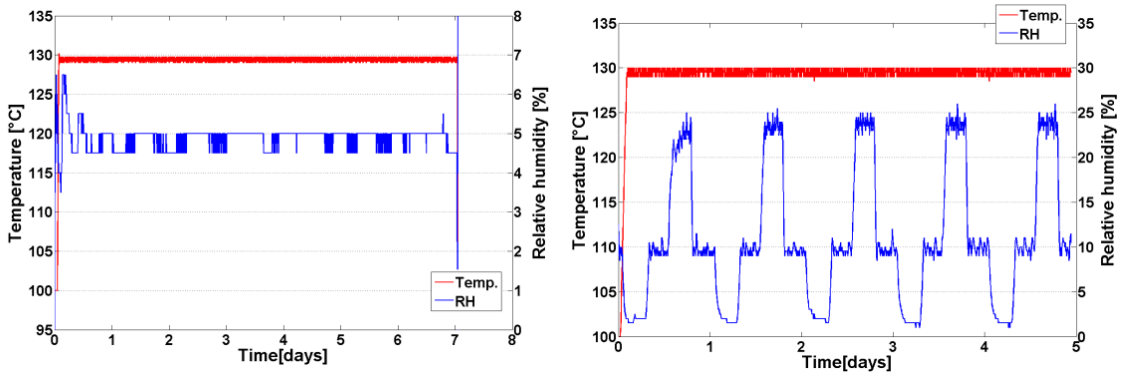

Figure 3.14: Recorded temperature and relative humidity in the treatment cell of the mono-cellular reactor (a) and of the tri-cellular reactor (b). In the latter case, the RH setting is variable over time.

3.2.4 Properties of thermally aged wood

Using the thermo-hydrous reactors, different treatments have been carried out to characterise the modifications of the treated wood properties and to compare them with naturally aged wood. Mechanical, physical and chemical measurements have been carried out and the results are presented in the following sections.

Treatments representation

The treatments parameters are represented by four numbers in brackets such as: (Temperature in °C - RH in % - Pressure in bars – Time in days), for instance: (130-10-1-10) stands for treatment at 130°C, 10% and 1bars during 10 days.

3.2.4.1 Mechanical modifications

3.2.4.1.1 Linear elastic behaviour

Figure 3.15 shows the radial Young's modulus and radial failure stress of non-aged, thermally aged and naturally aged spruce wood. The Young's modulus did not

change significantly as a result of TH treatments, and our results suggest that natural aging does not affect it either. Even long treatment at relatively high temperature, for example (140-10-1-65), did not modify the stiffness. However, the radial strength was invariably reduced by the treatments.

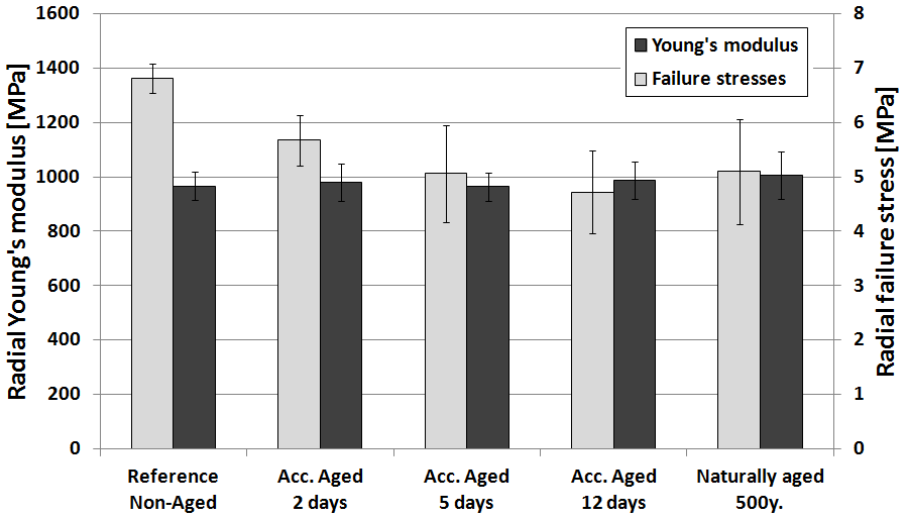

Figure 3.15: Comparison between non-aged, thermally aged and naturally aged wood. The TH treatment was done at 140°C, 10% RH and 1 bar.

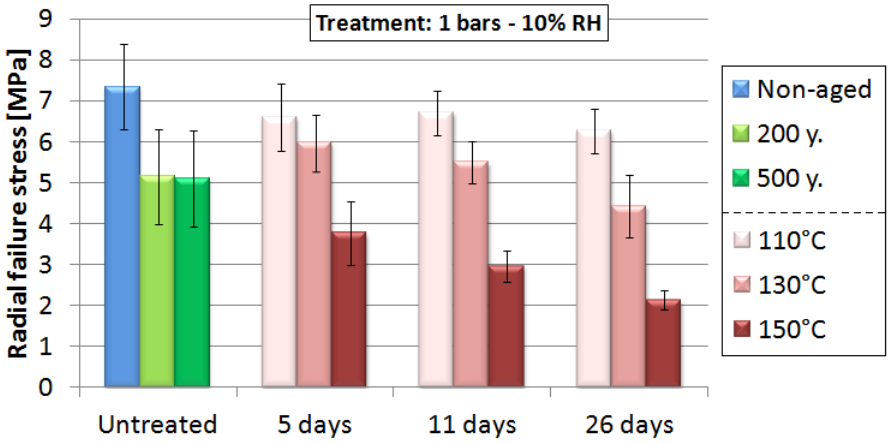

Figure 3.16: Influence of the treatment temperature on the radial failure stress for different treatments time.

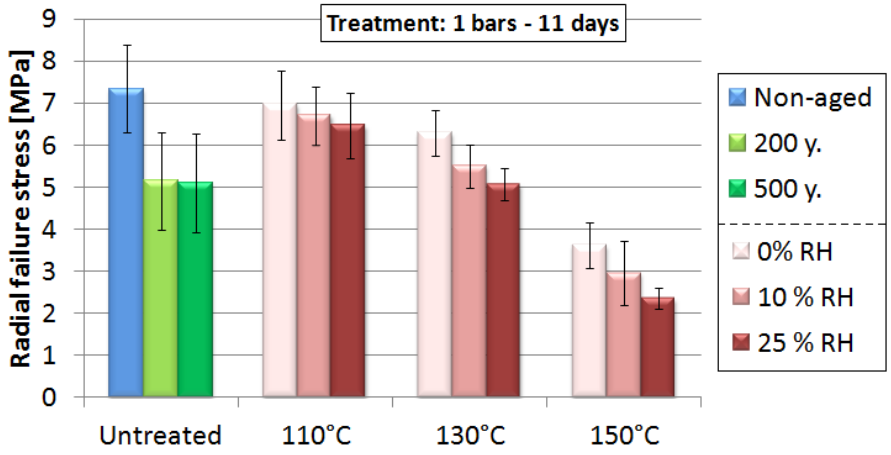

Figure 3.17: Influence of the treatment RH on the radial failure stress at different temperatures.

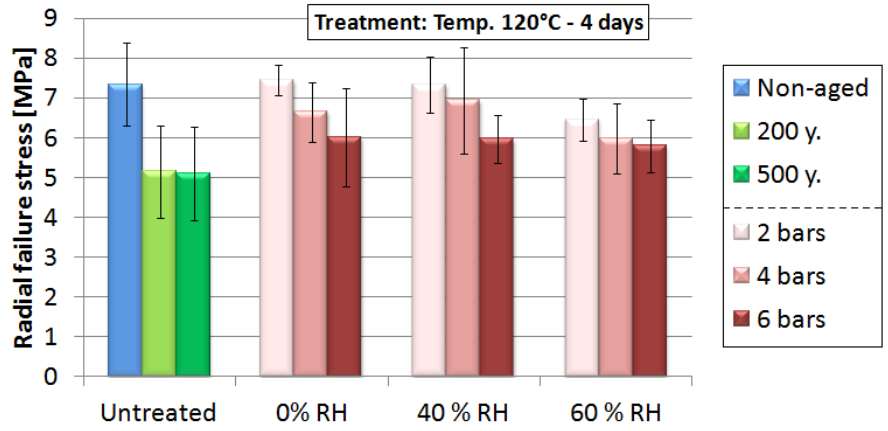

Figure 3.18: Influence of the reactor pressure on the radial failure stress at different treatment RH.

The influence of the treatment parameters are in accordance with general knowledge on thermal treatments (C. A. S. Hill, 2006). The loss of radial strength increases with the treatment time (figure 3.15), treatment temperature (figure 3.16), treatment RH (figure 3.17) and the reactor pressure (oxygen increases), (figure 3.18).

The effect of the treatment temperature on the strength is clearly non-linear. Indeed, Compared to 110°C, the 130°C values are about 15% lower for all durations, but the 150°C values are 55% lower.

The RH has an important influence on the loss of strength as well. Moreover, the influence of the RH seems to depend on the temperature. In the treatments presented in figure 3.17, the strength reduction between treatment at 0 and 10% RH is about 3.6% at 110°C and 18.3% at 150°C.

The treatment pressure has also a strong effect: Treatments (120-0-j-4) show about 10% strength reduction between 2 and 4 bars and 20% between 2 and 6 bars as shown in figure 3.18. This difference can be explained by the different amount of

oxygen in the reactor atmosphere: at higher pressure, more oxygen is able to oxidize the wood components.

On the other hand, the difference between the closed and the flux controlled pressure vessels is negligible (less than 1%). The difference between them is that in the closed system, the reaction gas released by the wood during the treatments remains in the reactor and can act as chemical catalyser.

The reproducibility of the thermal treatments is good. Two treatment (120-0-0-2) and (110-2-1-2) have been repeated on two sets of 5 specimens each, resulting in only 0.56% and 1.16%, respectively, of difference between each pair, much below the coefficient of variation within each set:12%.

Several tests have been carried out along L direction to compare our TH treatments with the results given in the literature. The L Young's modulus and failure stress for different treatment conditions are presented in figure 3.19. Our results are in good accordance with the results given in (C. A. S. Hill, 2006). The failure stress gets reduced with treatments temperature, moisture content and time. On the other hand, the Young's modulus is increased a little bit during the first days of the treatments: for example 2% after 26 days at (140-10-1). Afterwards, it decreases: -15% after 50 days of treatment (140-10-1).

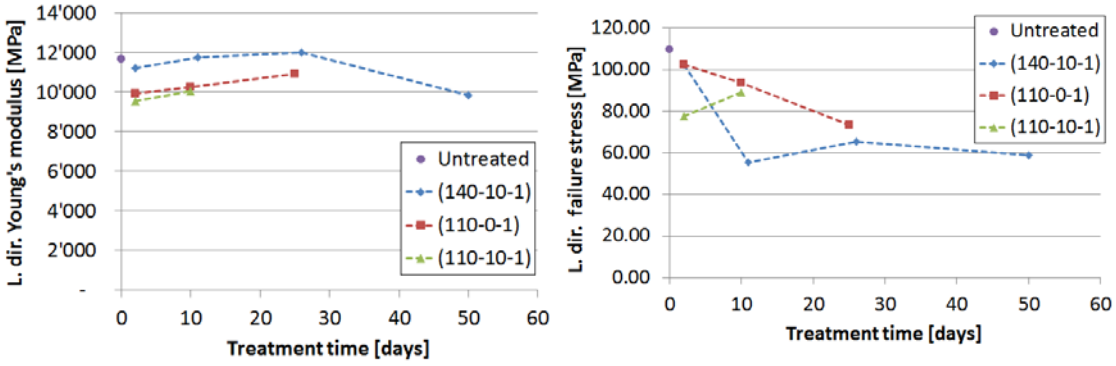

(a) (b)

Figure 3.19: Longitudinal Young's modulus in (a) and longitudinal failure stresses in (b) of non-aged and thermally aged samples by TH treatments.

3.2.4.1.2 Time dependent behaviour

Viscoelastic tests have been carried out with the micro-tensile testing device, following the experimental procedure described in section 2.3.3.3.

Figure 3.20 shows the relative creep for non-aged wood and some thermally aged wood. As for naturally aged wood, no change and no trend was detected in the time dependent behaviour.

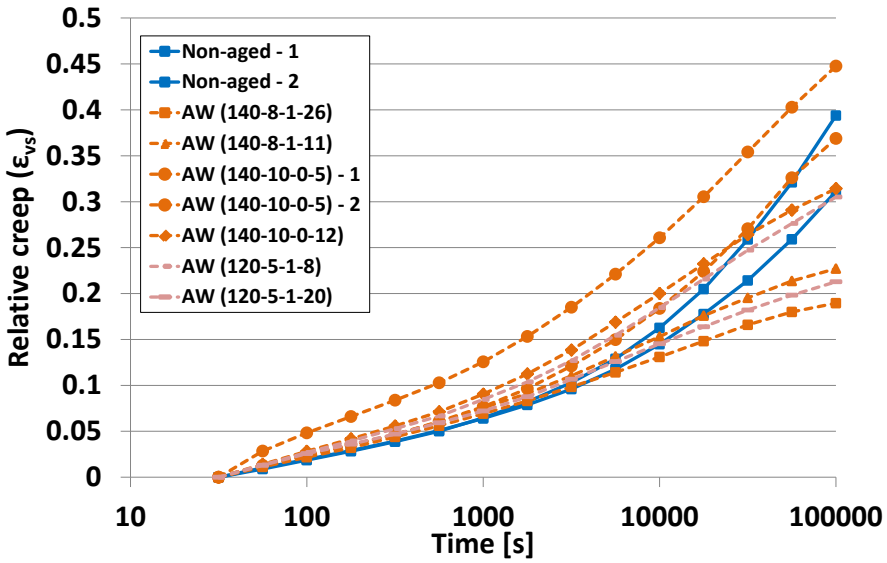

Figure 3.20: Radial relative creep strain ε_{VS} versus log time for non-aged and thermally aged spruce wood samples. Tests have been carried out at 22% RH and 23°C.

3.2.4.1.3 Mechanosorption

The mechanosorption tests have been carried out following the experimental procedure described in the section 2.3.3.4. Standard-shape samples have been used with a section of about *4.5x8 mm TxL*. The results are shown in table 3.5.

A marked decrease of mechanosorptive strain can be seen in the two treated wood samples, compared to naturally aged wood where no significant change has been observed (section 3.1.2.2.3). These results are in agreement with the strong reduction (or elimination) of the mechanosorption behaviour shown recently by (A. Straže *et al.*, 2012).

This loss has also to be related to the loss of hygroscopicity of treated wood (see next sections). However, for these two treated wood samples, the difference of the MC steps during the RH step from 76 to 22% is only 0.22% compared to non-aged wood.

Table 3.5: Mechanosorptive strain. ε_0 is the instantaneous strain; $\varepsilon_{ms,\ c1}$ and $\varepsilon_{ms,\ c3}$ are the strain after one and three cycles of relative humidity (RH) respectively; ε_{irr} is the final irreversible mechanosorptive strain after the final two RH cycles. Finally, each strain value is given relative to the instantaneous strain.

	Non-Aged 1	Non-Aged 2	AW (140-10-1-11)	AW (140-10-1-26)
ε_0	0.117	0.113	0.107	0.112
$\varepsilon_{ms,\ c1}$	0.377	0.335	0.236	0.211
$\varepsilon_{ms,\ c3}$	0.342	0.340	0.215	0.170
ε_{irr}	0.150	0.119	0.063	0.025
$(\varepsilon_{ms,\ c1} - \varepsilon_0)/\varepsilon_0$	2.22	1.97	1.20	0.88
$(\varepsilon_{ms,\ c3} - \varepsilon_0)/\varepsilon_0$	1.93	2.03	1.00	0.52
$\varepsilon_{irr}/\varepsilon_0$	1.28	1.06	0.59	0.22

3.2.4.2 Colour change of thermally aged wood

Accordingly to the experimental procedures described in section 2.5.3, the colour of the thermally aged wood samples has been measured by colorimetry in the CIELAB colour space.

The lightness L^* get invariably reduced by thermal treatment as shown in figure 3.21(a). The parameters a^* and b^* show non-linear changes with treatment times. These results are in accordance with the works of others authors (M. M. Gonzalez-Pena and M. D. C. Hale, 2009a, M. Matsuo et al., 2010). Moreover, the tendency seen in the naturally aged wood is similar, specifically for the lightness.

Figure 3.21(b) shows the chromatic parameters against the lightness. A linear relationship is seen in the lightness range from 75 to 40. That means that the lightness can be taken as a general indicator of the colour.

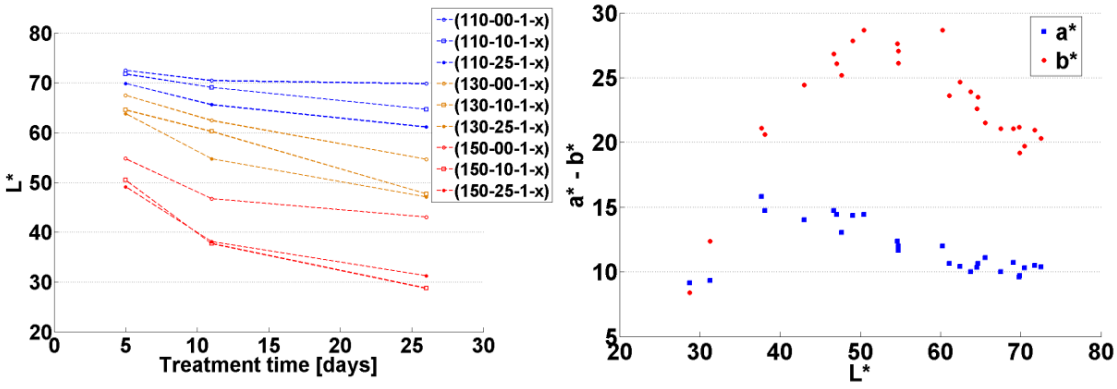

(a) (b)

Figure 3.21: (a) Change in lightness against treatment time. Chromatic parameters a* and b* against the lightness.

3.2.4.3 Sorption and diffusion modifications

3.2.4.3.1 Diffusivity

The diffusion coefficients along the longitudinal direction for different treatment conditions have been measured using the isothermal sorption chambers. The experimental procedure is described in section 2.4.2. The results are shown in figure 3.22.

No significant change was observed. A slight trend of increasing axial diffusion is observed in the samples treated at 140°C and 180°C. These increases can be due to the degradation of the piths due to the relatively high treatment temperatures of these last samples.

Anyway, comparing these coefficients with naturally aged wood, the accelerated aging samples did not exhibit similar changes. Indeed, it has been seen in section 3.1.2.5.1, that the diffusion along the L direction is reduced in old wood. This is clearly not the case for the accelerated aging. This fact can corroborate our theory that the loss of axial diffusion in old wood comes probably from a modification at the tissue or cell-wall level (e.g., pith obstruction) rather than a chemical modification of the wood material. Indeed, the effects of a potential chemical modification on D_L should be seen on the TH-treated samples.

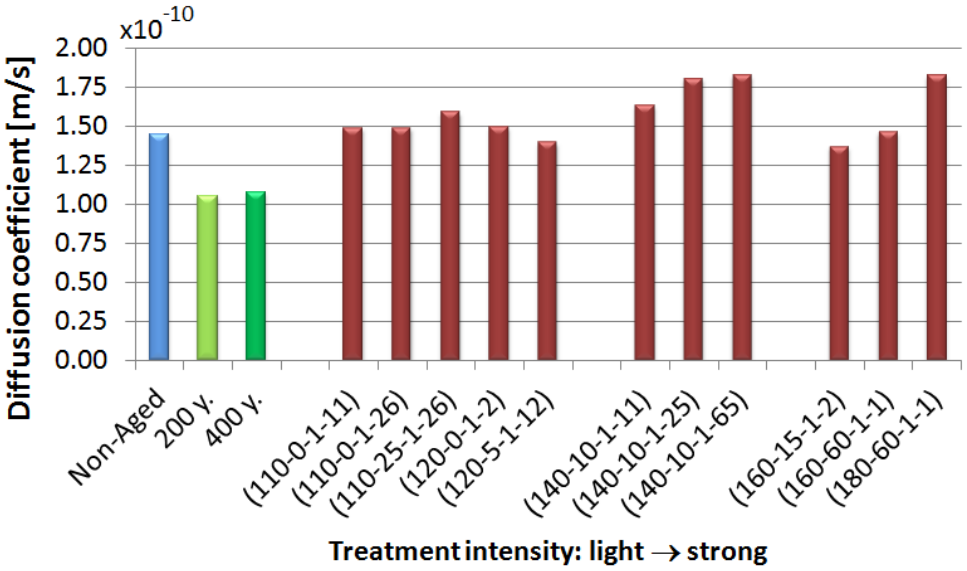

Figure 3.22: Longitudinal diffusion coefficients of non-aged, naturally aged and thermally aged spruce wood.

3.2.4.3.2 Sorption

The effect of the TH-treatment on the sorption behaviour of wood can be seen in figure 3.23. A reduction of the water-sorption is clearly seen. This reduction depends

closely on the treatment intensity. This is in accordance with the results found in literature (C. A. S. Hill, 2006).

As seen in section 3.1.2.5.2, natural aging of wood didn't show any important modification of the sorption behaviour. The loss of hygroscopicity of treated wood can be explained by the loss of sorption sites (OH groups) due to the degradation of the hemicelluloses. It can be deduced that the hemicelluloses are not similarly degraded during the natural aging than during the TH treatments.

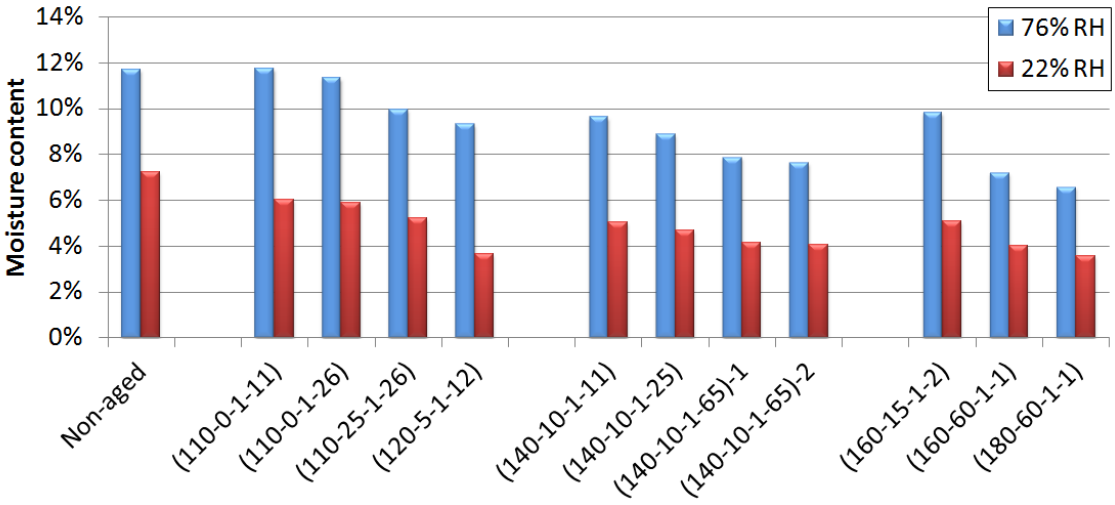

Figure 3.23: Comparison of the moisture content of non-aged and thermally aged spruce wood at 76 and 22 % of RH.

3.2.4.4 Chemical analysis

Thanks to the works of C. Ganne-Chédeville during a STSM at the Aalto University in Finland, FTIR-ATR (*Fourier Transform Infrared spectroscopy - Attenuated Total Reflection*), UVRR (*Ultraviolet Resonance Raman spectroscopy*) and XPS (*X-ray photoelectron spectroscopy*) characterisation of non-aged, naturally aged and thermally aged wood have been carried out (C. Ganne-Chédeville et al., 2011, L.-S. Johansson *et al.*, 2012).

These spectroscopy methods are fast and semi-invasive (they require just small chips) and give indications on the chemical composition of wood. In figure 3.24, the normalized FTIR spectra of the non-aged wood samples are shown with the identification of 22 peaks on characteristic bands. Each peak can be attributed to one specific chemical compound (E. Sjöström and R. Alén, 1992).

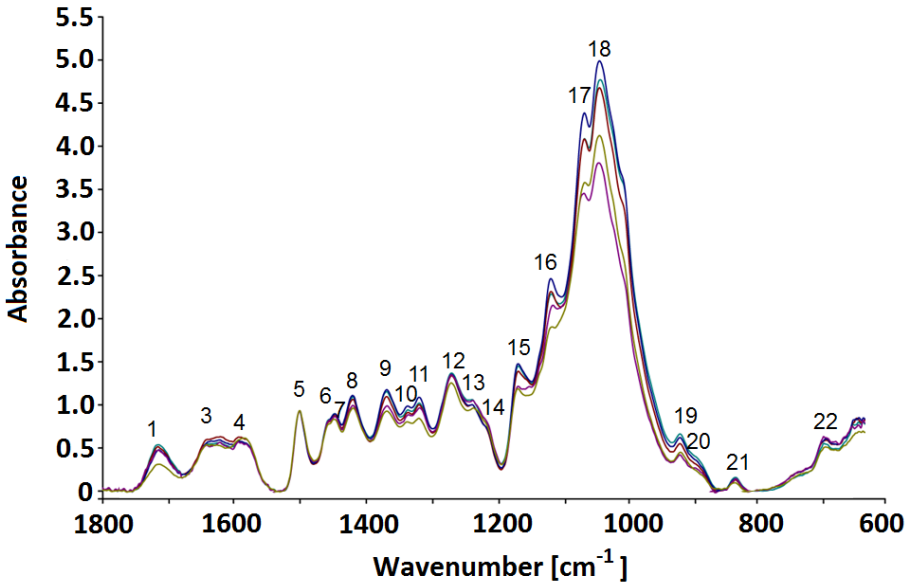

Figure 3.24: FTIR-ATR spectra of the non-aged sample. The numbers correspond to the band assignment.

No significant changes have been detected in the FTIR, UVRR and XPS spectra of the naturally aged wood. Mainly deterioration of hemicelluloses could be observed in FTIR spectra. UVRR spectra of naturally aged wood samples show that the small differences compared to non-aged spruce wood were due to acetone-extractable compounds. These compounds could include degradation products of the lignin or unsaturated wood extractives. As for the mechanical and physical characterisation, no time correlation has been found between the different naturally aged samples.

For artificial ageing treatment up to 160°C, the changes in the wood lignin were significant as shown in figure 3.25(a). This figure shows the comparison of corrected intensity ratios against carbohydrates. The carbohydrates are found in cellulose and should be not modified in an extensive way. The ratios show that the carbonyls groups decrease strongly for the samples (160-60-1-2) and (180-60-1-1). The thermal process (160-14-1-2) shows quite similar ratio to the natural ageing concerning the hemicelluloses. The results show though those modifications in the carbohydrate and lignin are happening.

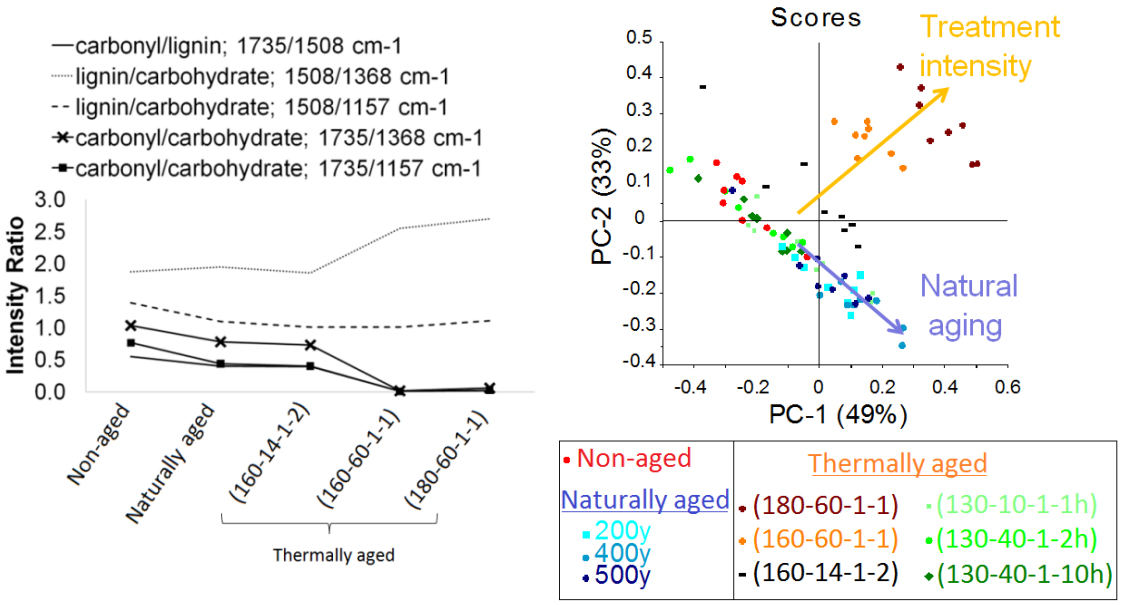

(a) (b)

Figure 3.25: (a) Corrected intensity ratio of the FTIR absorption bands which are characteristic for carbonyl, carbohydrate and lignin. (b) PCA analysis on UVRR spectra. Note: the times of treatments at 130°C are in hours.

Using the UVRR spectra a PCA[1] (*Principal component analysis*) using the NIPALS algorithm (*Nonlinear Iterative Partial Least Squares*), has been calculated as shown in figure 3.25(b). This analysis shows that treatment at high temperature (> 160°C) induce dissimilar reaction compare to natural aging. On the other hand the treatments done at 130°C are more comparable to the natural aging.

3.3 Aging Law

3.3.1 Analysis between natural and accelerated aging

The comparison between naturally aged and thermally aged wood carried out in the previous sections has shown some similarities but some differences as well.

The changes in the chemistry of thermally and naturally aged wood concern hemicelluloses and the lignin. From our results on sorption, the changes in hemicelluloses seem to differ. On the other hand radial strength and colour lightness show similar trends.

[1] PCA is a mathematical analysis used to simplifying a data set. It consists to reduce multidimensional data sets to lower dimensions. The resulting principal components (PC-i) are classified by variance (i.e. PC-1, the first PC has the largest possible variance). PCs don't have any physical meaning.

It is known that radial wood failure occurs at cells interfaces, between S1 and S2 or in the middle lamella. These locations are mainly composed of lignin. Lignin is quite stable thermally, its degradation starts above 200°C. However, some structural changes, and some oxidation have been detected in the lignin at only 50°C (C. A. S. Hill, 2006). Borgin *et al.* show oxidation of lignin on naturally aged oak and pine samples 900 to 4400 years old (K. Borgin et al., 1975a). In conclusion, the changes (mainly oxidation and hydrolyse) in the lignin seems to be similar between natural and accelerated aging.

No clear correlation with time (age) was found between naturally aged samples. This shows that not only aging time plays a role in the kinetics of the chemical reactions. As mentioned above, the thermodynamics states that wood should tend to minimise it free energy. However, to reach a new, more stable state energetic barriers (quantified by an activation energy) must be passed over. Environmental condition, specifically the temperature and relative humidity, can modify this activation energy resulting in a modification of the kinetics of the reactions.

Objective N°3:

Our third objective will be to verify the existence of a law for wood aging. The modification taking place during the accelerated thermo-hydrous treatments will be fitted to the kinetic chemical law. Next, an extrapolation at ambiance condition will be performed to simulate the natural aging.

3.3.2 Aging law investigation

From the comparison between naturally and thermally aged wood the aging law will be applied first on the radial strength property. Relatively low temperature and low RH of the accelerated aging treatments have been used to avoid strong degradation of polymeric molecules of wood. No treatment above 150°C and 25% RH was included in the fitting of the aging law. This decision is made following the results obtained by chemical analysis given in figure 3.25(b).

In order to build the aging law from the accelerated aging experiments, the following hypotheses are considered:

1. Chemical reactions are similar between thermally aged wood and naturally aged wood
2. Radial strength properties is proportional to the aging chemical reactions

We define the relative radial strength γ as:

$$\gamma = \frac{\sigma_f}{\sigma_{f0}} \tag{3-4}$$

with σ_f the radial failure stress and σ_{f0} the radial failure stress of non-aged spruce wood. The kinetic law of a chemical reaction such as $A + B \leftrightarrow C$ is the following:

$$\frac{\mathrm{d}[A]}{\mathrm{d}t} = -k[A]^{\alpha}[B]^{\beta} \tag{3-5}$$

with *[i]* the concentrations of the chemical specie *i*, *k* the rate constant and $\alpha + \beta$ define the order of the reaction. In our case, *A* represent wood lignin and/or hemicellulose and *B* oxygen and/or water. As oxygen and water are in excess, the evolution of their concentration over time is null. Therefore $\beta = 0$. From hypothesis number 2, γ is assumed proportional to *[A]*:

$$\frac{\mathrm{d}\gamma}{\mathrm{d}t} = -k(T, m, p_{O2})\gamma^{\alpha} \tag{3-6}$$

This equation gives the rate of strength degradation in terms of *k* which is function of temperature, wood moisture content and oxygen (given by partial pressure). The integration of this equation depends on the order of the reaction *α*. For the moment, let consider the order α equal 1, which gives:

$$\gamma(t) = e^{-k(T,m,p_{O2})t} \tag{3-7}$$

Using this last equation on experimental data, different $k(T_i, m_i, p_i)$ have been calculated for different treatment settings. These calculations for treatments at 130°C are shown in figure 3.26: A set of treatments has been done at constant temperature, RH and pressure for different treatment times. Then, linear regression is done on the natural logarithm of *γ*. Three treatment temperatures: 110, 130 and 150°C and three treatments RH 0, 10 and 25% have been investigated. Only atmospheric pressure has been considered. A set of 9 rate constants have been calculated as shown in table 3.6.

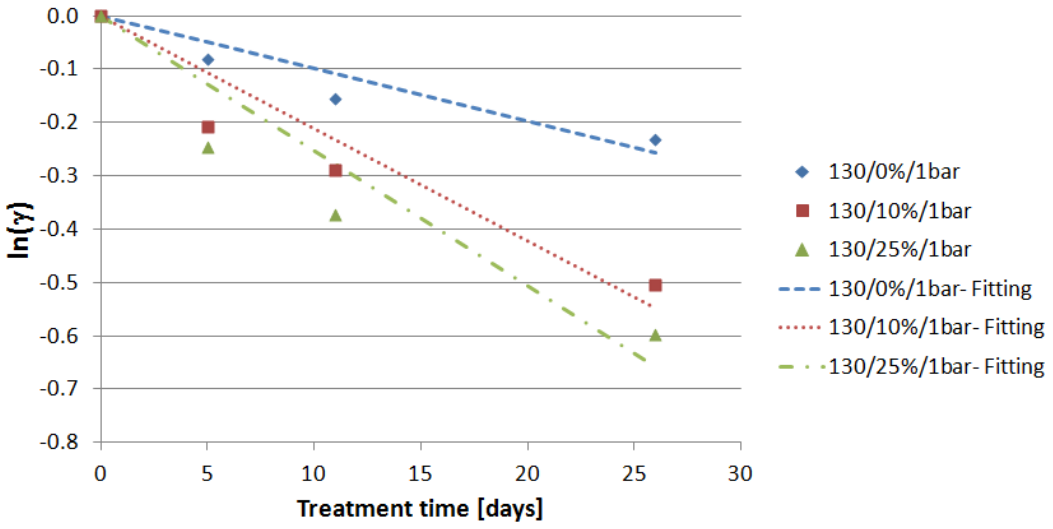

Figure 3.26: Calculation of the rate constant *k* by linear regression of the natural logarithm of γ for reaction order α equal 1.

Some corrections have been made on the strength values of the treatments at 10 and 25% of RH. Indeed, our TH-reactors can maintain constant RH during the treatment. However, the sorption behaviour of wood depends on the temperature. Therefore, the moisture content at 10% RH for treatments at 110°C is not the same as the ones at 150°C for example. The correction has been made on the treatment at 110 and 150°C. The ones at 130°C have been taken as the MC of reference. The differences of MC between 10 and 25 % of RH has been calculated using the equation (2-2) from the generalized BET model (see section 2.1.2 for more information). Next the difference of strength between the treatments at 10 and 25% RH has been determined and a linear correction has been made from the differences of MC. These corrections induce a change of ±*0.05* MPa on the strength (i.e. ±*6%*).

Table 3.6: Rate constant $k(T_i, m_i)$ for the different TH-treatments [days^{-1}]*10^3.

	110°C	**130°C**	**150°C**
0% RH	2.85	8.49	29.76
10% RH	4.47	17.92	42.75
25% RH	9.73	21.91	75.85

Next, the dependence of k upon the temperature has been assumed to follow an Arrhenius law:

$$k(T) = k_0 e^{-\frac{E_a}{RT}} \tag{3-8}$$

where E_a is the activation energy of the reaction and R is the gas constant (*8.314 J K^{-1}mol^{-1}*). Here also, a linear regression on the natural logarithm of this equation has been used to determine k_0 and E_a with the different rate constants as shown in figure 3.27.

The activation energy E_a is slightly lower than other studies: Millet et al. (1972) found 28.7 [kcal mol^{-1}] which gives 120 [kJ mol^{-1}] and Matsuo et al. (2010) in their colour change investigation found activation energies between 95 and 117 [kJ mol^{-1}]. However, both of them have worked on dry thermal treatments only.

The activation energy seems to depend weakly on the moisture content. Therefore, the impact of the treatment MC has been integrated into k_0. The evolution of $k(m)$ has been estimated with an exponential law as shown in figure 3.28.

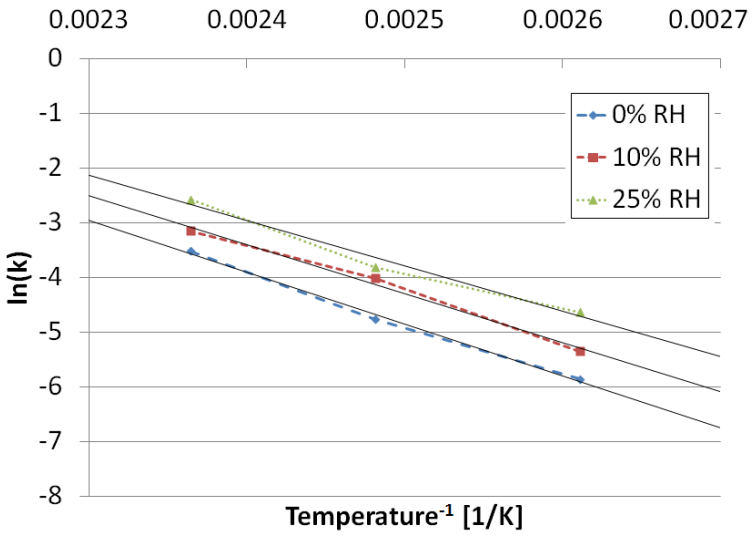

Figure 3.27: Representation of the natural logarithm of the Arrhenius equation (3-8). The slope of this curve is E_a/R.

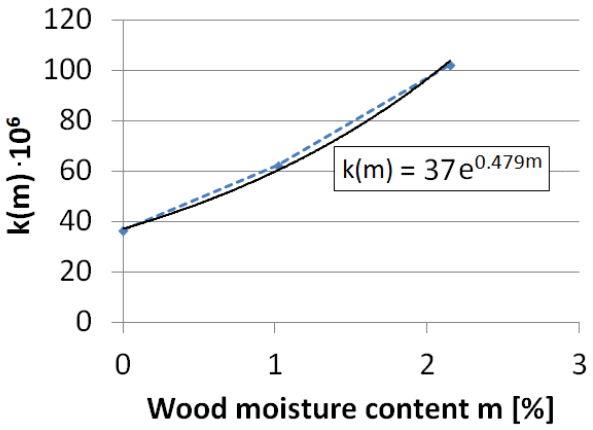

Figure 3.28: Rate constant $k_0(m)$ with respect to the wood moisture content during the treatment. This function has been fitted on an exponential law.

The final form of the law of aging is then:

$$\gamma(T,m,t) = \exp\left(k_0 \cdot t \cdot e^{Bm} \cdot e^{-\frac{E_a}{RT}} \right) \tag{3-9}$$

where the calculated parameters from the experimental results are E_a, B and k_0. In order to optimise the precision of the parameters, fitting of the law using the minimisation of the mean square differences by a *generalised reduction gradient* algorithm (GRG) have been carried out. The final value of the parameters is:

k_0 = $700 \cdot 10^6$ [days-1]
E_a = 82'500 [J mol-1]
B = 33 [-]

Extrapolation of the aging law

The aging law defined in equation (3-9) can be first used to predict the degradation of the radial strength after thermal treatment. The range of validity of the law is for temperatures lower than 150°C, treatment RH between 0 and 25% and under atmospheric pressure. An example of such comparison can be seen in figure 3.29 where experimental strength is compared with simulations. However, the law can also be extrapolated to standard climate conditions, in order to predict the effect of natural aging. The aging time for a given strength loss can be derived from equation (3-9):

$$t = \frac{\ln(\gamma)}{-k_0 \cdot e^{Bm} \cdot e^{-\frac{E_a}{RT}}} \tag{3-10}$$

For example, for a typical loss of strength of 20%, under of 20°C and 10% MC, the time of natural aging would be about 250 years as shown in figure 3.30.

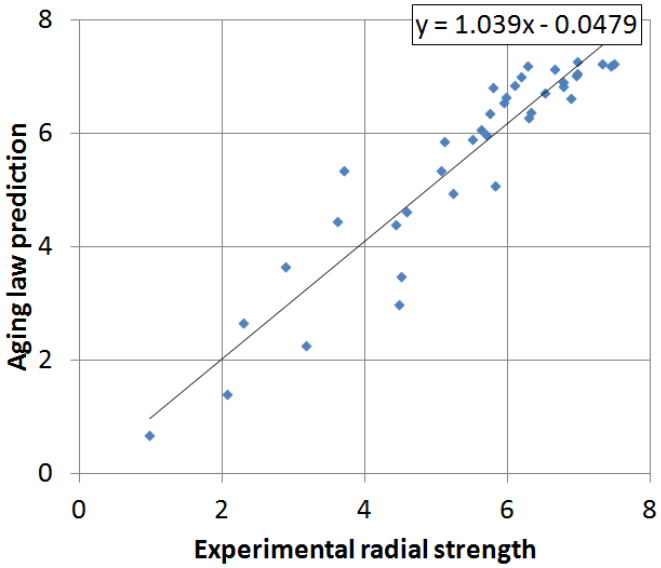

Figure 3.29: Prediction of the radial strength of the aging law with respect to the experimental strength.

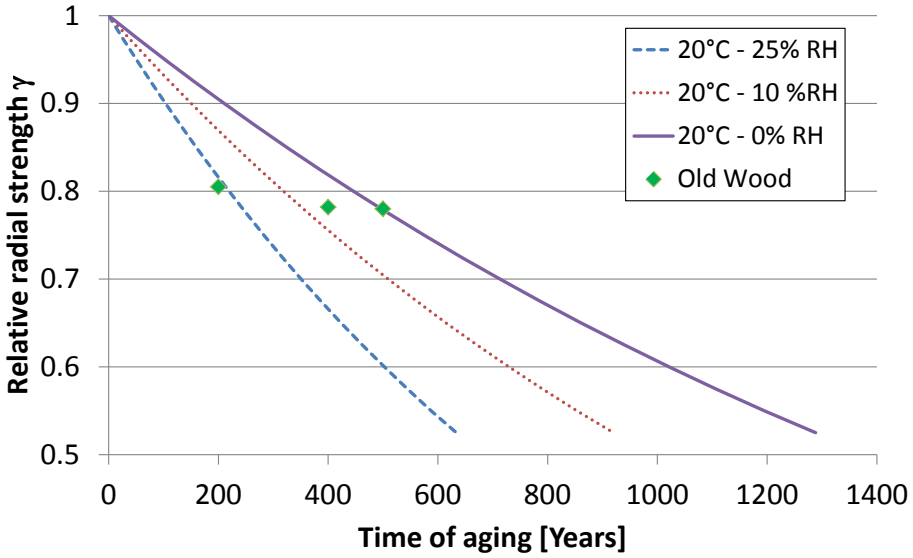

Figure 3.30: Extrapolation of the aging law for natural aging. Degradation of the radial strength is shown for three humidity-temperature conditions and compare to the natural aging.

3.3.3 Mathematical analysis of the aging law

The prediction of the law of aging required the knowledge of the *average climate history (ACH)* of the old wooden artworks (i.e. the mean temperature and moisture content of the wood during his past history). This information is in fact difficult to acquire precisely. However, the procedure for determining the aging law parameters can be done on other materials properties such as the colour. Indeed, colour does not require a destructive testing and therefore can be accessible on an old painting. If the colour changes happened to be linked with the radial strength losses, the ACH could be estimated with the colour and next the strength could be estimated for that ACH.

3.3.3.1 Reaction order

In the previous section, the reaction order has been taken as *1*, which leads to equations (3-7). The comparison between the experimental and simulated strength values shows quite good matching as shown in figure 3.29. However, according to (J. Dlouhà *et al.*, 2009), the matching has to be done on the strength values but also on the slope against time. A phase diagram can be built, representing the strength against its log time derivative. The axis values are the following:

$$\begin{aligned} X &: \sigma_f \\ Y &: \frac{-\mathrm{d}\sigma_f}{\mathrm{d}\log(t)} \cong -t\frac{\mathrm{d}\sigma_f}{\mathrm{d}t} \end{aligned} \qquad (3\text{-}11)$$

A phase diagram, including the experimental and the model values was plotted in figure 3.31. With *n = 1* (i.e. equivalent to a reaction order of *1*), the model does not really match the slope of the experimental data.

As shown above, the theory of chemical kinetic includes an order of the reaction, as shown in equation (3-6). The problem with such equation is that if $\alpha \neq 1$, there is a time limit of the reaction (i.e. the time to reach 100% of loss stresses in not infinity). Therefore, the reaction order parameter has been changed to *n* using the follow expression:

$$\sigma_f(t) = \sigma_0 \exp\left(-k(T,m)\cdot t^n\right) \tag{3-12}$$

The slope for the phase diagram becomes:

$$\frac{\mathrm{d}\sigma_f}{\mathrm{d}\log(t)} = \sigma_0 t^n k(T,m) n e^{-k(T,m)t^n} \tag{3-13}$$

The phase diagram in figure 3.31 shows that a reaction order of about *n = 0.5* matches better the experimental values than *n = 1* for both, the radial strength and the lightness.

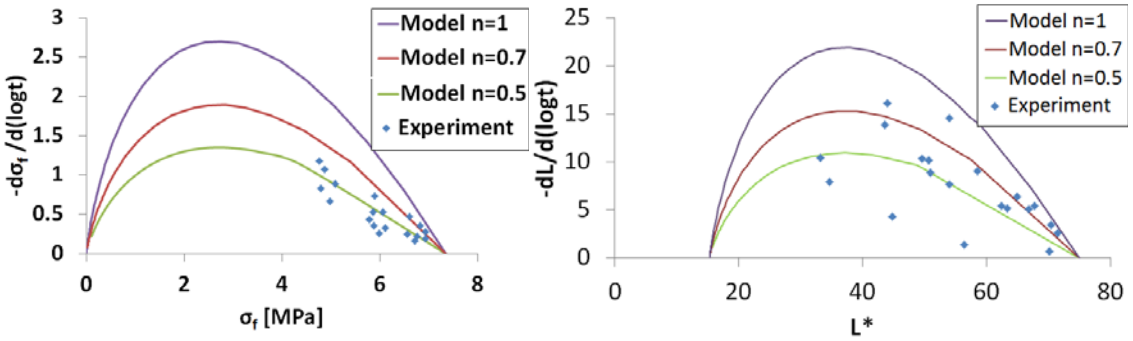

(a) (b)

Figure 3.31: Phase diagram showing the radial strength (a) and the lightness (b) against its slope for different reaction order *n*.

3.3.3.2 Fitting and extrapolation

Figure 3.32 shows the experimental radial strength against the lightness. A clear linear relation can be seen between each other. Therefore, by knowing the colour lightness *L** of an old wood, the strength can be calculated simply with:

$$\sigma_f = 0.1294 \cdot L^* - 2.19 \tag{3-14}$$

The figure 3.32 shows in red the strength and the lightness of the old wood samples. It confirms that the lightness and the radial strength are modified in similar manners between the two processes.

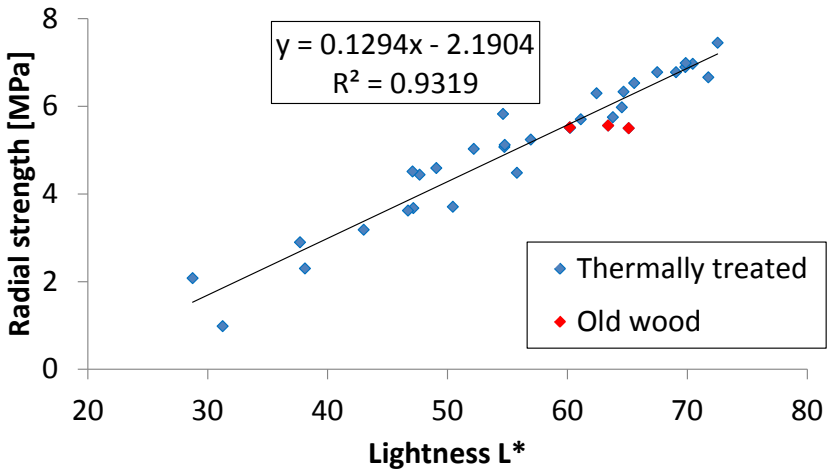

Figure 3.32: Linear relation between the radial strength and the lightness of thermally treated wood and old wood samples.

A direct fitting has been made for the radial strength σ_f and the colour lightness L^*, by minimising the mean square difference by a *generalised reduction gradient* algorithm (GRG). The variables of the fitting were: n, k_0, B, E_a, σ_0, L_0 and L_∞. The final aging equations are:

$$\begin{cases} \sigma_f(t) &= \sigma_0 e^{-k(T,m)\cdot t^n} \\ L^*(t) &= L_0^* e^{-k(T,m)\cdot t^n} + L_\infty^* \end{cases} \tag{3-15}$$

with:

$$k(T,m) = k_0 \cdot e^{Bm} \cdot e^{-\frac{E_a}{RT}} \tag{3-16}$$

The evolution of the lightness with treatment intensity does not tend to 0. This tendency can be clearly seen in figure 3.32. Therefore a limit lightness L_∞ has been incorporated to the aging law. The results of the fitting are shown in table 3.7. Figure 3.33 shows the fitting of the radial strength and lightness.

Table 3.7: Results of the fitting of the aging law on radial strength and lightness.

σ_0	7.49 [Mpa]	k_0	2.55E+07 [days^{-1}]
L^*_0	59.68 [-]	B	23.7 [-]
L^*_∞	15.34 [-]	E_a	66.0 [kJ mol^{-1}]
		n	0.51 [-]

The extrapolation for naturally aged samples is represented in red in figure 3.33 (a) and (b). The average climate history has been first estimated on the lightness aging law: Temperature of 25°C and MC of 8.8% (about 50% RH) has been calculated. The same ACH has been next used for the calculation of the strength.

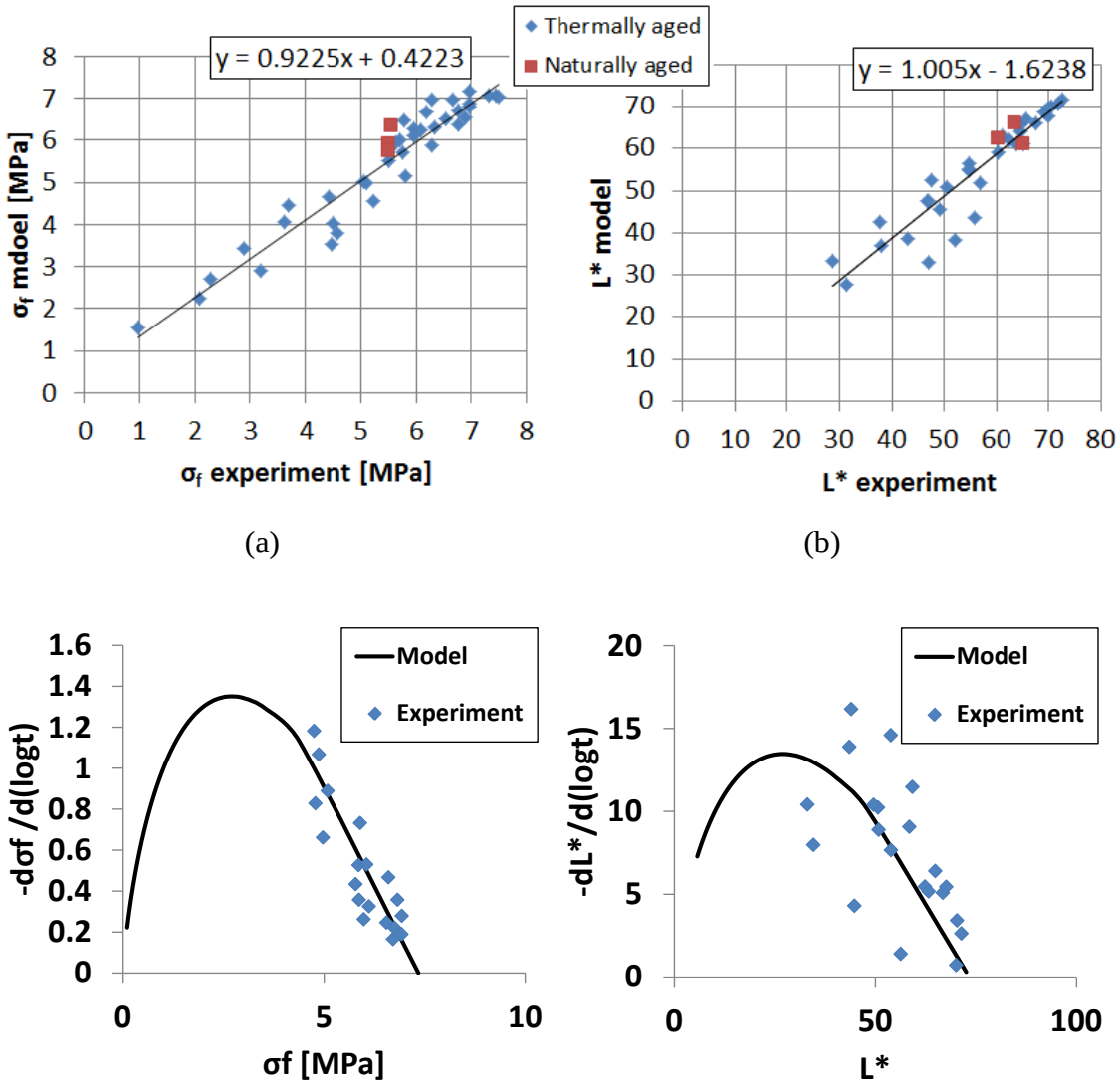

Figure 3.33: Fitting of the aging law for radial strength (a) and lightness (b). These last graphics show the model versus the experimental values of thermally aged wood (in blue) and naturally aged wood (in red). The fitting of the slope is seen on the phase diagrams (c) and (d) for the radial strength and lightness respectively.

3.4 Conclusion

An aging law of spruce wood for radial strength and as well as colour lightness has been successfully found. Natural aging depends on the time of aging - of course - but also on the climate history (temperature and RH). The application of the aging law requires the use of an “average climate history”. However, the radial strength and the colour lightness are linearly linked. Therefore, the loss of radial strength of an old painting can be estimated by the colour lightness. However, it is required to have access to an unpainted part of the old painting that has remained protected from light source or other surface aging, and that can be refreshed.

In order to predict the loss of strength of an old painting in the future, the ACH can be calculated from the aging law of the lightness and next the same ACH is applied on the radial strength.

This procedure will be applied in a case study on an old painting in chapter 6.

3.5 References

BORGIN, K., FAIX, O. & SCHWEERS, W. 1975a. The effect of Aging on Lignins of wood. *Wood Science and Technology,* 9**,** 207-211.

BORGIN, K., PARAMESWARAN, N. & LIESE, W. 1975b. The effect of aging on the ultrastructure of wood. *Wood Science and Technology,* 9**,** 87-98.

DLOUHÀ, J., CLAIR, B., ARNOULD, O., HORÀCEK, P. & GRIL, J. 2009. On the time-temperature equivalency in green wood: Characterisation of viscoelastic properties in longitudinal direction. *Holzforschung,* 63**,** 327-333.

ERHARDT, D. & MECKLENBURG, M. 1996. Accelerated vs Natural Aging: Effect of Aging Conditions on the Aging Process of paper. *Material Issues in Art and Archaeology IV,* 352**,** 247-270.

ERHARDT, D., MECKLENBURG, M. F., TUMOSA, C. S. & OLSTAD, T. M. 1996. New versus old wood: differences and similarities in physical, mechanical, and chemical properties. *ICOM Preprints, 11th Triennial Meeting,* 2**,** 903-910.

FROIDEVAUX, J., VOLKMER, T., GANNE-CHÉDEVILLE, C., GRIL, J. & NAVI, P. 2012. Viscoelastic behaviour of aged and non-aged spruce wood in the radial direction. *Wood Material Science and Engineering,* 7**,** 1-12.

GANNE-CHÉDEVILLE, C., JÄÄSKELÄINEN, A. S., FROIDEVAUX, J., HUGHES, M. & NAVI, P. 2011. Natural and artificial ageing of spruce wood as observed by FTIR-ATR and UVRR spectroscopy. *Holzforschung,* 66**,** 163-170.

GEREKE, T. 2009. *Moisture-induced stresses in cross-laminated wood panels.* ETH Zürich.

GONZALEZ-PENA, M. M. & HALE, M. D. C. 2009a. Colour in thermally modified wood of beech, Norway spruce and Scots pine. Part 1: Colour evolution and colour changes. *Holzforschung,* 63**,** 385-393.

GONZALEZ-PENA, M. M. & HALE, M. D. C. 2009b. Colour in thermally modified wood of beech, Norway spruce and Scots pine. Part 2: Property predictions from colour changes. *Holzforschung,* 63**,** 394-401.

HILL, C. A. S. 2006. *Wood modification: chemical, thermal and other processes,* John Wiley \& Sons.

JOHANSSON, L.-S., CAMPBELL, J. M., HÄNNINEN, T., GANNE-CHÈDEVILLE, C., VUORINEN, T., HUGHES, M. & LAINE, J. 2012. XPS and the medium-dependent surface adaptation of cellulose in wood. *Surface and Interface Analysis.*

KOHARA, J. 1952. Studies on the durability of wood I, mechanical properties of old timbers. *Bulletin of Kyoto Prefectural University,* 2**,** 116-131.

KOHARA, J. 1953. Studies on the permanence of wood V, shrinkage and swelling of old timbers about 300-1300 years ago. *Bulletin of Kyoto Prefectural University,* 5**,** 81-88.

KOHARA, J. 1954a. Studies on the permanence of wood VI, the changes of mechanical properties of old timbers. *Bulletin of Kyoto Prefectural University,* 6**,** 164-174.

KOHARA, J. 1954b. Studies on the permanence of wood VII, the influence of age on the components of wood (Chamaecyparis obtusa Endlicher). *Bulletin of Kyoto Prefectural University,* 6**,** 175-182.

KOHARA, J. 1955a. On permanence of wood II, differences between the ageing processes of cypress wood and zelkova wood. *Wood industry,* 10**,** 395-399.

KOHARA, J. 1955b. Studies on the permanence of wood XV, the influence of age on the components of wood (Zelkowa serrata Makino). *Mokuzai Gakkaishi,* 1**,** 21-24.

KOLLMAN, F. 1951. *Technologie des Holzes und der Holzwerkstoffe,* 2. Auflage, Springer, Berlin.

MATSUO, M., YOKOYAMA, M., UMEMURA, K., GRIL, J., YANO, K. I. & KAWAI, S. 2010. Color changes in wood during heating: kinetic analysis by applying a time-temperature superposition method. *Applied Physics A-Materials Science \& Processing,* 99**,** 47-52.

MATSUO, M., YOKOYAMA, M., UMEMURA, K., SUGIYAMA, J., KAWAI, S., GRIL, J., KUBODERA, S., MITSUTANI, T., OZAKI, H., SAKAMOTO, M. & IMAMURA, M. 2011. Aging of wood: Analysis of color changes during natural aging and heat treatment. *Holzforschung,* 65**,** 361-368.

MILLETT, M. A. & GERHARDS, C. C. 1970. Accelerated Aging: Residual Weight and Flexural Properties of Wood Heated in Air at 115° to 175°C. *Wood science,* 4**,** 193-201.

OBATAYA, E. 2007. Caractéristiques du bois ancien et technique traditionnelle japonaise de revêtement pour la protection du bois. *Actes de la journée d'étude Conserver aujourd'hui : les vieillissements du bois.* Cité de la Musique, Paris, France.

OBATAYA, E. Effects of ageing and heating on the mechanical properties of wood. Wood Science for Conservation of Cultural Heritage, Proceedings of the International Conference held by COST Action IE0601, 2009 Florence, Italy. 16-23.

SIAU, J. F. 1984. *Transport processes in wood,* Springer-Verlag.

SJÖSTRÖM, E. & ALÉN, R. 1992. *Analytical Methods in Wood Chemistry, Pulping, and Papermaking,* Springer.

STRAŽE, A., GORIŠEK, Z., PERVAN, S., FROIDEVAUX, J. & NAVI, P. 2012. Mechano-sorptive creep of heat treated and innate beechwood. *In:* LORRAINE, U. D. (ed.) *COST Action FP0904: Current and Future Trends of Thermo-Hydro-Mechanical Modification of Wood. Opportunities for new markets ?* Nancy, France.

YOKOYAMA, M., GRIL, J., MATSUO, M., YANO, H., SUGIYAMA, J., CLAIR, B., KUBODERA, S., MISTUTANI, T., SAKAMOTO, M., OZAKI, H., IMAMURA, M. & KAWAI, S. 2009. Mechanical characteristics of aged

Hinoki wood from Japanese historical buildings. *Comptes Rendus Physique*, 10**,** 601-611.

Chapter 4
Paint aging

Paintings are composed of a substrate and a multi-layered paint. In the previous chapter the aging of the wooden substrate has been defined and investigated. However, aging also occurs in the paint. The aging in terms of mechanics, physics and chemistry of the multi-layered paint is investigated in this chapter. Parts of the following work on the multi-layered paint have been carried out by the team of BFH-HKB (Bern University of Applied Sciences – Bern University of the Arts).

4.1 Multi-layered paint

4.1.1 Description

The paints materials used in paintings can vary considerably due the different pigments and materials used. A representative medieval multi-layered paint has been selected in this project. It is composed of two layers: a ground layer and a paint layer as shown in figure 4.1. The paint layer consists of linseed oil with white lead pigments (G. H. Hutchinson, 1973). The ground layer is composed of chalk and glue.

4.1.2 Preparation

The medieval multi-layered paint selected to investigate the painting behaviour has been produced by the team of BFH-HKB. The multi-layered paint has been applied on two different substrates, on wood panels to reproduce paintings, and on plastic sheet (Silicone coated Hostaphan® RNT 36 - Kremer GmbH & Co. KG) to isolate the different layers (paint and ground) from the substrate. The application of the different layers was made with a *Film Applicator Model 360* to control precisely the thickness of the layers. The drying of the paint layers was done at room temperature (23°C – 50% RH) under dark condition during 1 week.

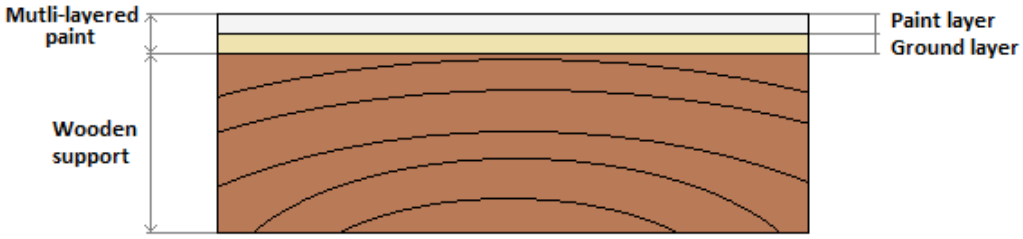

Figure 4.1: Sketch of the multi-layered paint selected in this project. The multi-layered paint is composed of two layers: paint and ground layers.

4.2 Accelerated ageing of oil paint

To study the mechano-physical behaviour and chemical alterations of old painted layers, series of oil paint samples were produced and aged artificially. The idea was to find, as for wood, an aging law able to predict the properties of an old paint. These technics are well known for polymeric materials (A. Miszczyk and K. Darowicki, 2001, P. L. Bégin and E. Kaminska, 2002, R. L. Feller, 1994). However, it is known that for many polymeric materials the principle of time-temperature equivalence, as described for instance by the Arrhenius equation, does not apply due to many competing reactions occurring simultaneously during aging (M. Celina *et al.*, 2005). The glass transition temperature (M. Warren and J. Röttler, 2008) or the diffusion of oxygen in the polymer (L. Audouin *et al.*, 1994) could also have an important effect on the accelerated treatments. However, under low thermal condition (40 – 60 °C), this principle might be applicable, resulting in the possibility to accelerated the aging in a predictable way.

The ground layer has not been incorporated in this aging study. This aging investigation and the chemical analysis have been done by the team from BFH-HKB and has been published (S. Zumbühl et al., 2011).

4.2.1 Experimental procedures

To accelerate the chemical reactions occurring during natural aging of the paint layer (first layer of the multi-layered paint), the temperature has to be raised up. However, as for wood, the RH and the oxygen content of the atmosphere play also an important role. Moreover, the light and specifically the UV light can induce chemical changes on photosensitive chemical components.

Accelerating aging treatments chambers have been built in BFH-HKB. These chambers are able to maintain a constant temperature, relative humidity, oxygen partial pressure and UV-light exposure during a determined amount of time. A picture of such system is shown in figure 4.2.

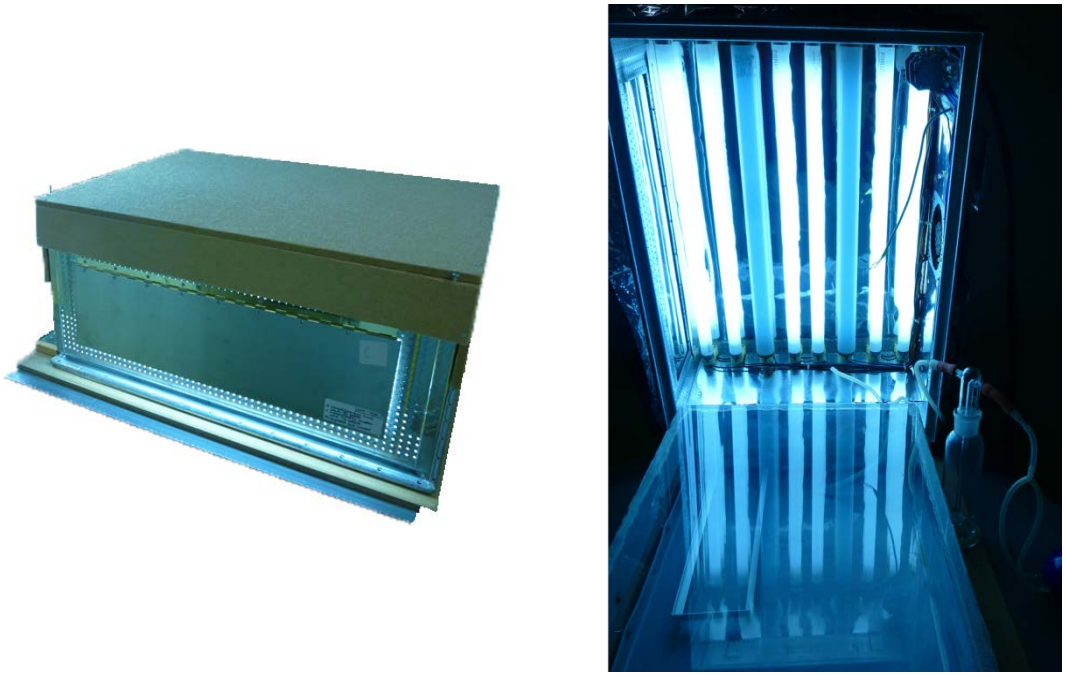

(a) (b)

Figure 4.2: Paint aging chamber. Close (a) and open (b) condition.

In this investigation four different accelerated aging conditions (Temperature-RH): 40-55, 40-75, 60-55 and 60-75 over periods of 3, 6 and 9 weeks for each were considered. Moreover, two different old paints were taken as reference for the chemical analysis: one containing lead white 106 years-old and another containing zinc white 108 years-old. These old paints came from small sampling on old paintings and therefore the quantity was very limited.

4.2.2 Chemical analysis

The chemical investigation was done by FTIR (Fourier transform infrared spectroscopy) and GCMS (Gas chromatography mass spectrometry) by the team of HKB-BFH.

The possible reactions in the oil paint are numerous and are strongly dependent on the treatment conditions (E. N. Frankel, 1998). Moreover these reactions can occurs simultaneously or sequentially. Some are photosensitive, some not. The different reactions pathways for the lipid oxidation are shown in figure 4.3. The sensitivity to temperature and light is indicated.

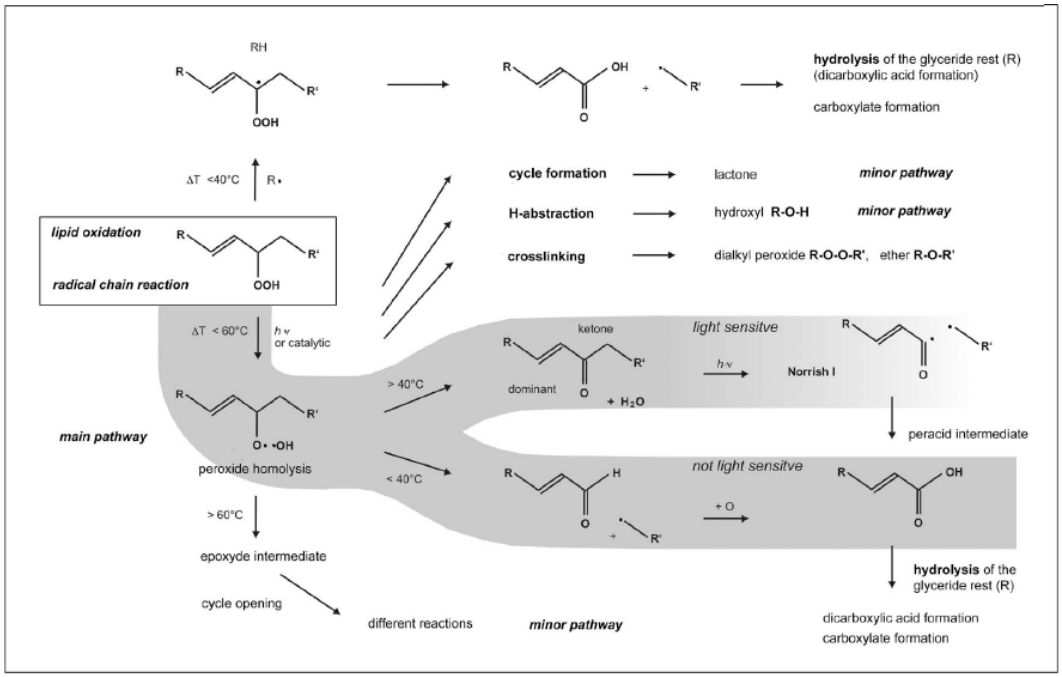

Figure 4.3: Reaction pathways of lipid oxidation and fragmentation (S. Zumbühl et al., 2011).

When comparing old paint with artificially aged paint, significantly different reactions are evidenced (S. Zumbühl et al., 2011). Therefore the accelerated treatments cannot be regarded as similar to natural aging. The multitude of reactions that occurs during the natural aging cannot be accelerated equally even at 40°C. These results show that to justify the accelerated aging of the paint layer still needs considerable research efforts.

4.3 Characterisation of the multi-layered paint

4.3.1 Permeability

The permeability of the non-aged and thermally aged paint layer has been measured in BFH-HKB with the cup method by M. Müller and G. Di Pietro. The permeability of the multi-layered paint has been calculated through inverse methodology using mass loss values measured with the isothermal sorption chambers developed in BFH-AHB. This latter measurement is important for the materials properties as input for the numerical modelling described in chapter 5.

4.3.1.1 Cup method

The cup-method used to determine the permeability has been carried out in BFH-HKB on the paint layer. The installation is sketched on the figure 4.4(a) and a picture is shown in figure 4.4(b).

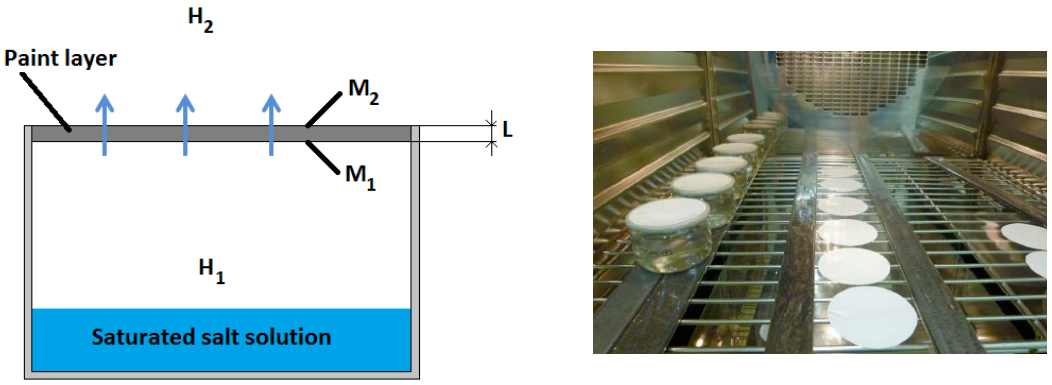

(a) (b)

Figure 4.4: Sketch and picture of the permeability measurements of the paint layer using cup method. (a) H_1 and H_2 are the relative humidity in and outside the cup respectively and M_1 and M_2 are the moisture content boundary conditions.

Circular paint layer samples were produced. The thickness of the samples has been carefully controlled with the Film Applicator Model 360 such as described in section 4.1. Two thicknesses were investigated: 100 and 200 µm. The samples are then placed and fixed on the top of a cup. These cups were filled with a water salt saturated solution to set a given RH inside the cup. This inner RH was set at 93% with potassium nitrate salt solution. Finally, the cups were placed in climatic chambers at 23°C and 50% RH.

With such experimental setting, the samples are subject to non-symmetric boundary conditions between their two surfaces. Therefore, after a certain amount of time, a steady state is reached and a flux of water goes through the paint layer. This flux can be determined by weighting the cups periodically. It is important to wait that the steady state is reached before calculating the permeability. This is achieved by waiting constant mass variation of the cups. The permeability is finally determined by:

$$P = \frac{\mathrm{d}\,w}{A\,\mathrm{d}\,t} \tag{4-1}$$

with P the permeability in [$g\ \ s^{-1}\ cm\text{-}2$], dw/dt the mass variation with respect to time and A the area of the samples exposed to the RH conditions. The permeability of the paint layer is dependent upon the thickness of the layer. The diffusion coefficient of the paint layer can be calculated from the permeability (i.e. the steady water flux) and the first Fick's law (equation (2-7)). As described in section 2.1.3, a variable change is made on the Fick equation $\mathrm{c}(x,t) = \left(\mathrm{m}(x,t) G \rho_w\right)/100$, where G is the specific gravity of the paint and ρ_w is the density of water. The moisture flux though the sample becomes:

$$\frac{\mathrm{d}\,w}{A\,\mathrm{d}\,t} = -\frac{G\rho_w D}{100}\cdot\frac{\mathrm{d}\,m}{\mathrm{d}\,z} \tag{4-2}$$

where *dm/dz* is the moisture content variation with respect to the thickness of the sample. From this equation, *D* can be solved by expressing the derivate as a ratio of differences:

$$D = \frac{100L(w_2 - w_1)}{\rho_w GA(t_2 - t_1)(m_2 - m_1)} \tag{4-3}$$

where *L* is the thickness of the sample. In order to know m_1 and m_2 from the two relative humidities h_1 and h_2, the sorption isotherm of the paint has to be known.

4.3.1.2 Inverse method

Inverse algorithm using the mass loss measured with isothermal sorption chambers has been applied on painted wood samples. The method has been described in section 2.4 where the diffusion parameters of wood have been measured. With this method, an estimation of the permeability of the multi-layered paint (ground + paint layers) is calculated. The experimental weight loss $w_e(t)$, equation (2-39), are obtained according to the following experimental setting: Spruce paint samples (Multi-layered paint) of *50x30x8* mm (LxTxR) were cut. Then, the samples were equilibrated at 76%RH. Next, the non-paint faces were sealed to water sorption with aluminium foil. Finally, the samples were placed in the analysis chambers and the equilibrium at 76% RH was checked during at least two weeks. Then a relative humidity step of 76 to 22% was imposed and the mass loss was recorded. Finally the dry mass was determined by drying the samples in an oven at 103°C.

The calculated weight $w_c(t)$, equation (2-29), is calculated by a unidirectional finite element simulation of the samples using ANSYS. In this model, the permeability of the paint is set as a boundary condition (see section 2.4.3 for more information about the numerical model):

$$J = E_m\left(m_{ref} - m\right) \tag{4-4}$$

where E_m is an emission parameter. J can be seen as the permeability of the paint layer, dependent on the moisture differences.

4.3.1.3 Results

The results of the permeability measurement are shown in table 4.1. The graph in figure 4.5 shows the evolution of the mean permeability of the paint against the accelerated aging treatment time. There is a loss of permeability with the treatment time. However, the thermally aged paint becomes brittle and cracks appear during the treatments. Therefore, because of the cracks, after 9 weeks of treatments the

permeability is the highest. Unfortunately it was not possible to avoid these cracks for the long time and high temperature treatments.

Table 4.1: Paint permeability for different accelerated aging treatments. Permeabilities after 9 weeks of treatment show huge variation due to cracks.

	Non-aged		3 Weeks	6 Weeks	9 Weeks
Thickness [µm]	100	200	200	200	200
Cup method - P [g s^{-1} m^{-2}] $\cdot 10^{-5}$	14.1±9.7%	9.81±5.4%	3.92±5.4%	2.77±5%	~12±200%
Inverse method - P^{IM} [g s^{-1} m^{-2}] $\cdot 10^{-5}$	2.67±22%	2.02±18%	0.51±1.3%	-	-

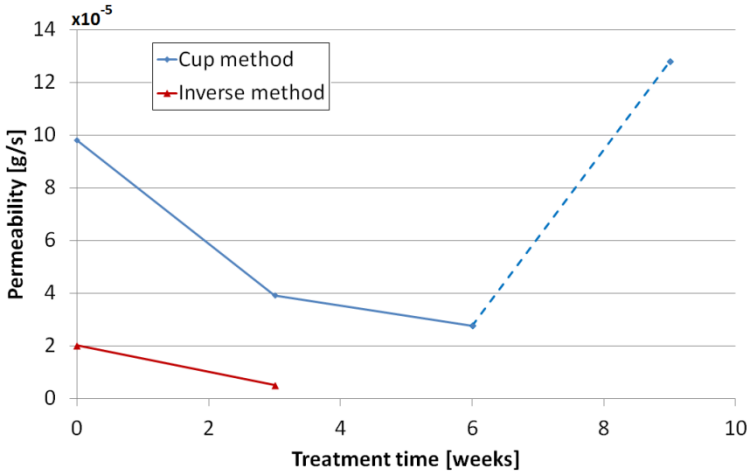

Figure 4.5: Mean permeability of the paint against the accelerated aging treatment times measured with the cup method and calculated by inverse method. The paint of 9 weeks treatment shows inevitable cracks.

The advantage of the inverse method, compared to the cup method, is that the ground layer and all interface zones of the multi-layered paint on the wooden support are taken into account. Indeed, the cup method determined only the permeability of the paint layer. As described above, the inverse method gives the emission factors E_m of the painted surfaces. In order to compare the two methods, the permeability is estimated from the emission factors by:

$$P_{IM} \cong E_m \cdot \Delta m \tag{4-5}$$

where P_{IM} is the estimated permeability of the inverse method and Δm is the wood moisture content difference between the two relative humidity of the measurements. The estimated permeability calculated with the inverse method is less than the cup-method. This is due to these interface zones that are taken into account.

The permeability of only the ground layer on a wooden support has been calculated through inverse method. The inverse algorithm didn't converge. This means that the water diffusion through the ground layer is higher than the diffusion

along the radial direction of wood. Therefore, the permeability of the ground layer has been neglected.

4.3.2 Mechanical properties

The mechanical properties of the paint layer and of the ground layer were determined using the micro-tensile testing device presented in section 2.3.1. These materials have been considered as isotropic. The Young's modulus, Poisson's ratio, failure stress and failure strain were measured.

4.3.2.1 Experimental procedures

First the paint and ground layer were prepared on a plastic foil as described in section 4.1.2. Then, these layers were removed from the plastic foil and specimens with a rectangular shape of about *7x50* mm were cut[2].

Next, the samples were placed in the micro-tensile testing device. An imposed displacement of 0.001 mm/s was set. Due to the brittleness of the samples, the inductive extensometer cannot be fixed. Therefore to record the axial and transverse deformation optical analysis was performed. To achieve this, a gauge of 25 mm was placed on the fixing grip of the testing device as shown in figure 4.6. A black background was placed below the sample to maximize the contrast and black lines were painted on the samples to follow the deformation.

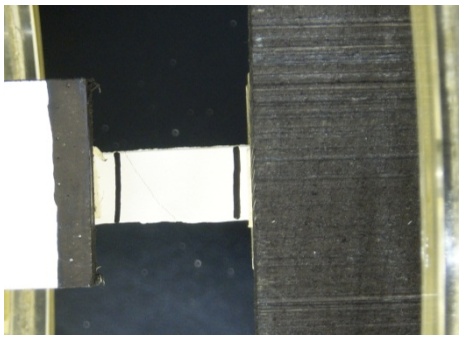

Figure 4.6: Paint layer samples fixed in the tensile testing device. The gauge of 25mm is placed on the left grips.

During the test, pictures (as presented in figure 4.6) were taken every 2 seconds. Matlab image analysis was programmed; lateral and axial elongations of the samples were calculated automatically by the program as well as the gauge length. Figure 4.7 shows the evolution of the length of a paint layer sample during a tensile test. Next, in order to correlate these strains values with the stresses from the tensile device, a linear regression was carried out as shown in figure 4.7.

[2] Due to the important brittleness of the ground layer and artificially aged paint, no standard tensile-sample shape could be produced.

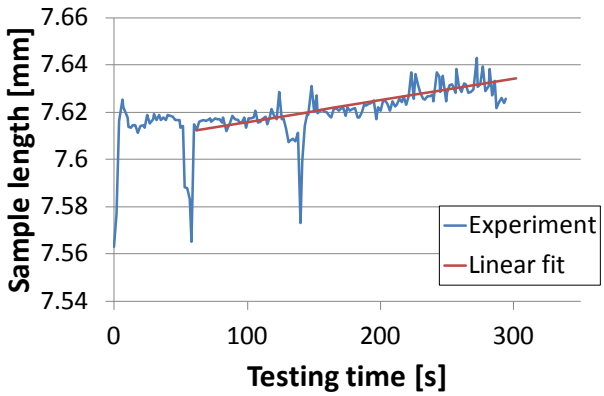

Figure 4.7: Evolution of the length of a paint layer sample during tensile test. It has been measured with optical analysis. In red, the linear regression is shown.

4.3.2.2 Results

Table 4.2 shows the different mechanical properties for paint and ground layers. The paint layer shows low stiffness with a Young's modulus of only 7.5 MPa. On the other hand, the stiffness of the paint after 3 weeks of accelerated aging treatment shows an increase of the modulus, estimated at about 25 MPa (the treated paint was very brittle, therefore the tested data show important scattering). In figure 4.8, the brittleness of the non-aged and thermally aged paint layers are shown.

Table 4.2: Mechanical properties of the paint and ground layers: E the Young's modulus, υ the Poisson ratio, ε_f and σ_f the failure strain and failure stress respectively.

	E [MPa]	**υ**	**σ_f [MPa]**	**ε_f [%]**
Non-aged paint	7.5±2	0.25±0.03	1.34±0.41	0.12±0.03
Acelerated aged paint	~25	~0.25	~0.45	~0.09
Ground layer	1350±140	0.35±0.05	4.44±1.02	0.30±0.02

The ground layer has a completely different mechanical behaviour than the paint layer. Indeed, the ground layer is very stiff with a Young's modulus of about 1350 MPa.

4.4 Conclusion

The aging of the paint seems to be much more difficult to estimate compared to wood due to many reaction pathways that can be thermally activated.

The kind of characterisation of the different paint layers can be achieved only on freshly paint. In case of the multi-layered paint of an old painting, the determination of the permeability and the stiffness becomes more difficult.

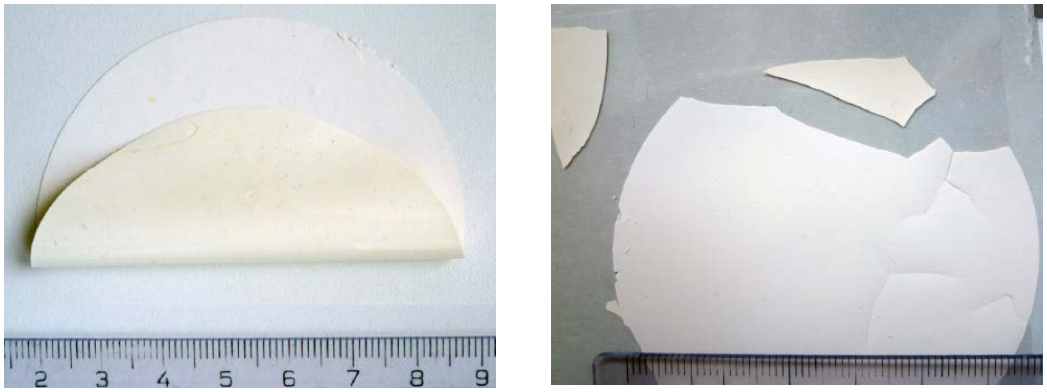

(a) (b)

Figure 4.8: Pictures showing the brittleness of the paint layer. Non-aged paint layer is shown in (a) and thermally aged paint layer is shown in (b).

4.5 References

AUDOUIN, L., LANGLOIS, V., VERD, J. & J.C.M., B. 1994. Role of Oxygen Diffusion in Polymer ageing - Kinetic and mechanical aspects. *Journal of Materials Science,* 29**,** 569-583.

BÉGIN, P. L. & KAMINSKA, E. 2002. Thermal accelerated ageing test methods development. *Restaurator,* 23**,** 89-105.

CELINA, M., GILLEN, K. T. & ASSINK, R. A. 2005. Accelerated ageing and lifetime prediction - review of non-Arrhenius behaviour due to two competing processes. *Polymer Degradation and Stability,* 90**,** 395-404.

FELLER, R. L. 1994. *Accelerated ageing - photochemical and thermal aspects*, Getty Conservation Institute, Los Angeles.

FRANKEL, E. N. 1998. *Lipid Oxidation,* Oily Press, Dundee Scottland.

HUTCHINSON, G. H. 1973. Some aspects of drying oil technology. *Journal of Oil Chemists Association,* 56**,** 44-53.

MISZCEZYK, A. & DAROWICKI, K. 2001. Accelerated ageing of organic coating systems by thermal treatment. *Corrosion science,* 43**,** 1337-1343.

WARREN, M. & RÖTTLER, J. 2008. Modification of ageing dynamics of glassy polymers due to a temperature step. *Journal of Physics: Condensed Matter,* 20**,** 1-6.

ZUMBÜHL, S., SCHERRER, N., FERREIRA, E., HONS, S., MÜLLER, M., KÜHNEN, R. & NAVI, P. 2011. Accelerated ageing of drying oil paint - an FTIR study on the chemical alteration. *Journal of Art Technology and Conservation / Zeitschrift für Kunsttechnologie und Konservierung,* 2**,** 137-149.

Chapter 5
Wood panels painting simulation

The first steps of the numerical modelling have been made in my master thesis: "*Simulation of the mechanical behaviour of wood under relative humidity changes*" (J. Froidevaux, 2009). In that work, the hygromechanical behaviour of wood panels was calculated using 2D finite elements in the TR plane. Next, the free swelling and shrinkage was introduced in a linear elastic anisotropic model (plane strain). This model was able to account for the annual rings orientation.

In the present work, the model will be extended to 3D and wood will be considered as an anisotropic viscoelastic material. Next, the painted layer will be added: its rigidity will be taken into account and the hygroscopic behaviour of the paint will be introduced as a boundary condition. Finally, the simulation will be validated using two different experimental techniques.

5.1 Numerical model

The numerical simulation of wood as a continuous medium has been often used to describe its behaviour as reviewed in (A. Hanhijiirvi, 2000), who summarises the modelling of two important mechanisms of wood under varying RH condition: creep and mechanosorption. In case of paintings, such behaviour cannot be neglected for a precise description of the mechanics of wood. In his PhD thesis (J. Colmars, 2011) developed a model including creep, mechanosorption and non-linear compression deformation, known as "*compression set*" (R. B. Hoadley, 1969).

The objective of the numerical model of this project is to calculate the behaviour of old panels painting under RH variation. The aging of the material parameters were determined and included in the model and results analysis.

The numerical model, mainly based on that of (S. Ormarsson et al., 1998, S. Ormarsson *et al.*, 1999, S. Ormarsson *et al.*, 2000, S. Ormarsson, 1999), is described in the following sections.

5.1.1 Wood hygroscopicity

The hygroscopic behaviour of wood has been calculated using the thermal model of ANSYS. Indeed, the thermal conductivity in a continuum media can be described by the Fourier's law:

$$\frac{\partial T}{\partial t} = \frac{\partial}{\partial \vec{r}}\left(\frac{\lambda}{\rho C_p} \frac{\partial T}{\partial \vec{r}} \right) \tag{5-1}$$

where T is the temperature field, λ is the thermal conductivity, ρ is the density and C_p is the heat capacity. This equation is similar to the second Fick's law (section (2-7)):

$$\frac{\partial m(\vec{r},t)}{\partial t} = \frac{\partial}{\partial \vec{r}}\left(D_m(m) \frac{\partial m(\vec{r},t)}{\partial \vec{r}} \right) \tag{5-2}$$

To convert the Fourier equation to the second Fick's law, the density ρ and heat capacity C_p are set to *1* and λ is set as the diffusion coefficient D_m. As shown by equation (5-2), the model takes into account the dependence of the diffusion coefficient on the moisture content. The anisotropy of the water diffusion is also considered.

The simulation of the temperature field has been neglected. The model assumes a constant temperature.

5.1.2 Wood mechanics

The anisotropic linear elastic model has been coupled to the moisture field using the hygroexpansion coefficients (section 2.2.2). The local coordinate system was rotated around the L axis to take into account the ring orientation, considered as perfectly cylindrical.

5.1.2.1 3D anisotropic viscoelastic model

To simulate the anisotropic viscoelastic behaviour, a model has been developed and implemented using *user programmable feature* (UPF) of ANSYS that allows one to implement in ANSYS a user-defined constitutive equation.

Our model is based on the following studies: (Z. A. Taylor et al., 2009, H. Poon and M. F. Ahmad, 1998, A. Guidoum, 1994). It consists of the generalized Maxwell model given in figure 5.1. The total stress of the model $\sigma(t)$ is the sum of the stresses of all parallel branches:

$$\sigma_i(t) = E_\infty \varepsilon(t) + \sum_{i=1}^{N} E_i\left(\varepsilon(t) - a_i(t)\right) \tag{5-3}$$

where N is the number of branches, E_i the modulus of elasticity of the spring of branch i and a_i the strain of its dashpot.

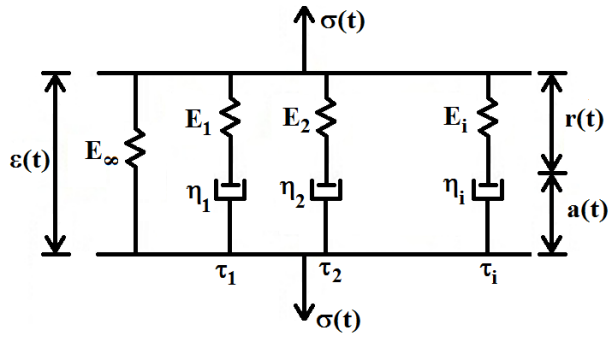

Figure 5.1: Generalized Maxwell model.

The extension to the 3D anisotropic case yields:

$$\sigma_{ij}(t) = D^{\infty}_{ijkl}\varepsilon_{kl}(t) + \sum_{i=1}^{N}\left(D^{i}_{ijkl}\right)\left(\varepsilon_{kl}(t) - a^{i}_{kl}(t)\right) \tag{5-4}$$

where D^{i}_{ijkl} is the orthotropic elasticity tensor for branch i. The D^{i}_{ijkl} are calculated from experimental relaxation tests. In each branch, the stress on the spring is equal to the stress on the dashpot (serial assembling), leading to:

$$\dot{a}^{i}_{kl}(t) + \frac{a^{i}_{kl}(t)}{\tau_i} = \frac{\varepsilon_{kl}(t)}{\tau_i} \tag{5-5}$$

with $\tau_i = E_i / \eta_i$ the relaxation time of the branch i. The relaxation times have been taken equal for all directions R, T, and L, so they were set to scalar values for each branch. The resolution of these differential equations leads to:

$$a^{n}_{kl}(t) = \varepsilon_{kl}(t) - \int_{-\infty}^{t} \exp\left(\frac{s-t}{\tau_n}\right)\frac{d\varepsilon_{kl}(s)}{ds}ds \tag{5-6}$$

Introducing equation (5-6) into equation (5-4) yields:

$$\sigma_{ij}(t) = D^{\infty}_{ijkl}\varepsilon_{kl}(t) + \sum_{i=1}^{N}\left(D^{i}_{ijkl}\right)h^{i}_{kl}(t) \tag{5-7}$$

The $h^{i}_{kl}(t)$ functions, representing the integral term of the equation (5-6), can be computed with an iterative procedure and by using state variables:

$$h^{i}_{kl}(t+\Delta t) = \int_{-\infty}^{t+\Delta t} \exp\left(\frac{s-t-\Delta t}{\tau_i}\right)\frac{d\varepsilon_{kl}(s)}{ds}ds \tag{5-8}$$

$$= \exp\left(\frac{-\Delta t}{\tau_i}\right) \cdot \int_{-\infty}^{t} \exp\left(\frac{s-t}{\tau_i}\right) \frac{d\varepsilon_{kl}(s)}{ds} ds + \int_{t}^{t+\Delta t} \exp\left(\frac{s-t-\Delta t}{\tau_i}\right) \frac{d\varepsilon_{kl}(s)}{ds} ds$$

The first integral (from -∞ to t) is equal to $h_{kl}^{i}(t)$ and the second can be computed using the mid-point rules:

$$\int_{x_1}^{x_2} f(x)dx = \Delta x \cdot f(x_1 + \Delta x/2) \tag{5-9}$$

which yield:

$$h_{kl}^{i}(t+\Delta t) = \exp\left(\frac{-\Delta t}{\tau_i}\right) \cdot h_{kl}^{i}(t) + \Delta\varepsilon_{kl} \cdot \exp\left(\frac{-\Delta t}{2\tau_i}\right) \tag{5-10}$$

Finally, the material Jacobian is computed as:

$$\frac{d\sigma_{ij}(t+\Delta t)}{d\varepsilon_{kl}(t+\Delta t)} = D_{ijkl}^{\infty} + \left(D_{ijkl}^{n} - D_{ijkl}^{\infty}\right)\left[\exp\left(\frac{-\Delta t}{\tau_n}\right) \cdot \frac{dh_{kl}(t)}{d\varepsilon_{kl}(t)} + \exp\left(\frac{-\Delta t}{2\tau_n}\right)\right] \tag{5-11}$$

5.1.2.2 Mechanosorption

It has been seen that under load, a hygroscopic variation induces mechanosorptive deformation. Unfortunately, due to lack of time, this behaviour has been neglected. Indeed, the implementation of a mechanosorption model, together with its validation and the measurement of its parameters, would have required an important effort. Moreover, the mechanosorptive deformation state of an old painting is very difficult to determine.

5.1.3 Multi-layered paint behaviour

The multi-layered paint (composed of ground and paint layers as described in section 4.1) has been considered in the model through plate elements following the *Mindlin-Reissner* plate theory (extension of the *Kirchhoff–Love* plate theory). The constitutive equation of the plate theory assumes that:

- Straight lines normal to the mid-surface remain straight after deformation.
- The thickness of the plate does not change during a deformation.

The mechanics of the paint layer was neglected. Indeed, as shown in section 4.3.2, the paint layer has a low stiffness compared to the ground layer (about 200 times lower). Therefore, the paint elements of the model are set with the ground layer stiffness and **thickness**.

No moisture diffusion was introduced into the paint elements, because it requires the knowledge of the sorption isotherm of the paint materials which is unknown and

difficult to determine. The permeability of the paint was introduced in the boundary condition. A third kind of boundary condition using a convection film was used:

$$J = E_m\left(m_{ref} - m\right) \tag{5-12}$$

where E_m is the emission parameter and J can be seen as the permeability of the paint layer dependent on the moisture difference. m_{ref} correspond to the initial MC (when the panel is flat).

5.2 Materials and model parameters

5.2.1 Spruce properties

5.2.1.1 Sorption properties

The sorption isotherm for spruce wood (*Picea abies Karst. (L.)*) has been determined during my master work (J. Froidevaux, 2009). The resulting curves are presented in figure 5.2. These curves were fitted on a BET model, using 12 experimental points from 9 to 97 % RH, for both adsorption and desorption. The three parameters of the BET model are tabulated in table 5.1.

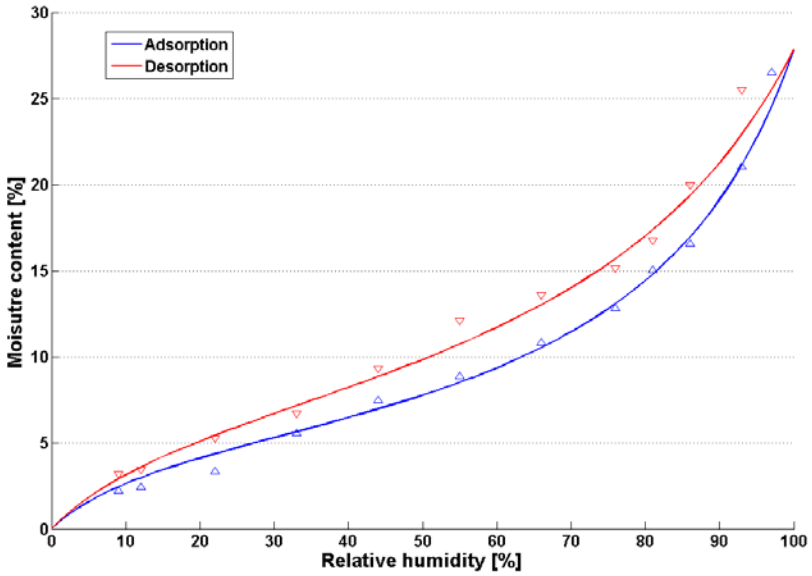

Figure 5.2: Sorption isotherm curves at 20°C calculated with BET model (2-2) for spruce (*Picea abies Karst. (L.)*). The triangles correspond to the experimental measurements (J. Froidevaux, 2009).

Table 5.1: BET model constants *A*, *B* and *C* of equation (2-2) for absorption and desorption, respectively, for spruce wood (*Picea abies* Karst. (L.)) *at 20°C* (J. Froidevaux, 2009).

	Adsorption	Desorption
A	2.4623	2.2888
B	0.1476	0.09867
C	0.001363	0.001109

5.2.1.2 Diffusion properties

The diffusivity coefficients D_m of spruce wood (*Picea abies* Karst. (L.)) were measured using the isothermal sorption chambers for all three main directions as described in section 2.4. 7 RH steps were imposed to the samples from 86 to 9% RH. Each direction was measured twice and the mean values are shown in figure 5.3.

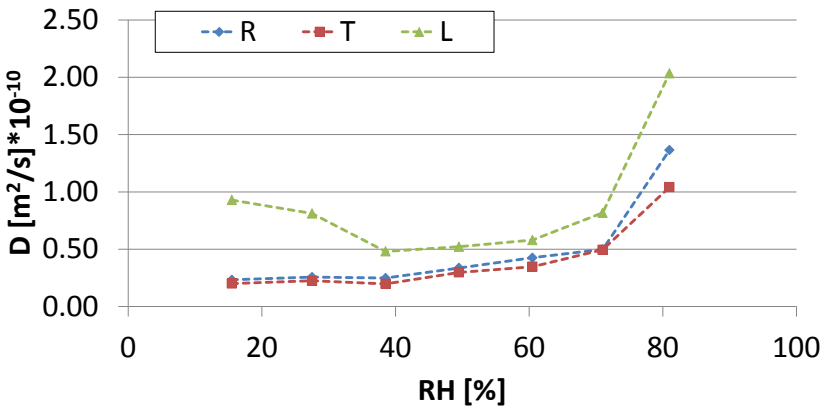

Figure 5.3: Diffusion coefficients for the three main direction of spruce wood with respect to the relative humidity. These values were measured using the isothermal sorption chambers.

5.2.1.3 Mechanical properties

The wood hygroexpansion coefficients have been determined during my master thesis and are presented in table 5.2 (J. Froidevaux, 2009).

Table 5.2: Hygroexpansion coefficients for spruce wood (*Picea abies* Karst. (L.)) determined during adsorption and desorption at 20°C (J. Froidevaux, 2009).

	Adsorption	Desorption	Mean
α_r	14.59	15.85	15.22
α_t	31.71	32.31	32.01
α_l	1.88	1.54	1.71

The tensile mechanical properties of spruce were determined using the micro-tensile testing device (section 2.3.3). The elastic and viscoelastic parameters were measured in the three main directions. The elastic shear modulus and the Poisson

ratio were taken from literature (P. Navi and F. Heger, 2005). The elastic parameters are shown in the first column of table 5.3.

The viscoelastic parameters of the generalised Maxwell model were calculated for the three main directions according to the data processing described in section 2.3.3.3. The different relaxation times and Young's modulus of the generalised Maxwell model are presented in table 5.3. The viscoelastic parameters along the R direction are mean values from 9 creep and relaxation tests, and from 3 creep tests for the L and T directions.

For the computation, the time-dependent compliance matrix must be estimated:

$$\begin{pmatrix} S_{rr}(1+f_{rr}(t)) & S_{tr}(1+f_{tr}(t)) & \dots \\ S_{rt}(1+f_{rt}(t)) & S_{tt}(1+f_{tt}(t)) & \dots \\ \dots & \dots & \dots \end{pmatrix} \quad (5\text{-}13)$$

where the S_{ij} refers to the instantaneous value and $f_{ij}(t)$ is the relative creep measured in i direction for a uniaxial loading in j direction. The functions $f_{ii}(t)$ were obtained directly from tensile creep tests, but due to time and equipment reason, the time dependent Poisson's ratio and shear modulus were not measured. To produce estimates of the coupling terms between directions and to ensure that the compliance matrix remains symmetric over time, average of these pairs is taken:

$$f_{tr}(t) = f_{rt}(t) = \frac{f_{rr}(t) + f_{tt}(t)}{2} \quad (5\text{-}14)$$

The instantaneous value S_{ij} (for $i \neq j$) are calculated with the elastic Poisson'ratio given in table 5.3. Concerning the shear moduli, the time function of the radial Young's modulus was used:

$$G_{ij}(t) = G_{ij}^{0}(1+f_{rr}(t)) \quad (5\text{-}15)$$

5.2.2 Multi-layered paint properties

The emission parameter E_m of the paint layer plate model was determined through inverse method as presented in section 4.3.1.2. The value chosen for the simulation is $E_m = 22.4 \cdot 10^{-5}$ [g s^{-1} m^{-2}].

The rigidity of the paint layer was neglected, but that of the ground layer was taken into account. The ground layer was assumed isotropic. Its Young's modulus and Poisson's ratio, measured as described in section 4.3.2, were 1300 MPa and 0.3 respectively. The thickness of the ground layer, measured using image analysis, was 0.3±0.01 mm.

Table 5.3: Elastic and viscoelastic parameters of the model. The E-modulus and viscoelastic modulus along R, T and L were determined using the micro-tensile testing device (black

values). The Poisson's ratios and the shear modulus come from literature (P. Navi and F. Heger, 2005) (red values). The viscoelastic shear moduli were calculated with equation (5-15) (green values).

	Elastic	Maxwell viscoelatic parameters					
		∞	N°1	N°2	N°3	N°4	N°5
E_r	885	473	67	76	99	87	82
E_t	580	244	63	45	27	134	67
E_l	16'130	13'605	473	317	553	677	505
G_{tl}	438	209	40	36	35	72	46
G_{rl}	533	254	49	43	43	88	56
G_{rt}	41	20	4	3	3	7	4
τ [hres]			0.032	0.316	3.162	31.62	316.20
υ_{rt}				0.45			
υ_{rl}				0.02			
υ_{tl}				0.03			

5.2.3 Wood anatomical properties

An important parameter of the model is the orientation of the annual ring in the panel. As mentioned above, the simulated wood panel is taken as flat-sawn. Therefore the distance of the panel from the tree pith has to be known. It can be calculated geometrically as sketched in figure 5.4.

From the transverse cut of a panel, the length *y* and *e* can be measured for different rings. Then the following relations apply:

$$\begin{cases} d = r - e \\ r = \sqrt{d^2 + \frac{y^2}{4}} \end{cases} \tag{5-16}$$

From these two equations, the distance *d* is deduced:

$$d = \frac{y^2}{8e} - \frac{e}{2} \tag{5-17}$$

The *d* is calculated on many rings of the panels and a mean is taken.

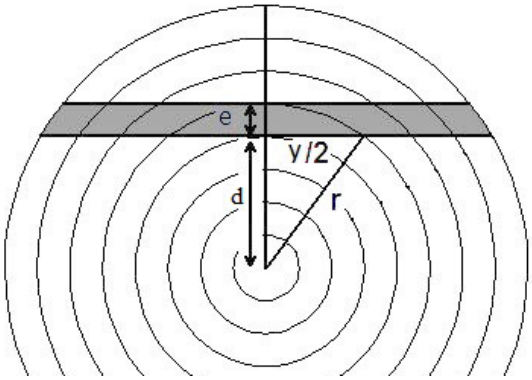

Figure 5.4: Determination of the position of a flat-sawn plank from the pith. The distance *x* corresponds to the distance from the pith to the plank.

5.2.4 Solver and mesh parameters

The ANSYS elements used for wood are SOLID226. They are composed of 20 nodes and include coupled field solutions. SHELL181 elements have been used for the paint. They are plate elements with 4 nodes.

Quadratic mesh was used as shown in figure 5.5. Sensitivity analysis on the mesh parameters has been carried out to ensure optimal mesh size. Finally 18 elements were used along the panel width and length with a parabolic reduction of the element size from the centre to the border. Across the thickness, 10 wood elements and 3 paint elements were used to precisely calculate the moisture through them. The maximal aspect ratio for the wood elements was about 20 for a 30cm panel wide. It corresponds to the maximum recommended by the code notice. The typical total numbers of elements was about 1300 and nodes about 6330. Transient solver was used with 200 time steps.

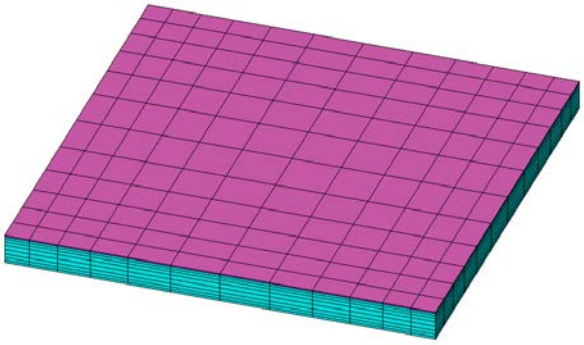

Figure 5.5: Mesh of the numerical model. In light blue the wood elements (SOLID226) and in violet the paint plate elements (SHELL181).

5.3 Model validation – materials and methods

To confirm the model, two experimental techniques and one analytical formulation were used to determine the deformation of panels subject to an RH step

change. The first experimental approach, called "Deformometric Kit", measured continuously the cupping of a panel. The second one was an optical technique using fringe projection and measuring the 3D shape of a panel at a certain time. These two experimental settings and the experimental procedures are described in the following sections. Then an analytical formulation corresponding to the difference between two equilibrium conditions will be detailed.

5.3.1 Definitions

Before investigating the confirmation experiments of wood and painted panels, the definition and the quantification of the deformation have to be defined as well as the coordinate system. Figure 5.6 shows a 3D sketch of a wooden panel. The paint layer can be applied on the bark or the pith oriented face.

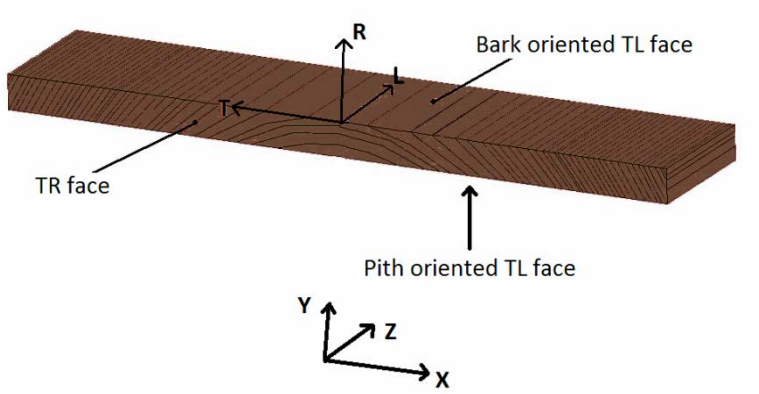

Figure 5.6: 3D sketch of a wooden panel with the faces definitions. The global XYZ and a local coordinate system RTL are shown as well.

The TR face is shown with a cup-deformation in figure 5.7. The amount of cupping c is quantified by the deflection taken at a certain width W. It is defined positively when the cupping is convex relative to bark side such as seen in figure 5.7, and negative when it is concave.

The global coordinate system is located at the pith location. Therefore the middle of the panel is at a width $x=0$ and the pith oriented face at $Y=d$ where d is the distance of the panel from the pith defined in equation (5-17).

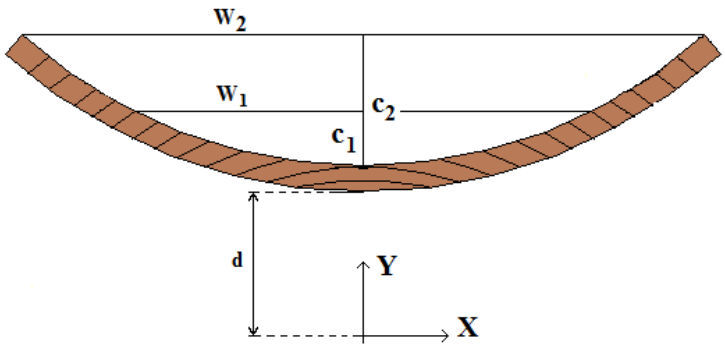

Figure 5.7: Cupped TR face. The amount of cupping is quantified by the length *c* taken at a certain width *W*. The local global coordinate system is located at the pith.

5.3.2 Deformometric Kit

5.3.2.1 Description

The first method is called "Deformometric kit" (DK). It has been developed in University of Florence (L. Uzielli *et al.*, 2009). It consists of the continuous measurement of the lengths of two linear displacement transducers, which are mounted on columns. The DK set up is presented in figure 5.8 and a sketch is given in figure 5.9. These columns are fixed with screws perpendicular to the wooden surface. During the cupping of the panel, the parallelism of the columns changes and due to geometrical relationships, the change in length of the two transducers can be used to calculate the amount of cupping of the panels.

(a) (b)

Figure 5.8: Installation of the Deformometric kit (DK) on a wooden panel (a). Wooden panel with DK in the climatic box controlled with salt solution (b).

Cupping determination

A sketch of the DK is shown in figure 5.9. The cupping is characterised by the deflection *c(t)*:

$$c(t) = R(t) - h(t) \tag{5-18}$$

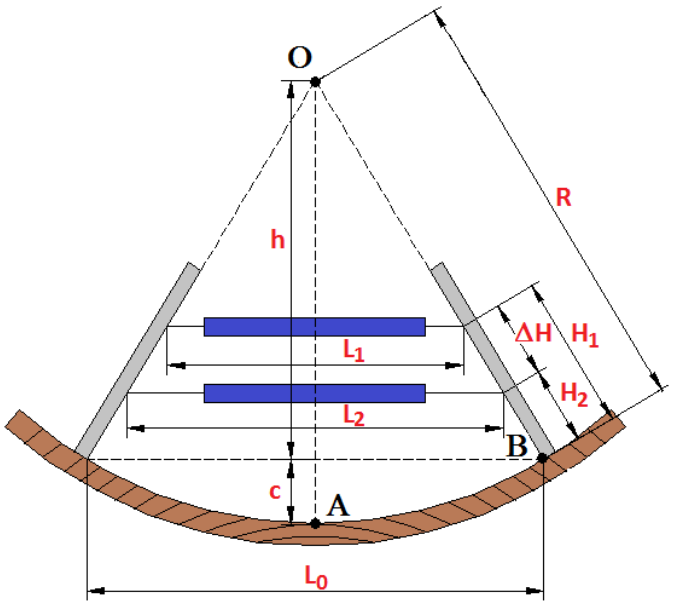

Figure 5.9: Sketch of the DK setting. The wood panel is supposed to cup as an arc of circle. The linear transducer (TD) are represent by the blue rectangles.

where *R(t)* corresponds to the cupping radius. The function $L_1(t)$ and $L_2(t)$ are known from the linear transducer (in blue on the sketch). Equation (5-18) assumes that the length *OA* and *OB* are equal to the cupping radius R. The length at the bottom of the columns $L_0(t)$ can be calculated as:

$$L_0(t) = L_2(t) + \frac{(L_2(t) - L_1(t))H_2}{\Delta H} \tag{5-19}$$

where $\Delta H = H_1 - H_2$, the height between the two TD. Finally by geometrical relations, we obtain:

$$\begin{aligned} R(t) &= \frac{L_0(t)H_1}{L_2(t) - L_1(t)} \\ h(t) &= \sqrt{R^2 - \frac{L_0^2(t)}{4}} \end{aligned} \tag{5-20}$$

5.3.2.2 Experimental procedures

The DK experiments have been carried out by M. Müller from BFH-HKB following these experimental procedures: The DK is fixed on the panels such it can be seen in figure 5.8. Next, the panels with the DK are put into a climatic box which has been built in order to keep the temperature and the RH stable over time. The temperature is controlled by the air conditioning system of the building and the RH is controlled by salt saturated solution. The panels are stabilized during at least one month under the starting climatic condition. Next the panel is weighted and the logging of the displacement data of the two transducers and as well as the

temperature and the RH is started. After an EMC control period of about 5 days, the salt saturated solution is changed to set another RH. At the end of the experiment, when the new EMC is reached, the panel is another time weighted. Finally, the panel is oven dried at 103°C during about 15 hours to determine its anhydrous mass.

5.3.3 Fringe projection technique

The second method used *fringe projection techniques* (FPT) for generating a 3D surface of the panels. These measurements were achieved in collaboration with EMPA (*Swiss Federal Laboratories for Materials Science and Technology*). FPT consists to project fringes pattern on an object and viewing it from a different direction as it has been reviewed by (S. S. Gorthi and P. Rastogi, 2010). A sketch of the installation is shown in figure 5.10 and a resulting 3 dimensional surface deformation of a wood panel is illustrated in figure 5.11.

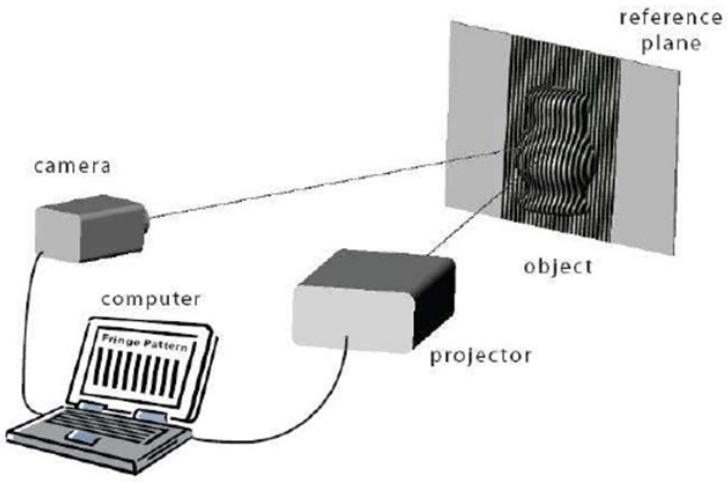

Figure 5.10: Sketch of the fringe projection techniques set-up (S. S. Gorthi and P. Rastogi, 2010).

5.3.3.1 Experimental procedures

The panels are stabilized during one month in boxes in which the RH is controlled by using salt saturated solution. The temperature is controlled by the air conditioning system of the building. This system was also capable to control the RH which is set to the final value.

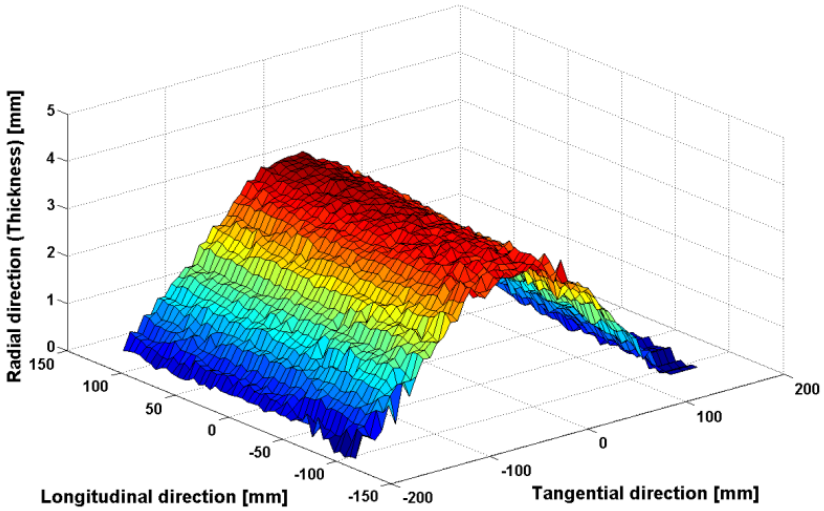

Figure 5.11: 3D deformation of the surface of a wooden panel subjected to an RH step from 66 to 45%, measured by fringe projection techniques after 50 hours from the RH step.

The panels are taken out of the climatized box inside the temperature and RH stabilized laboratory (LA160 at EMPA). Their shape and weight were measured periodically. In-between the recordings, the panels were placed upright on the table, while the natural panels were put horizontally on wooden spacer in order to allow the air to freely circulate around the panels. The shape measurement system covers an area of 35x25 cm2. The natural panels are measured form the upper side (bark oriented) and the painted panels are measured from the painted side. All panels are placed in upright position, and the bend is facing towards the camera.

5.3.3.2 Data processing

To correctly compare the different shapes of the panels at different time and compare them with simulated results, some data processing was required. First, all the measured shapes were rotated around the longitudinal and radial axis, in order to orientate the panels parallel to the XY plane in the Cartesian coordinate system. Afterwards, the Z deformation of the panels was smoothed using second order local interpolation to remove the scattering. Next, the middle of the panels was translated at coordinates *(0;0;0)*. Finally, the deformations of the panels were calculated: the initial shape has been removed at all shapes.

5.3.4 Calculation of the cupping of wooden panels between two equilibrium states using an analytical model

5.3.4.1 Model description

The swelling or shrinkage of a point *P(r,θ, l)* in the local coordinate system of wood (i.e. cylindrical coordinate system) subject to a moisture variation of *Δm* can be estimated as presented by (J. Colmars, 2011). The constitutive equation for an elastic behaviour on the local coordinate system is (2-15). Assuming a stress free hygroexpansion it remains as non-zero strain:

$$\begin{cases} \varepsilon_r &= \alpha_r \Delta m \\ \varepsilon_t &= \alpha_t \Delta m \\ \varepsilon_l &= \alpha_l \Delta m \end{cases} \tag{5-21}$$

Moreover:

$$\vec{\varepsilon} = \frac{1}{2}\left[\mathbf{grad}\left(\vec{U}\right) + \mathbf{grad}\left(\vec{U}\right)^T\right] \tag{5-22}$$

with *U(r, θ, l)* the displacement field in the local coordinate system, which leads after an appropriate rotation in the Cartesian coordinate system:

$$\begin{cases} U_x &= r\Delta m\left[\alpha_r \cos(\theta) - (\theta - \pi/2)\sin(\theta)(\alpha_t - \alpha_r)\right] \\ U_y &= r\Delta m\left[\alpha_r \sin(\theta) + (\theta - \pi/2)\cos(\theta)(\alpha_t - \alpha_r)\right] \\ U_z &= l\Delta m\alpha_l \end{cases} \tag{5-23}$$

Note: the gradient in cylindrical coordinate is:

$$grad(\vec{U}) = \begin{pmatrix} \frac{\partial U_r}{\partial r} & \frac{1}{r}\left(\frac{\partial U_r}{\partial \theta} - U_\theta\right) & \frac{\partial U_r}{\partial l} \\ \frac{\partial U_\theta}{\partial r} & \frac{1}{r}\left(\frac{\partial U_\theta}{\partial \theta} - U_r\right) & \frac{\partial U_\theta}{\partial l} \\ \frac{\partial U_l}{\partial r} & \frac{1}{r}\frac{\partial U_l}{\partial \theta} & \frac{\partial U_l}{\partial l} \end{pmatrix} \tag{5-24}$$

The cup deformation can be then determined by the height difference between two points: P_1 and P_2, the points at the middle and at the border of the panel respectively.

5.3.4.2 Model results

In figure 5.12, the cupping of a wood panel calculated with the analytical model is shown. A panel of *30 cm* wide and *1 cm* thick has been taken into account during two dryings with loss of moisture content Δ*m* of 5 and 10% respectively. In figure 5.12(a), the variation of the cupping against the position of the plank in the tree (distance *d* from the pith to the panel defined in equation (5-17)) is shown. In figure 5.12(b), the panel's profile is shown and compared with their corresponding arc of circle. It can be seen that the cupping profile of wooden panels didn't follow exactly

an arc of circle. This is due to the anisotropic shrinkage of the wooden surface. Indeed, the shrinkage difference between the bark oriented and pith oriented faces is more important at width $x = 0$ than at an infinite width (only radial).

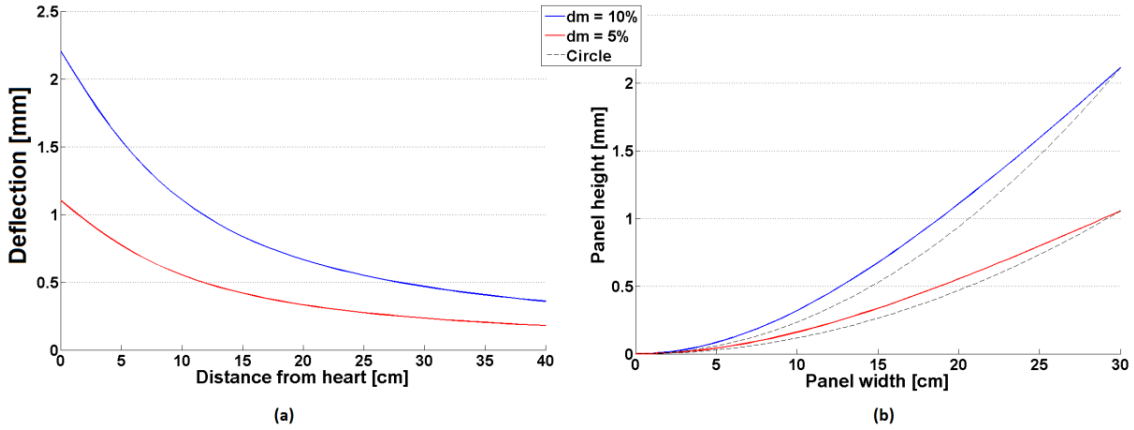

Figure 5.12: Results obtained with the analytical model of the deflection of a panel of 30 cm long and 1 cm thick subject to two moisture variations: 5 and 10% of drying respectively. The values are plotted against the position of the plank in the log in (a) and the panel profile (RT plane) is shown in (b).

5.3.5 Samples preparation

Validation of the model has been carried out on flat-sawn wooden panels and painted panels. The panels were carefully selected: regular annual tree rings, dry density of about $425\ kg/m^3$, few knots (only small ones) and no visible cracks.

Moreover, for achieving flat panels at the initial RH condition and also to avoid cracks, the panels were produced as follow: first they were planned at a thickness of about 2 cm. Then, they were stabilized at the initial RH condition during at least one month. Finally, the panels were planned again at the final thickness of about 1 cm. The choice of the thickness has been made for reaching the final EMC within about 2 weeks. Indeed, the moisture transfer inside the wood panel mainly occurs through the thickness.

The painting of the panels was produced by M. Müller in BFH-HKB. The preparation of the paint is described in section 4.1.2, with a constant thickness of $200\ \mu m$ for the paint and the ground layers.

The cupping of panels has been measured experimentally with the DK or by fringe projection technique. In order, to introduce precise boundaries conditions in the model, the starting and ending moisture contents of the panels should be known. Therefore, the panels have been weighted before starting the RH step and at the end of the measurements. Finally, the panels have been oven dried at 103°C for about 15 hours in order to determine their dry mass.

5.4 Model validation on wooden panels

5.4.1 Numerical simulation versus DK

Results

The experimental procedure described in section 5.3.2.2 has been carried out for a wood panel. The experiment and panel parameters are tabulated in table 5.4. The temperature and the RH during the experiment can be seen in figure 5.13 and the resulting cupping of the panel and the simulated results is shown in figure 5.14.

Table 5.4: Specification of wood panel and experimental setting of the DK measurement.

Panel information	Dimension (RxTxL) [m]	0.008 x 0.3 x 0.3
	Dry mass [g]	401.2
	Dry density [kg/m^3]	445.8
	Distance from the heart [m]	0.129 ±0.005
DK set	Length between the DK columns [m]	0.171
	Height of the first TD (H_1) [m]	17.96
	Height between TDs (dH) [m]	66.77
Climate condition	Mean temperature [°C]	22.76 ±0.56
	Starting condition • RH [%] • Weight [g] • MC [%]	 62% 450.9 12.4%
	Ending condition • RH [%] • Weight [g] • MC [%]	 12% 419.71 4.6%

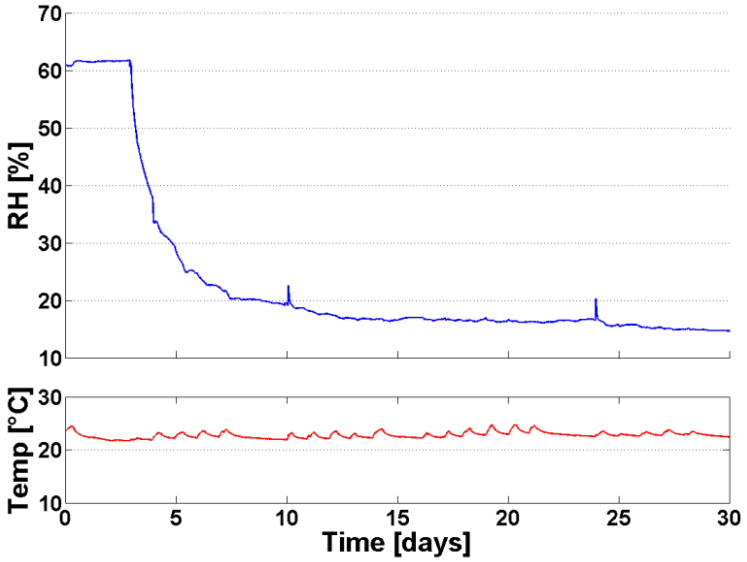

Figure 5.13: Climate conditions during the measurement of the cup-deformation with the DK.

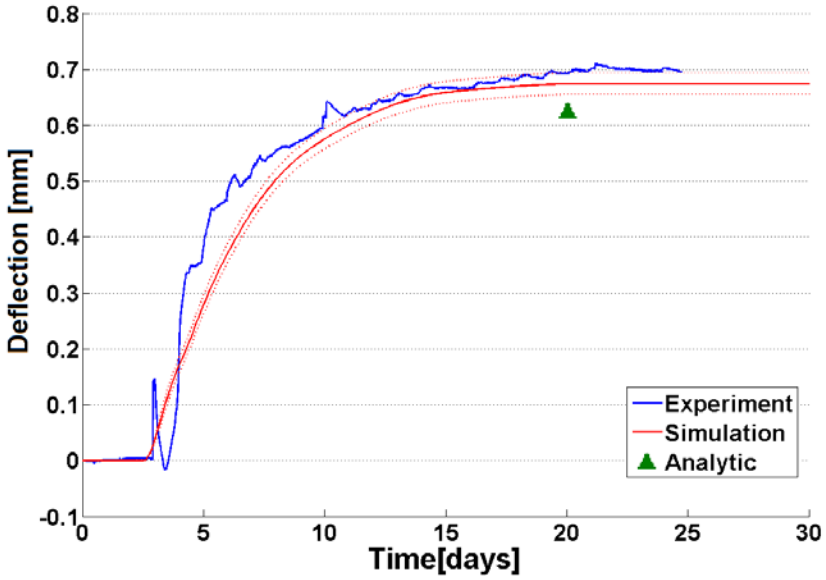

Figure 5.14: Cupping of a wood panel subject to an RH from 62 to 12% (climate in figure 5.13). Blue line corresponds to the experimental cupping measured with DK, red line corresponds to the simulated results and green triangle corresponds to the analytic model. Dashed red line corresponds to the uncertainty on the position of the panel in the log.

Analysis

The difference between the simulated deflection and the experimental one is small. The dynamics are similar: the EMC is reached more or less at the same time. It has to be noted that the boundary conditions imposed on the wooden surface of the DK experiment and the diffusion parameters determination setting are similar. Indeed, in both cases, wood is placed in sealed boxes with minimal air flow.

The simulated cupping is a little less than the cupping measured by the DK even by taking into account the uncertainty on the position of the wood plank in the log (±5 mm, it is plotted in the figure 5.14 with the dashed lines). However, DK measurements assume that the wood panel cups as an arc of circle (this assumption is made in the equation (5-18) where the length OA and OB are defined as equal to the radius). The analytical cupping shows an increasing radius with panel width. This comes from the higher anisotropy between the bark and pith oriented face at the middle of the panel. Therefore, normally the length OA is lower than OB. The calculation of the radius in equation (5-20) is then overestimated which implies an overestimate of the cupping *c(t)* for the DK results. This assumption can explain why the simulated results show a lower cupping than the DK experiment. These differences could also be due to the natural variation and defaults in the wood panel which is not taken into account in the numerical modelling.

Concerning the analytical model of the cupping, which can be seen in figure 5.14 with the green triangle, the deflection at the final EMC is under the simulation

and the DK experiments. The difference between the analytical model and the 3D numerical model should come from the discretisation of the numerical model.

5.4.2 Numerical simulation versus fringe projection

Results

The deformation of three wooden panels under an RH step from 76 to 44% has been measured using projection fringe techniques following the experimental procedure described in section 5.3.3.1. The panels and experiments specifications are tabulated in table 5.5.

Table 5.5: Specification of the wood panels and the experimental parameters of the projection fringe measurements.

		Panel N°1	Panel N°2	Panel N°3
Panels information	Dimension (RxTxL) [m]	0.01 x 0.32 x 0.24	0.01 x 0.31 x 0.25	0.01 x 0.33 x 0.4
	Dry mass [g]	317.55	335.65	566.55
	Dry density [kg/m^3]	413.5	433.1	429.2
	Distance from the heart [m]	0.061	0.062	0.074
Climate condition	**Starting condition**			
	• RH [%]	65%	65%	65%
	• Weight [g]	361.0	380.6	640.0
	• MC [%]	13.7%	13.4%	13.0%
	Ending condition			
	• RH [%]	43.9 ±1.8	43.9 ±1.8	43.9 ±1.8
	• Weight [g]	345.7	365.4	616.7
	• MC [%]	8.85%	8.85%	8.85%
	Mean temperature [°C]	20.53 ±0.08	20.53 ±0.08	20.53 ±0.08

The climate during the measurement was quite stable such as can be seen in figure 5.15. The RH was rather stable at 45%, but showed a few deviations below and beyond this value (min 38%; max 47.6%). The temperature was stable at 20.5°C (min 20.4°C, max 20.8°C). The different measurement shots are presented in figure 5.15 with the yellow triangles. The resulting 3D surface deformation after 50 hours can be seen in figure 5.11.

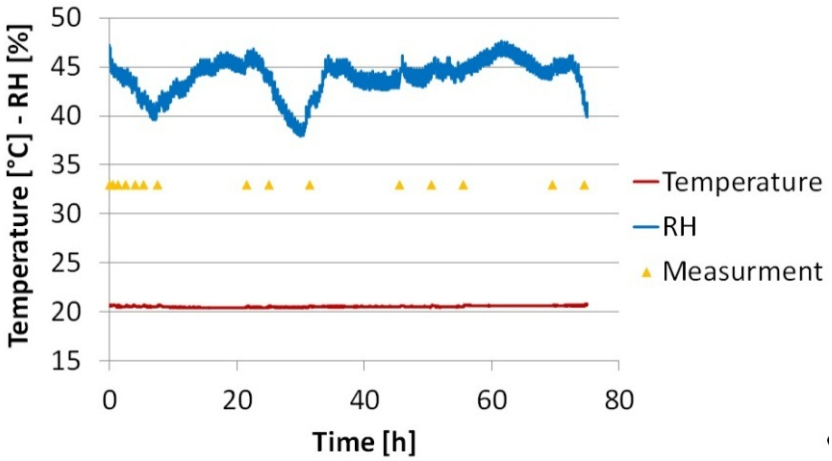

Figure 5.15: Temperature and RH evolution during the projection fringe measurement. The measurement times are shown with the triangles.

Figure 5.16(b) shows the comparison of the 2D profiles between simulation and experiment. These two profiles have been taken at the end of the experiment at about 71 hours. The 2D profiles are also compared with an arc of circle with the same deflection, indicated by the black dashed line in the figure.

Figures 5.17 and 5.18(a) show the cupping (deflection) of simulations and experiments by fringe projection techniques. The errors on the experimental curves indicate the standard deviation of the deflection along the longitudinal direction. The errors on the simulated results indicate the standard deviation of the determination of the position of the plank in the log. The analytical estimation of the cupping at the EMC is indicated on these graphics with green triangles.

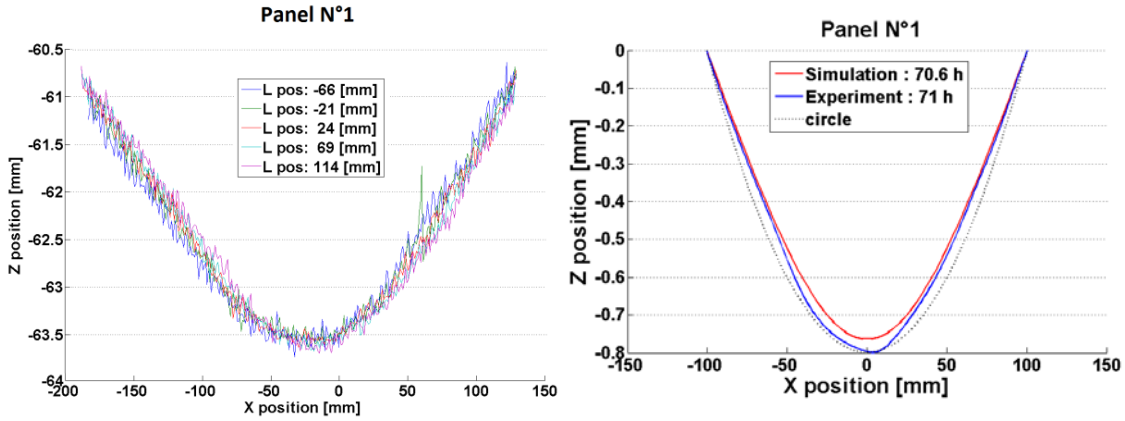

(a) (b)

Figure 5.16: (a) 2D profiles without any data processing taken at different location along the longitudinal direction. (b) Comparison of the experimental 2D-profile with simulation and arc of circle.

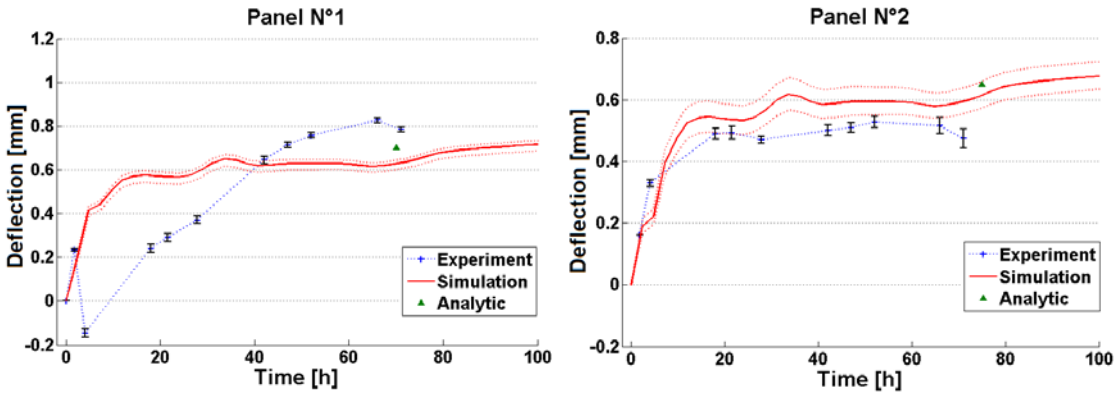

(a) (b)

Figure 5.17: Cupping (presented as the deflection of a 200 mm wide panel) of simulation and experiment by fringe projection techniques.

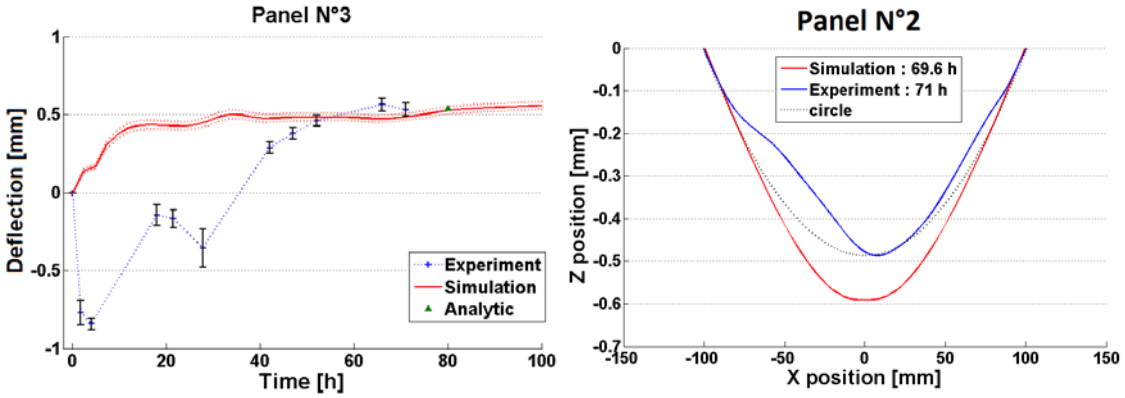

(a) (b)

Figure 5.18: Cup deformation and 2D profile of panel N°3 and N°2 respectively.

Analysis

According to the fringe projection measurements, the regularity of the annual rings of the panels can be checked such as can be seen in figure 5.16(a). On this figure, the 2D surface profiles are plotted at different heights along the longitudinal direction of the board. As it can be seen for the panel N°1, there is no significant difference between these profiles, which means that the panel has a symmetrical deformation along the L direction.

The profiles are rather similar between simulation and experiment and in both cases the shapes are not following the arc of circle as for the analytic case shown in figure 5.12(b). Concerning the profile of the panel N°2 in figure 5.18(b), it can be seen that it is not symmetric and shows a deviation on the left. This comes probably from a small knot (diameter of about 3 mm) located on the left side of the board. It can be shown here how sensitive is the cupping to fibre orientation.

By comparing the evolution of the deflection of the three panels, a slight difference in dynamics of the deformation between the experiment and simulation

can be seen. Indeed, the experiment seems to reach faster the equilibrium than the simulated results. No such difference was seen with the DK measurement as shown in figure 5.14. This is due to the different climatic conditions. Indeed, the DK experiment and the sorption experiment have been made in closed boxes with a minimum of air flow. Therefore the dynamics of the humidity changes between DK measurement and simulation give good correspondence. Concerning the fringe projection experiment, the panels were placed in the free air of the labs, controlled by an air conditioning system, which induces little air flow. This explains the difference of cupping dynamics.

Some problems have raised up for panel N°3 as shown by its cupping in figure 5.18(a). This cupping comes for the non-symmetrical boundary conditions imposed on the panel. Indeed, between the measurement shoots, the panels were placed in the room in a stack using wooden support to space them by about 2-3 cm. This has been done to allow air flow between the panels. However the spacing of 2-3 cm appears to have been insufficient. Therefore the top panel (N°3) did not experience the same humidity condition at the top and bottom faces. This experimental error shows the high sensitivity of wood panels to asymmetrical moisture conditions. In case of painted panels, it is clear that the paint layer induces asymmetrical condition but also the positioning of the panels. For example when one face is placed against a wall and the other exposed to the air.

The cupping at the end of the experiments gave similar value as both the simulated results and the analytical model.

5.5 Confirmation on painted panels

The second step of model confirmation takes into account the painted layers. Flat-sawn wooden panels carefully selected were used. The preparation of the panels is described in section 5.3.5 and the application of the paint in section 4.1.2. As for the wooden panels, DK and fringes projection were used to compare the deformation of the painted panels with the numerical simulations.

5.5.1 Numerical simulation versus DK

Results

The Deformometric Kit has been used to follow the cupping of a painted panel. The panel specifications and the experimental parameters are given in table 5.6.

RH steps from 64 to 46% and from 46 to 64% were applied as shown in figure 5.19. The mean temperature was 24.79°C. The relative humidity shows acceptable fluctuations (±1.6%) during the stabilisation parts. The resulting experimental cupping (deflection) and the simulated results are shown in figure 5.20.

Table 5.6: Specification of wooden painted panel and experimental setting of the DK measurement.

Panels information	Dimension (RxTxL) [m]	0.01 x 0.35 x 0.12
	Dry mass [g]	230.24
	Distance from the heart [m]	0.081
	Paint side	Pith
	DK Column distance	0.184
Climate condition	**Starting condition** • RH [%] • Weight [g] • MC [%]	 64% 255.4 10.9%
	Ending condition • RH [%] • MC [%]	 46 ±1.6 9.16%
	Mean temperature [°C]	24.79 ±0.47

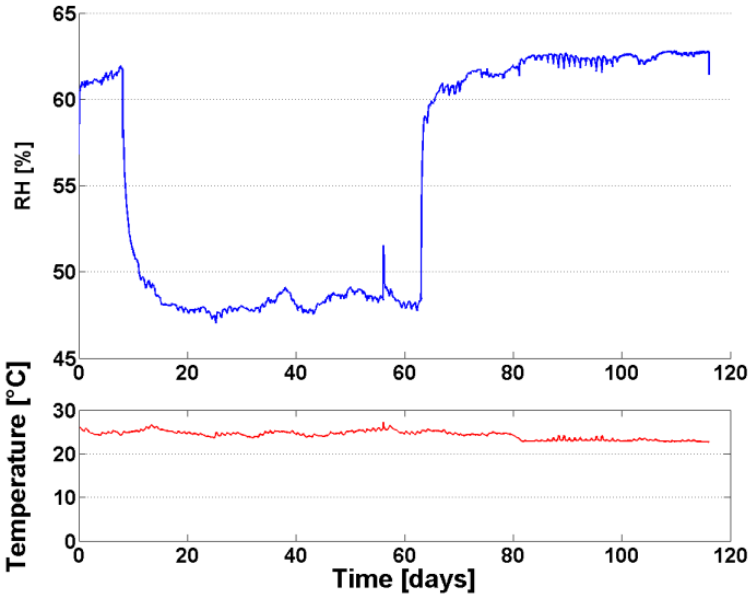

Figure 5.19: Climate conditions during the measurement of the cup-deformation with the DK of paint panels.

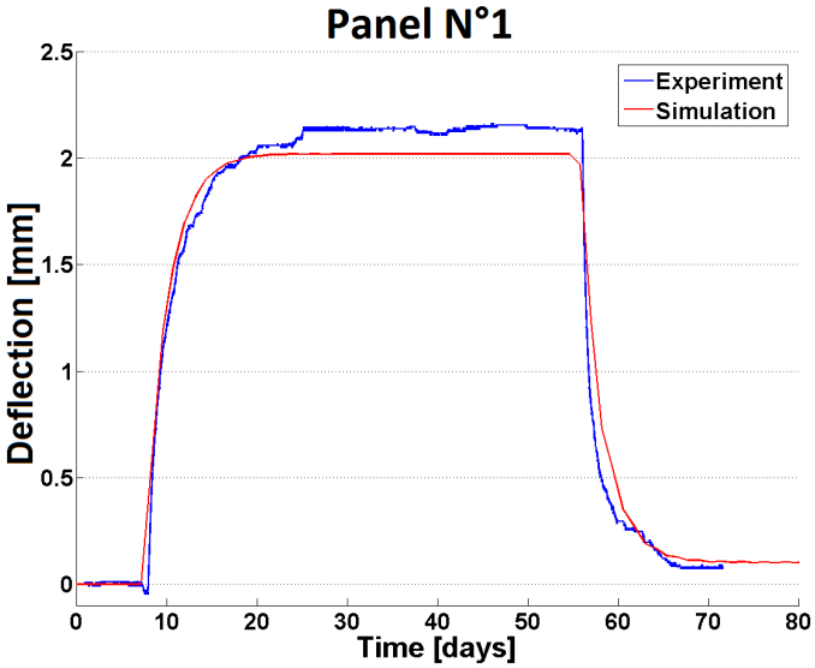

Figure 5.20: Cupping of a wooden paint panel subject to RH steps from 64 to 46% and back to 64%.

Analysis

As shown by the cupping of the painted panel in figure 5.20, the numerical model gives results similar to experiment. Indeed, the dynamics are the same, as well as the amount of cupping.

5.5.2 Numerical simulation versus fringe projection

Results

The deformation of four painted flat-sawn wooden panels under an RH step from 76 to 44% has been measured using fringe projection techniques following the experimental procedure described in section 5.3.3.1. The panels and experiments specifications are given in table 5.7. The climate during the measurement is shown in figure 5.15.

Table 5.7: Specification of the painted wood panels and the experimental setting of the projection fringe measurements.

		Panel N°4	Panel N°5	Panel N°6	Panel N°7
Panels information	Dimension (RxTxL) [m]	0.01 x 0.24 x 0.15	0.01 x 0.29 x 0.12	0.01 x 0.34 x 0.11	0.01 x 0.29 x 0.13
	Dry mass [g]	188.39	183.2	201.6	185.3
	Distance from the heart [m]	0.069	0.054	0.054	0.059
	Paint side	Pith	Bark	Bark	Pith
Climate condition	**Starting condition**				
	• RH [%]	65%	65%	65%	65%
	• Weight [g]	209.8	203.3	223.1	205.4
	• MC [%]	11.4%	11.0%	10.7%	10.8%
	Ending condition				
	• RH [%]	43.9 ±1.8	43.9 ±1.8	43.9 ±1.8	43.9 ±1.8
	• Weight [g]	205.1	199.4	219.4	201.7
	• MC [%]	8.85%	8.85%	8.85%	8.85%
	Mean temperature [°C]	20.53 ±0.08	20.53 ±0.08	20.53 ±0.08	20.53 ±0.08

The symmetry of the panels has been checked by plotting 2D-profiles along the L direction as shown in figure 5.21(a). All painted panels show good symmetry.

A comparison of the 2D-profiles between experiments and simulation of painted panel N°4 is presented in figure 5.21(b). Finally, the cupping profile (deflection) is shown for all painted panels in figure 5.22.

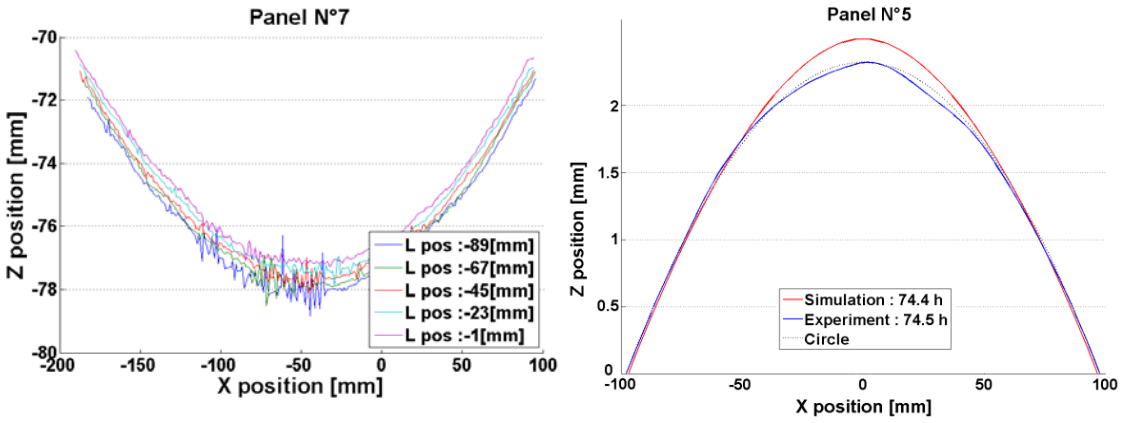

(a) (b)

Figure 5.21: (a) 2D profiles without any data processing taken at different location along the longitudinal direction. (b) Comparison of the experimental 2D-profile with simulation and arc of circle.

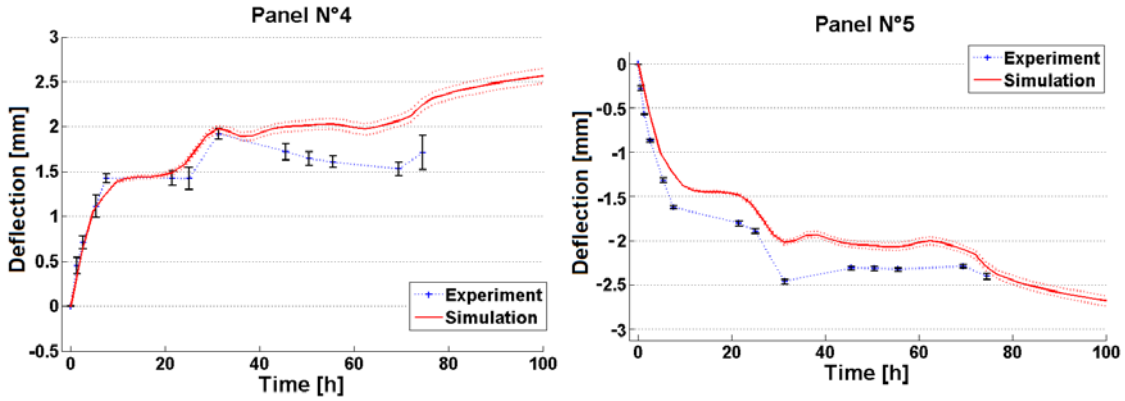

(a) (b)

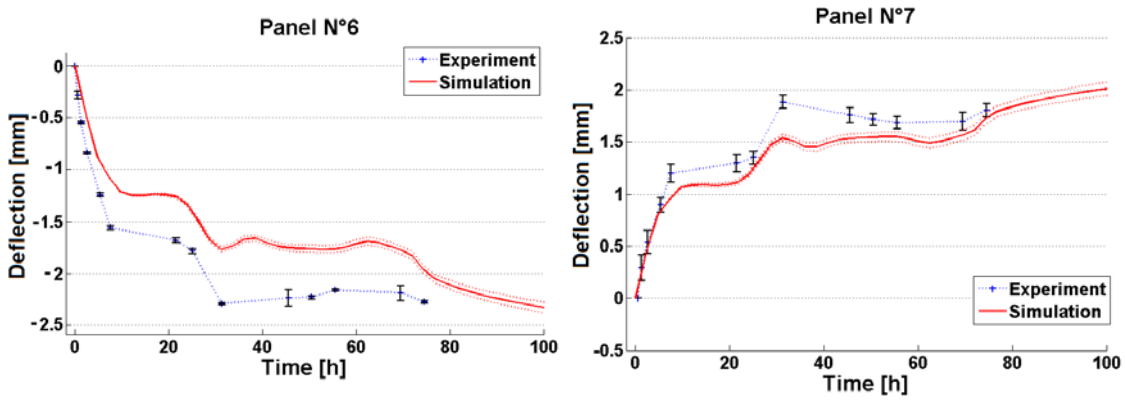

(c) (d)

Figure 5.22: Simulation and experimental cup deformations of four painted panels measured with fringe projection techniques.

Analysis

The cupping of the simulated painted panels is in good agreement with the experimental results as shown in figure 5.21(b). Moreover, the cupping profile follows better an arc of circle. This is due to the origin of the cupping as described in the next section (5.6.1).

The cupping of all four panels is also in good agreement with the corresponding simulation. The climatic variations can be directly correlated with the experimental and simulated cupping. Indeed, as shown in figure 5.15, the relative humidity shows a slight decrease followed by a strong increase at about 30 hours. This can be clearly seen on the experimental and simulated cupping. This effect of climate modification is less obvious in case of wood panels.

5.6 Behaviour and sensibility analysis of paintings

In this section, the behaviour of painted panels will be analysed and a sensibility analysis has been carried out on a set of parameters.

5.6.1 Importance/effect of the paint layer

It is well known that the hygroscopic deformation of flat-sawn wood panels is mainly cup deformation. This cupping comes from the anisotropy of the hygroexpansion. Indeed, the cupping changes with the panel width (i.e. in the middle of the wood panel, the anisotropy is maximal and at the far away border, it disappears as the panel orientation tends to quarter-sawn). This can be seen on the profile slope, plotted in figure 5.24(a). At a certain width (in our case about 50-75 mm) there is no anisotropic difference between the two faces of the panel and the slope becomes constant.

As shown by the cupping of the wood and painted panel in the previous sections, the paint layer induces a larger cupping compared to non-painted panels. Indeed, for similar conditions, the cupping deflection of wooden panels is about 0.5 – 0.7 mm, compared to 2.5 – 3 mm for painted panels.

Figure 5.23 shows the effect of the permeability of a non-stiff paint layer. The deformation starts with an important cup deformation during few hours which decrease afterwards. The final cupping, at EMC, depends on the ring orientation. This behaviour is due to the delay of moisture uptake in the painted side.

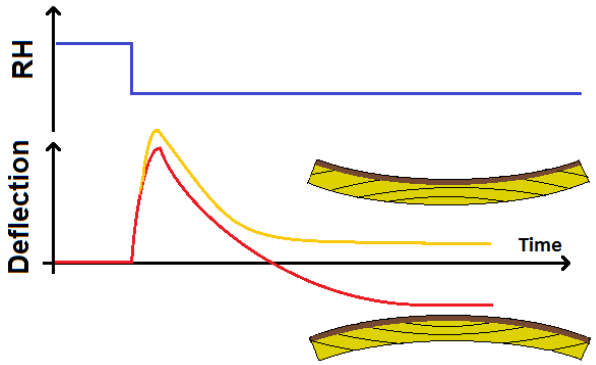

Figure 5.23: Qualitative cupping of painted panel in case of a drying. These cup deformations correspond to a non-stiff paint and depend on the position of the multi-layered paint relative to the ring orientation.

In our case, the deformation comes mainly from the deformation blocked by the painted face due to the important stiffness of the ground layer. The slope of profile never becomes constant as shown in figure 5.24(b). Indeed, all along the non-painted face, there will be a shrinkage and more or less no shrinkage of the paint face. However, the cupping is not following an arc of circle. Indeed, the slope of the simulated cupping shows an inflexion point at central position ($x=0$), compared to circle where the slope is linear. This is due to the fact that at the middle of the flat-sawn panel, the shrinkage is more important than at the ends due to the important amount of tangentially oriented wood.

Compared to the stiffness of radial and tangential wood (about 800 and 450 MPa) the ground layer is sufficiently stiff (about 1300 MPa) to contribute further to break the symmetry of the panel. As shown in figure 5.25(a), the paint stiffness has an important impact on the cupping and cannot be neglected if it is higher than about 50 MPa (for our spruce wood panels).

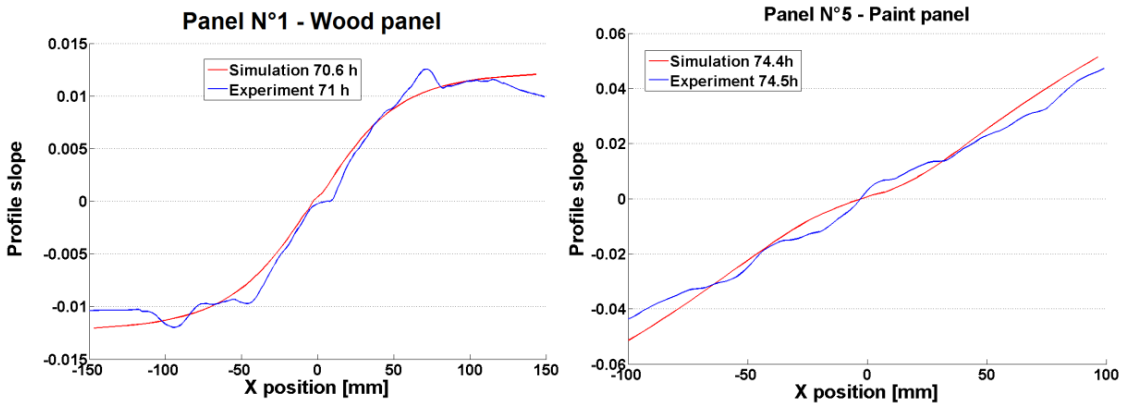

(a) (b)

Figure 5.24: Slope of the cupping (slope of the 2D-profile in the RT plane) for (a) a wooden panel and (b) a painted panel.

5.6.2 Sensibility analysis

It has been seen that the cupping of panel paintings depends strongly of the following parameters:

- Hygroscopic change
- Annual ring orientation
- Permeability of the multi-layered paint
- Stiffness of the multi-layered paint

Some sensibility analyses have been carried out on the previous parameters as shown in figure 5.25. The following simulations correspond to the painted panel N°4, subject to the RH step from 65 to 44%. The model parameters are shown in table 5.7.

It can be seen in the graphic (a) that the stiffness of the paint layer has an important effect on the cupping. A high stiffness will completely block the surface deformation of the painted side of the paintings. Therefore, the deformation is kept strongly cupped and does not decrease as for non-stiff paint as shown in figure 5.25(b). This last graphic shows the effect of the permeability for two different ground layer stiffness. In case of non-stiff-paint (1 MPa), the effect of the permeability is dominant. However, the variation of the permeability is shown for a stiff-paint (1300 MPa) also on figure 5.25(b). It can be seen that the effect is lower. This result is important when considering the characterisation of a painting. Indeed, much effort should be taken to characterise the multi-layered paint stiffness if it is high, and if it is low the efforts should be made for the permeability.

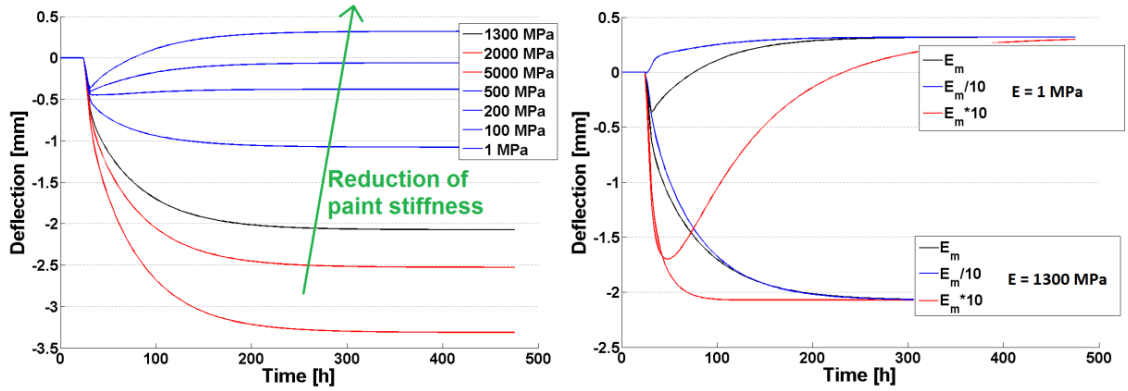

(a) (b)

Figure 5.25: Sensibility analysis on: (a) paint stiffness, (b) paint permeability for two different stiffness.

In figure 5.26, the two simulations of the same paint panel (always the paint panel N°4) are compared. One of the simulations has been made with the viscoelastic model and the other one with the elastic model. A significant difference can be seen between these two simulations of a painted panel. This is due to the high level of stresses that the stiff-paint imposes to the panel by blocking the paint face. The level of stresses is less important in the viscoelastic model due to the relaxation of the stresses as shown in figure 5.26(b). To simulate properly the behaviour of painted panel (with stiff paint layer), the viscoelastic behaviour cannot be neglected. In case of wood panel, no significant difference can be seen, because the level of stresses in lower.

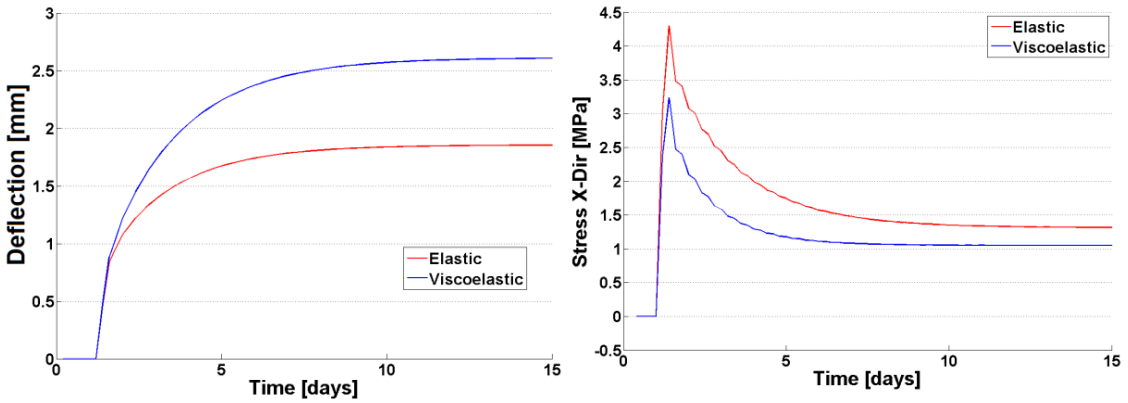

(a) (b)

Figure 5.26: Comparison between the elastic and viscoelastic model. (a) Deflection and (b) stress in the X direction below the paint layer in the middle of the paint panel.

5.7 Conclusions

The numerical model developed during this PhD is able to predict the deformation behaviour of painted panels as shown with the confirmation experiments that have been carried out. Is this model ready for predicting the behaviour of old paintings?

The wood of the panels used to confirm the model were almost perfect: The wood had regular and well aligned fibres with circular growth rings and without any visible default. The wood used for paintings was not always at such top quality. Anyway, the defaults in wood can at a certain extend be incorporated in the model. However, the paint layers were extremely regular: homogenous material and thickness. This is never the case for paintings. The authors of paintings used many pigments and materials for their paintings and the thickness is generally strongly inhomogeneous. The determination of the local permeability and stiffness of the paint is a very difficult task. Moreover, these two parameters are the most important ones for describing the paintings behaviour.

In terms of behaviour, the mechanosorption effect is neglected in the present model. Therefore, the simulations of complex climate condition are limited. Also for a single step of RH, the mechanosorption will induce important effects on stresses in the panel (R. Rémond, 2004). The effects include a stress reversal in the panel (A. Brandao and P. Perré, 1996). Indeed, during a drying the surface stresses are in tension and the bulk stresses in compression. By taking into account the mechanosorptive behaviour, these stresses, at the end of the RH steps will be reversed: compression at the surface and tension in the bulk. This effect cannot be seen in the model.

5.8 References

BRANDAO, A. & PERRÉ, P. The Flying Wood - A quick test to characterise the drying behaviour of tropical woods. 5th Int. IUFRO Wood Drying Conference, 1996 Quebec, Canada. 315-324.

COLMARS, J. 2011. *Hygromécanique du matériau bois appliquée à la conservation du patrimoine culturel : Etude sur la courbure des panneaux peints.* PhD, Université de Montpellier 2 (UM2).

FROIDEVAUX, J. 2009. *Simulation of the mechanical behavior of wood under relative humidity changes.* EPFL (Ecole Polytechnique Fédérale de Lausanne).

GORTHI, S. S. & RASTOGI, P. 2010. Fringe projection techniques: Whither we are? *Optics and Lasers in Engineering,* 48**,** 133-140.

GUIDOUM, A. 1994. *Simulation numérique 3D des comportements des bétons en tant que composites granulaires.* EPFL (Ecole Polytechnique Fédérale de Lausanne).

HANHIJIIRVI, A. 2000. Advances in the knowledge of the influence of moisture changes on the long-term mechanical performance of timber structures. *Materials and Structures / Matériaux et Constructions,* 33**,** 43-49.

HOADLEY, R. B. 1969. Perpendicular-to-grain compression set induced by restrained swelling. *Wood science,* 1**,** 6.

NAVI, P. & HEGER, F. 2005. *Comportement thermo-hydromécanique du bois: applications technologiques et dans les structures,* PPUR.

ORMARSSON, S. 1999. *Numerical analysis of moisture-related distortions in sawn timber.* Chalmers university of technology - Department of structural mechanics, Göteborg, Sweden.

ORMARSSON, S., DAHLBLOM, O. & PETERSSON, H. 1998. A numerical study of the shape stability of sawn timber subjected to moisture variation - Part 1: Theory. *Wood Science and Technology,* 32**,** 325-334.

ORMARSSON, S., DAHLBLOM, O. & PETERSSON, H. 1999. A numerical study of the shape stability of sawn timber subjected to moisture variation - Part 2: Simulation of drying board. *Wood Science and Technology,* 33**,** 407-423.

ORMARSSON, S., DAHLBLOM, O. & PETERSSON, H. 2000. A numerical study of the shape stability of sawn timber subjected to moisture variation Part 3: Influence of annual ring orientation. *Wood Science and Technology,* 34**,** 207-219.

POON, H. & AHMAD, M. F. 1998. A material point time integration procedure for anisotropic, thermo rheologically simple, viscoelastic solids. *Computational Mechanics,* 21**,** 236-242.

RÉMOND, R. 2004. *Approche déterministe du séchage des avivées de résineux de fortes épaisseurs pour proposer des conduites industrielles adaptées.* École Nationale du Génie Rural, des Eaux et des Forêts, Centre de Nancy.

TAYLOR, Z. A., COMAS, O., CHENG, M., PASSENGER, J., HAWKES, D. J., D., A. & S., O. 2009. On modelling of anisotropic viscoelasticity for soft tissue simulation: Numerical solution and GPU execution. *Medical Image Analysis,* 13**,** 234-244.

UZIELLI, L., DIONISI VICI, P. & COLMARS, J. 2009. Instrumentation pour le contrôle continu des panneaux peints en bois. *Technè,* 29**,** 27-27.

Chapter 6
Case study: old panel painting

Case study of an old panel painting is presented in this section. This painting is shown in figure 6.1. It has been rented from the *Swiss National Museum – Collection Centre* (Sammlungszentrum). It is a fake painting from an unknown artist and is composed of a multi-layered paint and a wooden support. The wood of this panel has been identified as spruce (*Picea abies* Karst. (L.)) of about 270 years old. The multi-layered paint is composed of a ground and a paint layer, similar to the multi-layered paint studied in chapter 4.

6.1 Old painting cupping measurement using fringe projection

The fringe projection technique has been used to measure the cupping of the old panel painting subjected to an RH variation. This was done as follows:

The stability of the EMC of the painting was controlled by weighing. Indeed, the painting was stored in a climate room controlled at 20°C and 50% RH and no significant mass variation has been detected over a period of one week. Next, the painting was wrapped in impermeable foil and transported to the EMPA laboratory. The final climate was set by the air conditioning of the laboratory: 20°C and 44% RH. To better stabilise the RH, a climatic tent was build all around the experimental setting as shown in figure 6.2(a & b). In this tent, the RH is maintained by salt saturated solution of potassium carbonate. The air conditioning system of the laboratory was also set at the same RH value. Next, the old panel painting was unwrapped from the foil and placed on a force sensor to follow the weight during the measurement. This sensor is shown in figure 6.2(c). It was placed inside the climatic tent. Finally, the shape is recorded by fringe projection techniques as shown in figure 6.2(d). The shape measurement system covers an area of $35x25cm^2$ presented by the

red rectangle in figure 6.1. The data processing of the measurement has been described in section 5.3.3.2.

Figure 6.1: The old wooden painting used for cupping measurement. A glue line is clearly visible (green arrow). The red frame indicates the fringe projection measurement area.

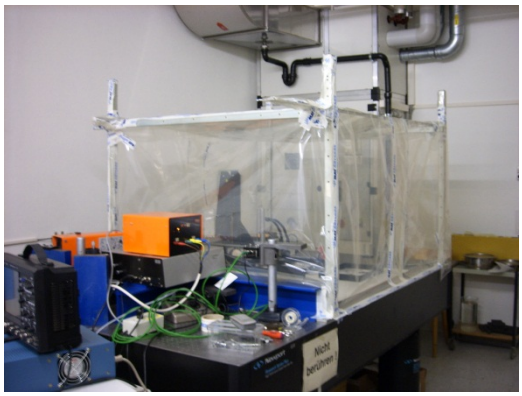

(a)

(b)

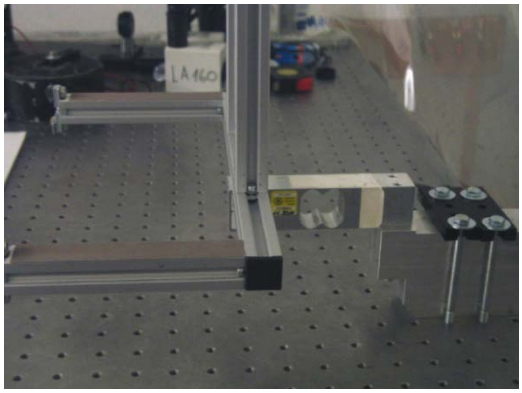

(c)

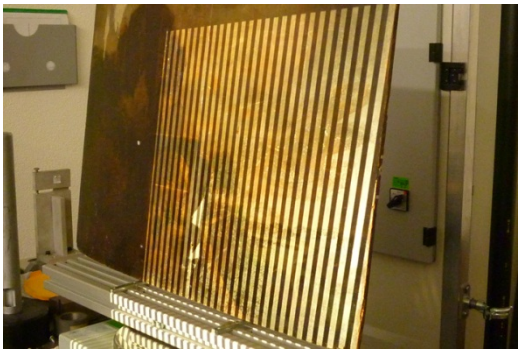

(d)

Figure 6.2: Photographs of the experimental setting for the fringe projection measurements. (a) Climatic tent constructed all around the experimental setting. (b) View from the panel inside the climatic tent. (c) Force sensor where the paintings where placed. (d) Fringe projection on the paintings.

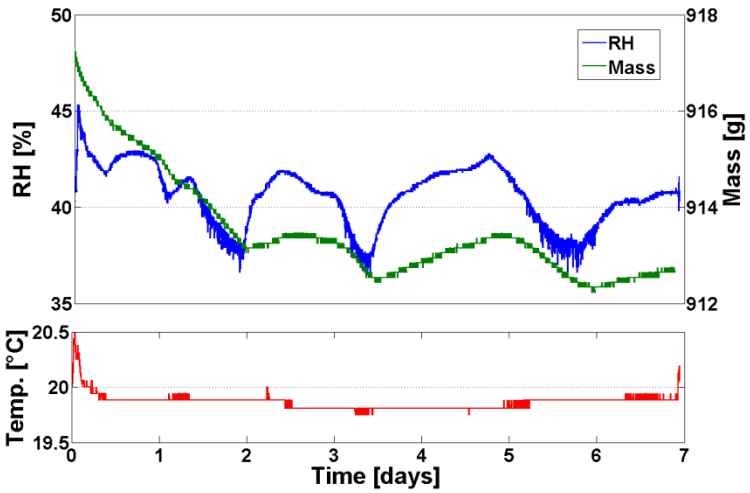

Figure 6.3: RH, mass and temperature evolution during the projection fringe measurement of the old paintings using the climatic tent shown in figure 6.2(a) and (b).

6.2 Characterisation of the painting

The characterisation of the old panel paintings is more difficult compared to the modern wood panels produced for the model confirmation experiments. No destructive testing can be carried out on real panel paintings. However, as the painting is a fake, we were authorised to sand the TR face as shown in figure 6.4.

Table 6.1 recapitulates the properties of the old painting and the experimental parameters of the fringe projection measurements. The values in black were measured, those in blue estimated, those in green calculated with the estimated blue ones and those in red unknown (taken from the multi-layered paint developed in chapter 4).

Figure 6.4: Sanded TR face of the old painting. The green arrow shows the glue line.

6.2.1 General characterisation of the panel painting

Firstly, it can be seen in figure 6.4, that the painting is composed of a unique wood panel, flat-sawn cut. The wood substrate has been identified as spruce wood (*Picea abies Karst. (L.)*). A glue line is visible on the painting as shown with a green arrow in figure 6.1 and figure 6.4. This glue line shows that the painting has been broken all along the longitudinal direction and it has been restored with glue.

Next, the age of the wood has been recognized by dendrochronology. This has been carried out by Dr. K. F. Kaiser from *Swiss Federal Research Institute for Forest, Snow and Landscape* in Birmensdorf. A non-interrupted sequence of 96

annual rings has been taken for the analysis. The age of cutting down of the tree is estimate at **1734**.

The annual ring orientation, i.e. the distance between the wood panel and the pit, is 48.9±5 mm, determined using the calculation shown in section 5.2.3. It can also be seen in figure 6.4 that the thickness of the wood panel is not constant. However, for the simulation an average thickness of 8 mm has been taken.

6.2.2 Wood panel characterisation

The wood colour was determined in the CIELAB colour space using the picture of the TR plane (figure 6.4) in Photoshop (graphics editing program). This last picture has been produced with a scanner. In order to be able to compare these colour parameters with the aging law, measured with a colorimeter, some samples of thermally aged wood have also been scanned. The differences between the scanned colour and the colour determined with the colorimeter have been taken into account for the characterisation of the old painting.

The mechanical and physical properties of wood have been taken equal to those of the non-aged wood (presented in table 5.3). Indeed, the elastic, viscoelastic and water diffusion parameters do not change significantly during aging.

The moisture content boundary and initial conditions were estimated by taking into account the mass loss measured with the force sensor during the RH step. Since the dry-mass of the painting is unknown, the equilibrium moisture content of the panel was estimated with the sorption isotherm of non-aged spruce wood. Next, from the measured mass losses, the dry-mass and the initial moisture content were calculated.

6.2.3 Multi-layered paint characterisation

Unfortunately, as shown in chapter 4, we failed to predict the properties of aged paint. However, it is known that the paint layers of paintings tend to crack with age. These cracks will decrease the stiffness and increase the permeability of the multi-layered paint. This can induce important change in the cupping dynamics of the painting as shown in section 5.6.2. In case of cracking, the permeability of the paint could become more influent on the cupping compared to the stiffness.

The old painting that has been investigated in this study didn’t show any crack in the multi-layered paint. Therefore, the aging of the stiffness and of the permeability will be neglected. Indeed, the effect of aging on the stiffness of the ground layer has not been investigated in our study, and the aging of the permeability does not induce important changes in case of a stiff ground (section 5.6.2). Moreover, due to the non-correspondence between naturally and thermally aged paint, the permeability of the latter paint cannot be used to estimate that of the former.

Permeability and stiffness of the multi-layered paint of the old painting can be measured only with destructive testing. However, the multi-layered paint of the old painting look similar than the paint study in chapter 4. Therefore, these values were taken as estimates for the non-aged paint.

The thickness of the paint was measured using the TR plane scan shown in figure 6.4. A mean value of 300 μm was taken for the whole painting.

6.2.4 Radial strength of aged wood

In chapter 3, the aging of the wood has been investigated. The objective is now to apply the wood aging law to the old panel painting to estimate the loss of radial strength. To calculate this strength, the age and the *average climate history* (ACH) of the old painting has to be known. The age has been calculated by dendrochronology and is about 277 years-old and the colour has been determined with the scan of TR plane (table 6.1).

Concerning the ACH of the old painting, aging law has been inversely applied with the colour data of the old painting. To reach a lightness of 53.74 after 277 years, the ACH is: 30°C with an MC of 10.1% (about 65% RH).

By applying this last ACH with the age of the paint in the aging law, or by using the linear relation between radial strength and lightness, the radial strength for the old painting spruce wood can be estimated as **5 MPa**.

6.3 Analysis through numerical modelling

6.3.1 Cupping

Figure 6.5 shows the 3D shape of the old painting and figure 6.6 shows the 2D profiles at different times. The glue line is clearly visible on each figure. The initial shape was already importantly cupped, with a deflection of 1.5 mm for a length of 180 mm.

In figure 6.7, the cupping and the mass of the old painting during the RH step is compared with the numerical model predictions. The simulated cupping is slightly higher than the real one, even by considering the uncertainty (shown by the dotted line) on the paint parameters (stiffness, thickness and permeability of the paint and the annual ring orientation). This can be due to the unknown paint stiffness and permeability which can significantly modify the amount of cupping. From the shape of the cupping curve, it can be deduced that the multi-layered paint is stiff. Indeed, a non-stiff paint should induce different cupping dynamics as detailed in section 5.6.

The climate changes, shown by the mass fluctuation, have been correctly simulated. A good correlation between the mass and the cupping is seen for both the simulation and the experiment.

Table 6.1: Old painting properties and experimental parameters of the fringe projection measurements. The value in blue are estimated, values in green are calculated from the estimated blue values and the red value are unknown (taken from the multi-layered paint developed in chapter 4).

		Old painting
Panels information	**Dimension [mm]**	
	• Thickness (R dir)	**8.00**
	• Wideness (T dir)	567
	• Length (L dir)	470
	Distance from the heart [m]	0.049±5
	Paint side	Bark
	Years - Age (in 2011)	1734 - 277
	Colour CIELAB*	
	• L*	53.75
	• a*	7.5
	• b*	26.25
	Dry mass [g]	**843**
	Dry density [kg m^{-3}]	**395**
Climate condition	**Starting condition**	
	• RH [%]	50%
	• Weight [g]	917.3
	• MC [%]	**8.83%**
	Ending condition	
	• RH [%]	40.6% ±1.5
	• Weight [g]	912.2
	• Weight difference [g]	5.1
	• MC [%]	**8.22%**
	Mean temperature [°C]	19.86±0.06
Multi-layered paint properties	Thickness [µm]	**300**
	Stiffness [MPa]	**1'350**
	Permeability [g s^{-1} m^{-2}]	**22.4e-5**

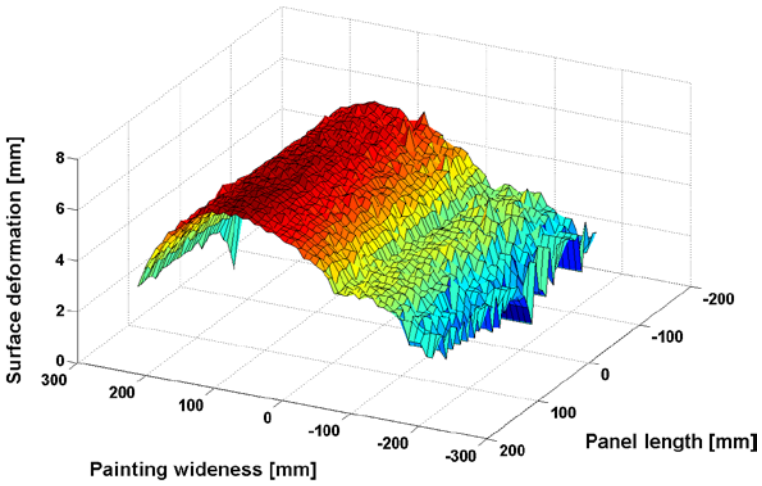

Figure 6.5: Surface shape of the old painting after one hours of RH step. The glue line of the wood panel can be seen at about -50 mm of the width.

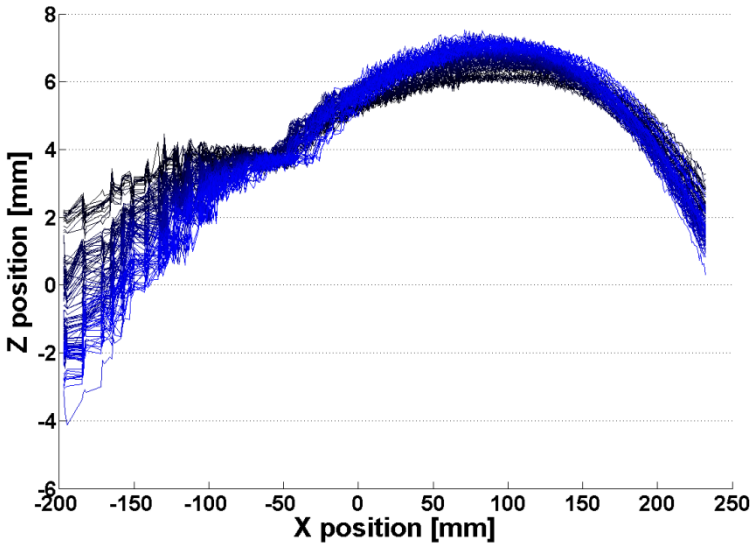

Figure 6.6: 2D profiles in the middle of the measurement zone, of the old painting taken at different times from 0 to 8 days from the black to the blue respectively.

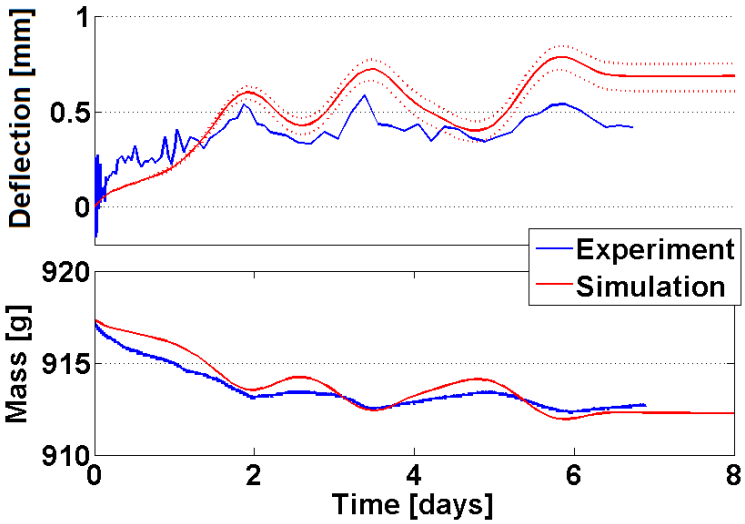

Figure 6.7: Mass and deflection (for a width of 180 mm) of the old painting compared to the simulation. The dotted lines correspond to the uncertainty of the painting characterisation. The RH step was from 50 to 40%.

6.3.2 Stress analysis

The stresses during the RH step of the old painting can be calculated by the numerical model. It is important to note that these stresses are calculated by not considering the possible mechanosorptive effects.

6.3.2.1 Wood panel and painted panel stress analysis

Figure 6.8 shows the stresses in the wood panel N°1 calculated with the numerical viscoelastic model after 100 hours (parameters are given in table 5.5). Firstly, it can be seen that the maximal stresses are developed in the middle part of

the panel. Secondly, during a drying, the surface stresses are positive (tension) and the bulk-stresses are negative (compression). Figure 6.9(a) shows the X-stresses in the wood panel against time at the surface and in the bulk. After 8 days, at EMC, the stresses are close to zero. This is not the case in reality, due to mechanosorption.

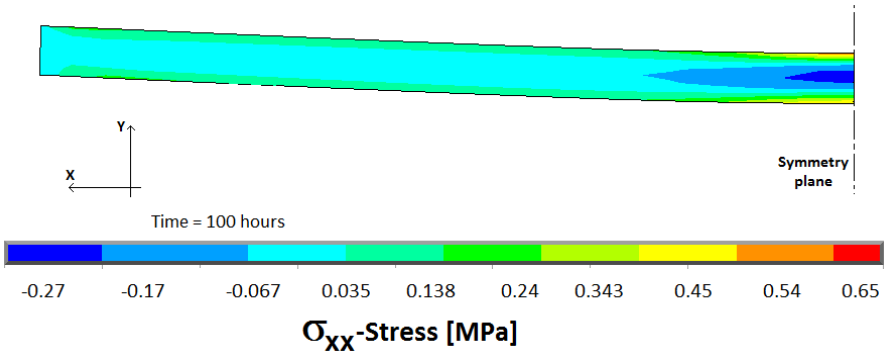

Figure 6.8:X-Stresses in the wood panel N° 1, after 100 hours of the RH step from 65 to 44% (table 5.5).

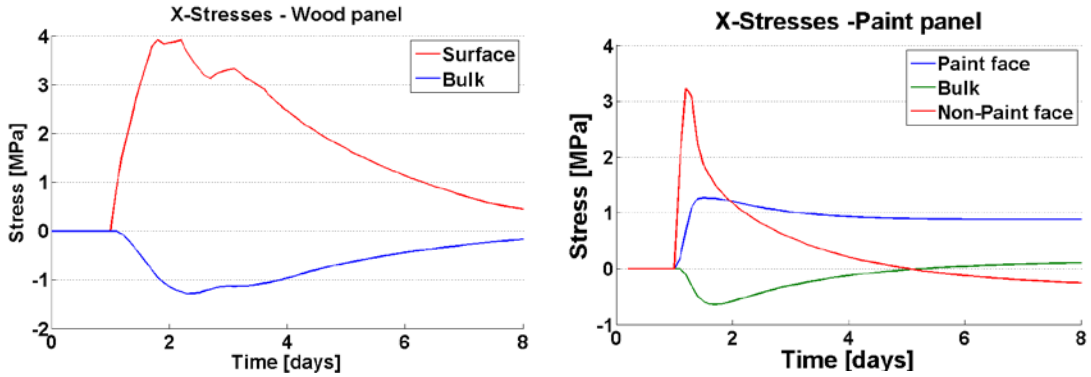

(a) (b)

Figure 6.9: X-Stresses against time at different location in a wooden panel (a) and in a painted panel (b).

Figure 6.10 and figure 6.11 show the stresses in the painted panel N°4 (parameters given in table 5.7) at 10 and 240 hours respectively. The evolution of the stresses in the wood against time at different locations is shown in figure 6.9(b).

Important stresses are developed under the multi-layered paint. It can be seen that the paint face is in tension, due to the high stiffness of the multi-layered paint which restrains the wood shrinkage. As for wooden panel, the bulk is compressed due to the shrinkage of the non-paint face, but afterwards the tension induced by the multi-layered paint diffuses in the bulk. Again, these stresses are mechanosorption-free and therefore are not exactly as in reality.

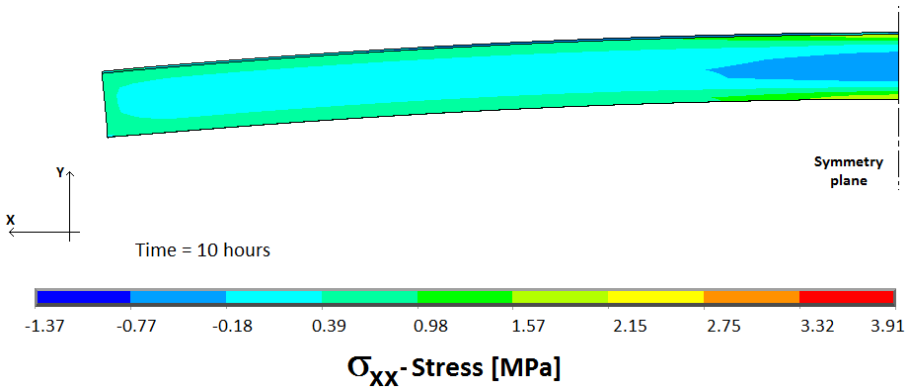

Figure 6.10: X-Stresses in the paint panel N°4, after 10 hours of the RH step from 65 to 44% (table 5.7).

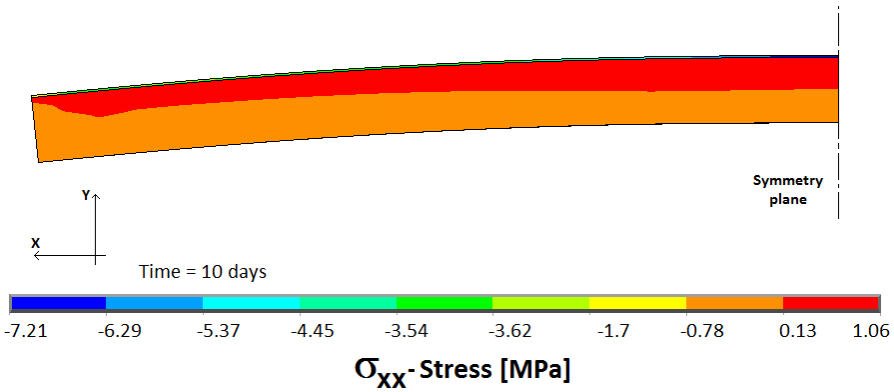

Figure 6.11: X-Stresses in the paint panel N°4, after 10 days of the RH step from 65 to 44%.

6.3.2.2 Old painting stresses

The X-stresses in the old panel paintings during the cupping measurement are shown against time in figure 6.12(a). Climate fluctuations induce important stress variations.

The RH step from 50 to 40% imposed to the old painting do not induce stresses above the failure stresses, even by considering the aging-reduced strength. Indeed, the maximum tensile stress in the radial direction (local coordinate system) in the wood is far from the radial strength: **0.48 MPa** as shown in figure 6.12(b).The maximal and minimal stresses are located on the painted and non-painted face, respectively, and at an *x* location of about *260 mm* (*x=0* is the middle of the panel), closed to the border (the *1/2* length is *283.5 mm*).

By considering a larger RH step, for example the RH step imposed to the dummy paint panel from 65 to 44% (section 5.4), the maximal radial stress became: **2.68 MPa**. This stress is also below the radial failure stress. However, based on the aging law, when the old panel painting will be 1770 years-old the radial strength would fall to that value of 2.68.

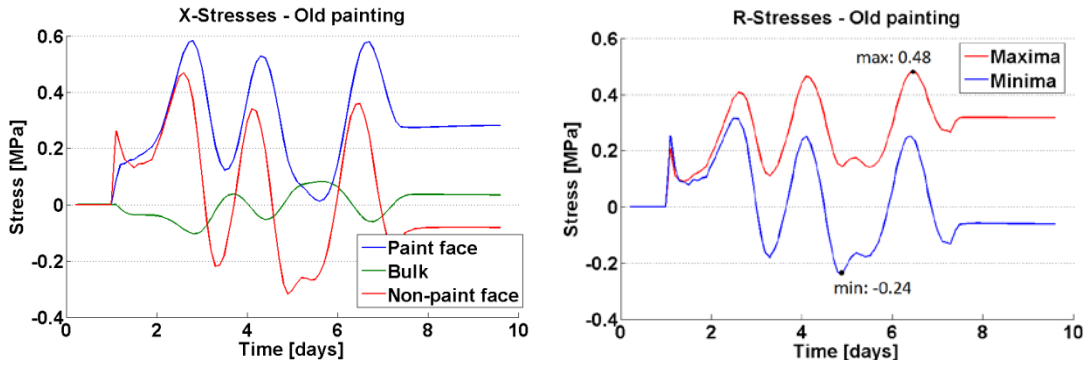

(a) (b)

Figure 6.12: Stress analysis in the old painting. (a) X-Stresses against time at different location in the old paintings during the RH step presented in figure 6.3. (b) Maximal and minimal R-stresses in the old painting.

6.3.2.3 Stress in the ground layer

The stresses in the multi-layered paint are localized in the stiff ground layer. Indeed, the paint layer is not stiff and its strain to failure is large as seen in section 4.3.2.2.

The maximal stresses, calculated by the numerical model, were *1.58* MPa in the ground layer during the cupping measurement. This is less than the failure stress of the ground layer which is *4.4±1.0* MPa. Again, by considering the climate variation from 65 to 44%, the stress in the ground layer increases to *6.4* MPa. This is definitely greater than the failure stress. The ground layer may crack.

6.4 Conclusion

If the old painting is kept under controlled ambient condition with slow and small changes in RH, no particular risk of failure is expected. The RH steps that we have investigated were quite strong for the panel painting. Indeed, the changes were important and instantaneous. This level of changes could be applied on panel painting only in case of accident or negligence. It could also occur in situations of transportation, when the changing of environment imposes important and instantaneous RH fluctuation if no precaution is taken. However, even with such RH variations, it has been shown that no damage should appear before a long time.

The most important risk of failure comes from the multi-layered paint as shown by our calculation.

Is it possible to calculate more precisely the stresses in the old panel paintings? The most important aspects of behaviour that have been neglected are mechanosorption and thermal coupling. Considering them will definitely increase the precision of the numerical model. However, the most important difficulty to calculate the behaviour of panel paintings is the determination of the initial state of the

moisture content and internal stresses. These initial states can only be estimated with the numerical model itself by simulating the complete history of the painting.

Further studies should been done by considering different mechanical boundary conditions. Indeed, the old painting that has been investigated during this project was free to move. Frames, for example, can limit the panel deformation and therefore induces stresses which could attain risk values.

Chapter 7
Conclusion and perspectives

7.1 General conclusion

The **first purpose** of this PhD thesis was to determine which, and how, mechanical and physical properties of wood and paint are modified by long aging time and if the aging could be obtained by accelerated methods using mild thermo-hydrous treatment.

The investigation on the wood aging was successful. The good durability (under appropriate climate condition) of spruce wood has been confirmed. Mechanical and physical properties such as moduli of elasticity, viscoelastic parameters, sorption of water and diffusion of water remain more or less unchanged after several centuries of aging. On the other hand, the colour of the wood is modified and the radial strength is rather strongly degraded.

In order to be able to predict the loss of strength and the loss of colour lightness, accelerated aging by thermo-hydro treatments was investigated. Two thermo-hydro reactors were developed to control precisely the treatment variables such as time, temperature, RH and pressure.

Thermally treated wood samples show some similarities with naturally aged wood. Indeed, the mechanical properties appear similar (no modification of the elastic and viscoelastic behaviour and a marked loss of radial strength). However, the sorption and diffusion of water in wood show differences. This indicated that the chemical changes in the hemicellulose are probably different between the thermally and naturally aged samples. On the other hand, the chemical changes in the lignin of the wood could be more similar. Taking this into consideration, radial strength and colour lightness of thermally aged wood samples were fitted on a kinetic law of chemistry. This law is dependent upon the treatment variables. Finally, this kinetic law were extrapolated at standard condition (i.e. as if the treatment was performed at ambient temperature and RH) in order to predict the natural aging. Thanks to a linear

relation between radial strength and colour lightness, the aging law has been used to predict the loss of radial strength of an old panel painting by using its colour.

Thanks to the collaboration with the university of the arts from Bern (BFH-HKB), similar investigations were done also on the paint layer (linseed oil with white lead pigments). Mechanical testing of the thin layers of paint and ground layer was developed and isothermal sorption chambers has been designed and constructed in order to determine their permeability by inverse algorithm. Aging chambers with controllable temperature and UV light exposure were designed and constructed to accelerate the paint aging. Unfortunately, the aging of the paint seems to be much more difficult to estimate compared to wood due to many reaction pathways that can be thermally activated. Indeed, even aging treatments at only 40°C induce dissimilar chemical reactions compared to natural aging. Consequently, no prediction on the paint layer was found.

The **second purpose** of this PhD work was to simulate numerically and to analyse the behaviour of non-aged and old painted panels under RH variations, and verify the modelling by experiments.

The 3D hygromechanical simulations of wood painted panels were done including an anisotropic viscoelastic model that we implemented in the FE-software ANSYS. This model was able to account for the annual rings orientation. The multi-layered paint has been simulated as one layer using plate elements, with the stiffness of the ground layer. The permeability of the paint layer has been taken as a boundary condition.

In order to confirm the model, two experimental measurement techniques were used: Deformometric kit (measurement of the length of two columns fixed perpendicular to the panel surface) and fringe projection technique (optical techniques based on the projections of fringes pattern of the panel and recording of the pictures at a different and known position). This model was able to predict the deformation behaviour of wood panels and painted panels compared with the confirmation experiments. These last experiments were performed on prepared paint panel with perfect multi-layered paint thickness and material (ideal case) and high quality wood but as well as within a well-defined climate condition. The model was also in good agreement compare to a real old panel painting but difficulties of the painting characterisation have been met, specifically for the multi-layered paint.

The stress analysis on the old panel painting shows that normal climate fluctuation should not promote cracks in the wooden support but the cracking of the ground layer is possible under fast RH changes.

7.2 Future development

This work shows that the prediction of the naturally aged wood properties is possible and should be taken into account. Aging law for spruce wood has been successfully fitted for colour and radial strength. The radial strength investigated during this project can give information on the risks of damages of non-damaged panel paintings. In case of fractured panel paintings, linear fracture mechanics analysis can be applied to calculate the stress concentration at crack tip and evaluate the instability conditions of existing cracks. Such analysis requires the knowledge of the crack length and stress intensity factors in the different modes of rupture. Future developments would be to find the aging law of such parameters. Moreover, different loading directions should be investigated such as the RL and TL plane, the strength along the T direction and possibly the L.

Another important mechanical aspect in panel paintings is the non-linear behaviour and more specifically in compression known as *Compression Set (P. Navi and D. Sandberg, 2012).* J. Colmars investigated the level of compression set that are developed in an old panel painting under varying humidity (J. Colmars, 2011). He didn't note any important irreversible deformation. However, his model was based on non-aged parameters for the compression set. If the elastic limit is reduced by aging such as strength, the level of irreversible compressed wood would be increased. The level of compressed wood in painting is important to be identified. Indeed, it could explain why the old panel paintings have a remaining convex (from the painted side) cupping.

A lot of works are still needed for better understanding the difference between the thermally aged wood and the natural aging in terms of chemistry. Indeed, due to the relatively low temperature and RH used for the accelerated aging, the levels of chemical changes are low. The different spectroscopy techniques used during this project (FTIR, UVRR, XPS), which are well suitable for standard thermal treatments (higher temperature level), are not able to clearly detect differences in the chemistry of naturally and thermally aged wood. Moreover, these techniques give mainly qualitative information. In order to clearly link the loss of radial strength and lightness with the chemical changes, quantitative value about the chemistry of lignin specifically should be measured.

This might be investigated with the following techniques:

Extraction of wood component – By extracting specifically the lignin and the hemicellulose from wood the relative quantity of these molecules in wood could be determined, and the level of oxidation could be estimated.

Analyse of the output gases of the TH reactors - This could be done directly by *Gas Chromatography - Mass Spectrometry* (GC-MS). The analysis of the soluble component of the output gases of the TH reactors could give also quantitative values.

It has to be noted that the acid level of this solution has been investigated by acidic titration using a solution of NaOH in this study. However, only in case of strong thermal treatment a slight increase of acidity has been detected. However, analysing this solution with more sensible techniques such as *High Performance Liquid Chromatography* (HPLC) could also give more quantitative indications.

The problem of the analysis of the output gases is that the results cannot be compared with the chemical change in the natural aging. However, rich information about the mild thermo-hydro treatments could be identified.

UV-Microspectrophotometry (UMSP) – With this technique the topochemical characterisation of modification of lignin can be made within individual cell layers as was applied on wood welded joint by (M. I. Placencia *et al.*, 2012). This could give us interesting information in the region where the radial failure occurs (i.e. between cell wall layers S1 and S2 and in the middle lamella).

As shown in chapter 4, the aging of the paint seems to be much more difficult to be estimated by accelerated method compared to wood. Indeed, many reaction pathways can be thermally activated. Moreover, the effects of RH and the light exposition should be added. It still needs considerable research efforts to justify an accelerated aging of the paint layer.

However, as seen during the investigation of the old panel painting in chapter 6, the characterisation of the permeability and the stiffness of the multi-layered paint is impossible directly without destructive testing. This is mainly due to the extreme inhomogeneity of the materials and its thickness, and added to this possibly a cracked pattern of the paint layers. Even with a good aging law for the paint layers, all these homogeneities cannot be precisely estimated. Inverse methodology, as applied by (J. Colmars, 2011), appears to be a more appropriate technique to determine such complex properties. It consists of measuring the 3-dimensional deformation of the old paintings, subjected to an RH change (typically measured with fringe projection techniques or other optical techniques) and minimise the differences with simulated results by varying the paint permeability and stiffness. An optimisation could be made for each paint layers elements.

The mechanosorption could be added too but the materials parameters should be determined as well as their aging.

7.3 References

COLMARS, J. 2011. *Hygromécanique du matériau bois appliquée à la conservation du patrimoine culturel : Etude sur la courbure des panneaux peints.* PhD, Université de Montpellier 2 (UM2).

NAVI, P. & SANDBERG, D. 2012. *Thermo-Hydro-Mechanical Wood Processing*, EPFL Press - Distibuted by CRC Press.

PLACENCIA, M. I., KOCH, G., PIZZI, A. & PICHELIN, F. 2012. Characterisation of the welding zone of spruce by UMSP. *In:* LORRAINE, U. D. (ed.) *COST Action FP0904: Current and Future Trends of Thermo-Hydro-Mechanical Modification of Wood. Opportunities for new markets ?* Nancy, France.

References

ACIDINI, A., CIATTI, M., BONSANTI, G., FROSININI, C., UZIELLI, L., CASTELLI, C. & SANTACESARIA, A. 2006. *Panel Painting - Technique and conservation of wood supports*, EDIFIR - Edizioni Firenze.

AUDOUIN, L., LANGLOIS, V., VERD, J. & J.C.M., B. 1994. Role of Oxygen Diffusion in Polymer ageing - Kinetic and mechanical aspects. *Journal of Materials Science,* 29**,** 569-583.

BÉGIN, P. L. & KAMINSKA, E. 2002. Thermal accelerated ageing test methods development. *Restaurator,* 23**,** 89-105.

BORGIN, K., FAIX, O. & SCHWEERS, W. 1975a. The effect of Aging on Lignins of wood. *Wood Science and Technology,* 9**,** 207-211.

BORGIN, K., PARAMESWARAN, N. & LIESE, W. 1975b. The effect of aging on the ultrastructure of wood. *Wood Science and Technology,* 9**,** 87-98.

BRANDAO, A. & PERRÉ, P. The Flying Wood - A quick test to characterise the drying behaviour of tropical woods. 5th Int. IUFRO Wood Drying Conference, 1996 Quebec, Canada. 315-324.

BURMESTER, A. 1978. Seasonal-Changes of Physical Wood Properties in Oak Wood (Quercus-Robur L). *Holz Als Roh-Und Werkstoff,* 36**,** 315-321.

CELINA, M., GILLEN, K. T. & ASSINK, R. A. 2005. Accelerated ageing and lifetime prediction - review of non-Arrhenius behaviour due to two competing processes. *Polymer Degradation and Stability,* 90**,** 395-404.

COLMARS, J. 2011. *Hygromécanique du matériau bois appliquée à la conservation du patrimoine culturel : Etude sur la courbure des panneaux peints.* PhD, Université de Montpellier 2 (UM2).

DLOUHÀ, J., CLAIR, B., ARNOULD, O., HORÀCEK, P. & GRIL, J. 2009. On the time-temperature equivalency in green wood: Characterisation of viscoelastic properties in longitudinal direction. *Holzforschung,* 63**,** 327-333.

DUREISSEIX, D. & MARCON, B. 2011. A partitioning strategy for the coupled hygromechanical analysis with application to wood structures of cultural heritage. *International Journal for Numerical Methods in Engineering,* 88**,** 228-256.

ERHARDT, D. & MECKLENBURG, M. 1996. Accelerated vs Natural Aging: Effect of Aging Conditions on the Aging Process of paper. *Material Issues in Art and Archaeology IV,* 352**,** 247-270.

ERHARDT, D., MECKLENBURG, M. F., TUMOSA, C. S. & OLSTAD, T. M. 1996. New versus old wood: differences and similarities in physical, mechanical, and chemical properties. *ICOM Preprints, 11th Triennial Meeting,* 2**,** 903-910.

FELLER, R. L. 1994. *Accelerated ageing - photochemical and thermal aspects*, Getty Conservation Institute, Los Angeles.

FRANKEL, E. N. 1998. *Lipid Oxidation*, Oily Press, Dundee Scottland.

FROIDEVAUX, J. 2009. *Simulation of the mechanical behavior of wood under relative humidity changes.* EPFL (Ecole Polytechnique Fédérale de Lausanne).

FROIDEVAUX, J., VOLKMER, T., GANNE-CHÉDEVILLE, C., GRIL, J. & NAVI, P. 2012. Viscoelastic behaviour of aged and non-aged spruce wood in the radial direction. *Wood Material Science and Engineering,* 7**,** 1-12.

GANNE-CHÉDEVILLE, C., JÄÄSKELÄINEN, A. S., FROIDEVAUX, J., HUGHES, M. & NAVI, P. 2011. Natural and artificial ageing of spruce wood as observed by FTIR-ATR and UVRR spectroscopy. *Holzforschung,* 66**,** 163-170.

GEREKE, T. 2009. *Moisture-induced stresses in cross-laminated wood panels.* ETH Zürich.

GONZALEZ-PENA, M. M. & HALE, M. D. C. 2009a. Colour in thermally modified wood of beech, Norway spruce and Scots pine. Part 1: Colour evolution and colour changes. *Holzforschung,* 63**,** 385-393.

GONZALEZ-PENA, M. M. & HALE, M. D. C. 2009b. Colour in thermally modified wood of beech, Norway spruce and Scots pine. Part 2: Property predictions from colour changes. *Holzforschung,* 63**,** 394-401.

GORTHI, S. S. & RASTOGI, P. 2010. Fringe projection techniques: Whither we are? *Optics and Lasers in Engineering,* 48**,** 133-140.

GRIL, J. 1988. *Une modelisation du comportement hygro-rhéologique du bois à partir de sa microstructure.* Université Paris 6, Sciences Physiques.

GRIL, J., RAVAUD, E., UZIELLI, L., DUPRÉ, J. C., PERRÉ, P., DUREISSEIX, D., ARNOULD, O., VICI, D. P., JAUNARD, D. & MANDRON, P. 2007. Le cas de la Joconde : modélisation mécanique de l'action du châssis-cadre. *Actes de la journée d'étude Conserver aujourd'hui : les vieillissements du bois.* Cité de la Musique, Paris, France.

GRIL, J., RAVAUD, E., UZIELLI, L., DUPRÉ, J. C., PERRÉ, P., DUREISSEIX, D., ARNOULD, O., VICI, P. D., JAUNARD, D. & MANDRON, P. Mona Lisa saved by the Griffith theory: Assessing the crack propagation risk in the wooden support of a panel painting. International Conference on Integrated Approach to Wood Structure, Behavior and Applications, ESWM and COST Action E35, May 2006 Florence (Italy).

GROSSMAN, P. 1976. Requirements for a model that exhibits mechano-sorptive behavior. *Wood Science and Technology,* 10**,** 163-168.

GUIDOUM, A. 1994. *Simulation numérique 3D des comportements des bétons en tant que composites granulaires.* EPFL (Ecole Polytechnique Fédérale de Lausanne).

HANHIJIIRVI, A. 2000. Advances in the knowledge of the influence of moisture changes on the long-term mechanical performance of timber structures. *Materials and Structures / Matériaux et Constructions,* 33**,** 43-49.

HEGER, F. 2004. *Etude du phénomène de l'élimination de la mémoire de forme du bois densifié par post-traitement themo-hydro-mécanique.* EPFL (Ecole Polytechnique Fédérale de Lausanne).

HILL, C. A. S. 2006. *Wood modification: chemical, thermal and other processes*, John Wiley \& Sons.

HOADLEY, R. B. 1969. Perpendicular-to-grain compression set induced by restrained swelling. *Wood science,* 1**,** 6.

HUNT, D. 1982. Limited mechano-sorptive creep of beech wood. *Journal of the Institute of Wood Science,* 9**,** 136-138.

HUTCHINSON, G. H. 1973. Some aspects of drying oil technology. *Journal of Oil Chemists Association,* 56**,** 44-53.

JOHANSSON, L.-S., CAMPBELL, J. M., HÄNNINEN, T., GANNE-CHÈDEVILLE, C., VUORINEN, T., HUGHES, M. & LAINE, J. 2012. XPS and the medium-dependent surface adaptation of cellulose in wood. *Surface and Interface Analysis*.

KOHARA, J. 1952. Studies on the durability of wood I, mechanical properties of old timbers. *Bulletin of Kyoto Prefectural University,* 2**,** 116-131.

KOHARA, J. 1953. Studies on the permanence of wood V, shrinkage and swelling of old timbers about 300-1300 years ago. *Bulletin of Kyoto Prefectural University,* 5**,** 81-88.

KOHARA, J. 1954a. Studies on the permanence of wood VI, the changes of mechanical properties of old timbers. *Bulletin of Kyoto Prefectural University,* 6**,** 164-174.

KOHARA, J. 1954b. Studies on the permanence of wood VII, the influence of age on the components of wood (Chamaecyparis obtusa Endlicher). *Bulletin of Kyoto Prefectural University,* 6**,** 175-182.

KOHARA, J. 1955a. On permanence of wood II, differences between the ageing processes of cypress wood and zelkova wood. *Wood industry,* 10**,** 395-399.

KOHARA, J. 1955b. Studies on the permanence of wood XV, the influence of age on the components of wood (Zelkowa serrata Makino). *Mokuzai Gakkaishi*, 1**,** 21-24.

KOLLMAN, F. 1951. *Technologie des Holzes und der Holzwerkstoffe*, 2. Auflage, Springer, Berlin.

MARCON, B. 2009. *Hygromécanique des panneaux en bois et conservation du patrimoine culturel : des pathologies...aux outils pour la conservation.* PhD, Université Montpellier 2 - Università degli studi di Firenze.

MATSUO, M., YOKOYAMA, M., UMEMURA, K., GRIL, J., YANO, K. I. & KAWAI, S. 2010. Color changes in wood during heating: kinetic analysis by applying a time-temperature superposition method. *Applied Physics A-Materials Science \& Processing,* 99**,** 47-52.

MATSUO, M., YOKOYAMA, M., UMEMURA, K., SUGIYAMA, J., KAWAI, S., GRIL, J., KUBODERA, S., MITSUTANI, T., OZAKI, H., SAKAMOTO, M. & IMAMURA, M. 2011. Aging of wood: Analysis of color changes during natural aging and heat treatment. *Holzforschung,* 65**,** 361-368.

MECKLENBURG, M. F., TUMOSA, C. & ERHARDT, D. Structural Response of Painted Wood Surfaces to Changes in Ambient Relative Humidity. Painted Wood: History and Conservation, 1998. Los Angeles: Getty Conservation Institute, 464-484.

MECKLENBURG, M. F. & TUMOSA, C. S. Mechanical behavior of paintings subjected to changes in temperature and relative humidity. *In:*

MECKLENBURG, M. F., ed. Art in transit: studies in the transport of paintings, 1991. NATL GALLERY ART, 173-216.

MILLETT, M. A. & GERHARDS, C. C. 1970. Accelerated Aging: Residual Weight and Flexural Properties of Wood Heated in Air at 115° to 175°C. *Wood science,* 4**,** 193-201.

MISZCEZYK, A. & DAROWICKI, K. 2001. Accelerated ageing of organic coating systems by thermal treatment. *Corrosion science,* 43**,** 1337-1343.

MOHEN, J. P., MENU, M. & MOTTIN, B. 2006. *Au coeur de La Joconde: Léonard de Vinci décodé - Centre de recherche et de restauration des musées de France*, Gallimard.

NAVI, P. & HEGER, F. 2005. *Comportement thermo-hydromécanique du bois: applications technologiques et dans les structures*, PPUR.

NAVI, P., PITTET, V. & PLUMMER, C. J. G. 2002. Transient moisture effects on wood creep. *Wood Science and Technology,* 36**,** 447-462.

NAVI, P. & SANDBERG, D. 2012. *Thermo-Hydro-Mechanical Wood Processing*, EPFL Press - Distibuted by CRC Press.

NEGI, A. 1999. Turbulence in the wood system with small and short stresses. *Wood Science and Technology,* 33**,** 209-214.

OBATAYA, E. 2007. Caractéristiques du bois ancien et technique traditionnelle japonaise de revêtement pour la protection du bois. *Actes de la journée d'étude Conserver aujourd'hui : les vieillissements du bois.* Cité de la Musique, Paris, France.

OBATAYA, E. Effects of ageing and heating on the mechanical properties of wood. Wood Science for Conservation of Cultural Heritage, Proceedings of the International Conference held by COST Action IE0601, 2009 Florence, Italy. 16-23.

OLEK, W., PERRÉ, P. & WERES, J. 2005. Inverse analysis of the transient bound water diffusion in wood. *Holzforschung,* 59**,** 38-45.

OLEK, W. & WERES, J. 2007. Effects of the method of identification of the diffusion coefficient on accuracy of modeling bound water transfer in wood. *Transport in Porous Media,* 66**,** 135-144.

ORMARSSON, S. 1999. *Numerical analysis of moisture-related distortions in sawn timber.* Chalmers university of technology - Department of structural mechanics, Göteborg, Sweden.

ORMARSSON, S., DAHLBLOM, O. & PETERSSON, H. 1998. A numerical study of the shape stability of sawn timber subjected to moisture variation - Part 1: Theory. *Wood Science and Technology,* 32**,** 325-334.

ORMARSSON, S., DAHLBLOM, O. & PETERSSON, H. 1999. A numerical study of the shape stability of sawn timber subjected to moisture variation - Part 2: Simulation of drying board. *Wood Science and Technology,* 33**,** 407-423.

ORMARSSON, S., DAHLBLOM, O. & PETERSSON, H. 2000. A numerical study of the shape stability of sawn timber subjected to moisture variation Part 3: Influence of annual ring orientation. *Wood Science and Technology,* 34**,** 207-219.

PERRÉ, P., RÉMOND, R. & GRIL, J. La simulation des effets de variation de l'ambiance. *In:* MOHEN, J. P., MENU, M. & MOTTIN, B., eds. Au coeur de

la Joconde: Léonard de Vinci décodé, 2006. Paris: Gallimard / Musée du Louvre, 53-55.

PFRIEM, A., ZAUER, M. & WAGENFUEHR, A. 2010. Alteration of the unsteady sorption behaviour of maple (Acer pseudoplatanus L.) and spruce (Picea abies (L.) Karst.) due to thermal modification. *Holzforschung,* 64**,** 235-241.

PITTET, V. 1996. *Etude expérimentale des couplages mécanosorptifs dans le bois soumis à variations hygrométriques contrôlées sous chargement de longue durée.* EPFL (Ecole Polytechnique Fédérale de Lausanne).

PLACENCIA, M. I., KOCH, G., PIZZI, A. & PICHELIN, F. 2012. Characterisation of the welding zone of spruce by UMSP. *In:* LORRAINE, U. D. (ed.) *COST Action FP0904: Current and Future Trends of Thermo-Hydro-Mechanical Modification of Wood. Opportunities for new markets ?* Nancy, France.

POON, H. & AHMAD, M. F. 1998. A material point time integration procedure for anisotropic, thermo rheologically simple, viscoelastic solids. *Computational Mechanics,* 21**,** 236-242.

RANTA-MAUNUS, A. 1975. Viscoelasticity of wood at varying moisture content. *Wood Science and Technology,* 9**,** 189-205.

RAPPAZ, M., BELLET, M. & DEVILLE, M. 1998. *Modélisation numérique en science et génie des matériaux,* Presses polytechniques et universitaires romandes.

RÉMOND, R. 2004. *Approche déterministe du séchage des avivées de résineux de fortes épaisseurs pour proposer des conduites industrielles adaptées.* École Nationale du Génie Rural, des Eaux et des Forêts, Centre de Nancy.

SIAU, J. F. 1984. *Transport processes in wood,* Springer-Verlag.

SJÖSTRÖM, E. & ALÉN, R. 1992. *Analytical Methods in Wood Chemistry, Pulping, and Papermaking,* Springer.

SKAAR, C. 1988. *Wood-water relations,* Springer-Verlag.

STRAŽE, A., GORIŠEK, Z., PERVAN, S., FROIDEVAUX, J. & NAVI, P. 2012. Mechano-sorptive creep of heat treated and innate beechwood. *In:* LORRAINE, U. D. (ed.) *COST Action FP0904: Current and Future Trends of Thermo-Hydro-Mechanical Modification of Wood. Opportunities for new markets ?* Nancy, France.

TAYLOR, Z. A., COMAS, O., CHENG, M., PASSENGER, J., HAWKES, D. J., D., A. & S., O. 2009. On modelling of anisotropic viscoelasticity for soft tissue simulation: Numerical solution and GPU execution. *Medical Image Analysis,* 13**,** 234-244.

TORATTI, T. & SVENSSON, S. 2000. Mechano-sorptive experiments perpendicular to grain under tensile and compressive loads. *Wood Science and Technology,* 34**,** 317-326.

UZIELLI, L., DIONISI VICI, P. & COLMARS, J. 2009. Instrumentation pour le contrôle continu des panneaux peints en bois. *Technè,* 29**,** 27-27.

UZIELLI, L., DIONISI VICI, P. & GRIL, J. Caractérisation physico-mécanique du support. *In:* MOHEN, J. P., MENU, M. & MOTTIN, B., eds. Au coeur de la Joconde: Léonard de Vinci décodé, 2006. Paris: Gallimard / Musée du Louvre, 52-53.

WARREN, M. & RÖTTLER, J. 2008. Modification of ageing dynamics of glassy polymers due to a temperature step. *Journal of Physics: Condensed Matter,* 20**,** 1-6.

YOKOYAMA, M., GRIL, J., MATSUO, M., YANO, H., SUGIYAMA, J., CLAIR, B., KUBODERA, S., MISTUTANI, T., SAKAMOTO, M., OZAKI, H., IMAMURA, M. & KAWAI, S. 2009. Mechanical characteristics of aged Hinoki wood from Japanese historical buildings. *Comptes Rendus Physique,* 10**,** 601-611.

ZUMBÜHL, S., SCHERRER, N., FERREIRA, E., HONS, S., MÜLLER, M., KÜHNEN, R. & NAVI, P. 2011. Accelerated ageing of drying oil paint - an FTIR study on the chemical alteration. *Journal of Art Technology and Conservation / Zeitschrift für Kunsttechnologie und Konservierung,* 2**,** 137-149.

ZÜRCHER, E., ROGENMOSER, C., KARTALAEI, A. S. & RAMBERT, D. 2012. Reversible Variations in Some Wood Properties of Norway Spruce (Picea abies Karst.), Depending on the Tree Felling Date *In:* NOWAK, K. I. & STRYBEL, H. F. (eds.) *Spruce: Ecology, Management and Conservation.*

Abstract - Wood and paint layers aging and risk analysis of ancient panel painting

Ancient wood panel paintings represent an important part of the European cultural heritage. Since long time it is known that the storing condition can degrade and damage them. Understanding of the actual state of old panel paintings and the prediction of their behaviour under various climatic conditions is essential to better conserve and restore them. Such analysis could be done by numerical modelling. However, numerical modelling can achieved good predictions only if the materials parameters are adequately determined.

In this work, the mechanical, physical and chemical modifications occurring during natural aging have been investigated for wood and paint layers. The possibility to accelerate the aging with thermo-hydro treatments has been successfully applied to wood. A wood aging law has been found for the radial strength and the lightness. Unfortunately, no such law has been found for the paint layers. The hygroscopic and mechanical behaviour of panel paintings has been then simulated in 3D by a finite element model taking into account the time dependent behaviour. The comparison between the model and experiments shows good agreement. Finally, risk analysis on an old painting shows that normal climate fluctuation should not promote cracks in the wooden support but the cracking of the ground layer is possible.

Résumé – Vieillissement du bois et des couches de peintres et analyse de risques d'anciens panneaux peints.

Les anciennes peintures sur bois représentent une part importante du patrimoine culturel européen. Depuis longtemps, il est connu que les conditions de stockage peuvent entraîner des dégradations et endommagements des panneaux. Une bonne compréhension de l'état actuel des peintures sur bois ainsi que la prédiction de leur comportement dans diverses conditions climatiques est essentielle pour mieux les conserver et les restaurer. De telles analyses peuvent être faites par le biais de la modélisation numérique. Cependant, la modélisation numérique n'est efficace que si les paramètres des matériaux sont proches de la réalité.

Dans ce travail, les modifications mécaniques, physiques et chimiques qui se produisent au cours du vieillissement naturel ont été étudiées pour le bois et les couches picturales. La possibilité d'accélérer le vieillissement par des traitements thermo-hydrique a été appliquée avec succès au bois. Une loi de vieillissement du bois a été trouvée pour la résistance radiale et la clarté de la couleur. Malheureusement, une telle loi n'a pas été obtenue pour les couches picturales. Ensuite, un modèle numérique tridimensionnel de comportement hygromécanique des panneaux peints a été développé. La comparaison entre ce modèle et des expériences donne un bon accord. Finalement, une analyse de risques sur une ancienne peinture a montré que des fluctuations normales d'humidité relative ne devraient pas provoquer de dommages dans le support en bois, mais la fissuration de la couche picturale est possible.